Inverse Modelling to Forecast Enclosure Fire Dynamics

Wolfram Jahn

A thesis submitted for the degree of Doctor of Philosophy.

The University of Edinburgh.

2010

Inverse Modelling to Forecast Enclosure Fire Dynamics

by

Wolfram Jahn

This thesis has been supervised by
Dr Guillermo Rein
Prof José Luis Torero

The examining committee was integrated by
Prof. dr. ir. Bart Merci
Dr Stephen Welch

This thesis was typeset by the author using the LaTeXdocument processing system.

Abstract

Despite advances in the understanding of fire dynamics over the past decades and despite the advances in computational capacity, our ability to predict the behaviour of fires in general and building fires in particular remains very limited. This thesis proposes and studies a method to use measurements of the real event in order to steer and accelerate fire simulations. This technology aims at providing forecasts of the fire development with a positive lead time, i.e. the forecast of future events is ready before those events take place. A simplified fire spread model is implemented, and sensor data are assimilated into the model in order to estimate the parameters that characterize the spread model and thus recover information lost by approximations. The assimilation process is posed as an inverse problem, which is solved minimizing a non linear cost function that measures the distance between sensor data and the forward model. In order to accelerate the optimization procedure, the 'tangent linear model' is implemented, i.e. the forward model is linearized around the initial guess of the governing parameters that are to be estimated, thus approximating the cost function by a quadratic function.

The methodology was tested first with a simple two-zone forward model, and then with a coarse grid Computational Fluid Dynamics (CFD) fire model as forward model. Observations for the inverse modelling were generated using a fine grid CFD simulation in order to illustrate the methodology. A test case with observations from a real scale fire test is presented at the end of this document.

In the two-zone model approach the spread rate, entrainment coefficient and gas transport time are the governing invariant parameters that are estimated. The parameters could be estimated correctly and the temperature and the height of the hot layer were reproduced satisfactorily. Moreover, the heat release rate and growth rate were estimated correctly with a positive lead time of up to 30 s. The results showed that the simple mass and heat balances and plume correlation of the zone model were enough to satisfactorily forecast the main features of the fire, and that positive lead times are possible.

With the CFD forward model the growth rate, fuel mass loss rate and other parame-

ters of a fire were estimated by assimilating measurements from the fire into the model. It was shown that with a field type forward model it is possible to estimate the growth rates of several different spread rates simultaneously. A coarse grid CFD model with very short computation times was used to assimilate measurements and it was shown that spatially resolved forecasts can be obtained in reasonable time, when combined with observations from the fire.

The assimilation of observations from a real scale fire test into a coarse grid CFD model showed that the estimation of a fire growth parameter is possible in complicated scenarios in reasonable time, and that the resulting forecasts at localized level present good levels of accuracy.

The proposed methodology is still subject to ongoing research. The limited capability of the forward model to represent the true fire has to be addressed with more detail, and the additional information that has to be provided in order to run the simulations has to be investigated. When using a CFD type forward model, additional to the detailed geometry, it is necessary to establish the location of the fire origin and the potential fuel load before starting the assimilation cycle. While the fire origin can be located easily (as a first approximation the location of the highest temperature reading can be used), the fuel load is potentially very variable and its exact distribution might be impractical to continually keep track of. It was however shown that for relatively small compartments the exact fuel distribution is not essential in order to produce an adequate forecast, and the fuel load could for example be established based on a statistical analysis of typical compartment layouts.

To my wife Marcela

Study the past if you would divine the future.

Confucius, 551-479 BC

Contents

Abstract **iii**

Contents **vii**

List of Figures **xi**

List of Tables **xv**

Preface **xvii**

Acknowledgments **xxi**

1 Introduction **1**

1.1 FireGrid 2

1.2 Dalmarnock Fire Tests 6

1.3 *A priori* Fire Modelling 8

1.4 Data Assimilation and Inverse Modelling 10

1.5 Review of Inverse Modelling of Fire Dynamics 12

2 The Challenge of *A posteriori* Modelling of the Growth Phase of Dalmarnock Fire Test One **17**

2.1 Introduction 17

2.2 Dalmarnock Test One 19

2.3 *A priori* vs. *A posteriori* Modelling 22

2.4 Computational Domain 23

2.5 Hot Layer Average Temperatures 25

2.6 Comparison of Field Variables 27

2.7 Conclusions 31

3 The effect of model parameters on the simulation of fire dynamics 35

3.1 Introduction . . . 35

3.2 Large-Scale Tests and Simulations . . . 36

3.3 Fire Dynamics Forecast and Model Parameters . . . 38

3.3.1 Pre-flashover Fire . . . 38

3.3.2 Post-flashover Fire . . . 39

3.3.3 Model Parameter . . . 39

3.4 Results of Sensitivity to Model Paramters . . . 40

3.4.1 Ignition Source . . . 41

3.4.2 Fire location, fire area and heat of combustion . . . 42

3.4.3 Thermal and ignition material properties . . . 45

3.4.4 Flame radiative fraction . . . 47

3.4.5 Heating from the smoke layer . . . 47

3.5 Conclusions . . . 49

4 Forecasting Fire Growth using an Inverse Zone Modelling Approach 55

4.1 Introduction . . . 55

4.2 Fire Modelling . . . 58

4.3 Modelling Approach . . . 58

4.3.1 Two-Zone Model . . . 58

4.3.2 Heat Release Rate . . . 60

4.4 Inverse Modelling . . . 61

4.4.1 Framework . . . 61

4.4.2 Cost Function . . . 62

4.4.3 Optimization . . . 62

4.5 Fire Growth Forecasting . . . 63

4.5.1 Slow Fire . . . 67

4.5.2 Fast Fire . . . 69

4.6 Concluding Remarks . . . 71

5 Inverse Modelling of Enclosure Fire Dynamics using a Tangent Linear Approach 75

5.1 Introduction 75
5.1.1 Inverse Modelling 77
5.2 Enclosure Fire Dynamics 79
5.2.1 Fuel Controlled Fire 79
5.2.2 Ventilation Controlled Fire 80
5.3 Fire Modelling 80
5.3.1 Fire Growth 81
5.4 Inverse Modelling 82
5.4.1 Framework 82
5.4.2 Cost Function 83
5.4.3 Optimization 84
5.4.4 Tangent Linear Model 85
5.5 Using the TLM for Parameter Estimation 89
5.5.1 Scenario 89
5.5.2 Single Parameter 91
5.5.3 Two Burning Items 92
5.5.4 Estimation of fuel burning rate 94
5.5.5 Sensitivity to Sensor Locations 94
5.5.6 Alternative sensors 96
5.6 Forecasting Fire Growth in a Compartment 98
5.6.1 Unknown Fuel Source 101
5.7 Conclusions 103

6 Estimation of the Fire Growth Rate in a Real-Scale Fire Test 109
6.1 Introduction 109
6.1.1 Simplified Forecast 110
6.2 Prior analysis 111
6.3 Model Details 113
6.3.1 Computational Domain 114
6.3.2 Grid Size 115
6.3.3 Modelling of the Fire 115
6.3.4 Data Assimilation 116

6.4 Forecast Result 116
6.5 Conclusions 119

7 Conclusions and Future Work **123**
7.1 Conclusions 123
7.2 Future Work 127
7.2.1 Experimental Testing 127
7.2.2 Inverse Modelling of pre- and post-flashover 127
7.2.2.1 Gradient based optimization 128
7.2.2.2 Adjoint modelling 129
7.2.2.3 Summary 130

A Details of the Tangent Linear Model **135**
A.1 Cost Function 135
A.2 Tangent Linear Model 136
A.3 Gradient of the Cost Function 136
A.4 For a Single Parameter 138
A.5 Efficiency Considerations 139
A.5.1 Finite Difference 139
A.5.2 Tangent Differentiation 140
A.5.2.1 Differentiate then discretize 140
A.5.2.2 Discretize then differentiate 140
A.5.3 Adjoint Model 142
A.5.3.1 Differentiate then discretize 142
A.5.3.2 Discretize then differentiate 143
A.5.4 Minimizing a Quadratic Function 144

List of Figures

1.1 Data assimilation process 4
1.2 Dalmarnock Fire Test layout 6
1.3 Dalmarnock average temperatures 7
1.4 Round robin HRR 9
1.5 Zone results from the round-robin study 9

2.1 Dalmarnock room layout with fuel load and location of sensors 19
2.2 Measurements from the Dalmarnock Test One 20
2.3 HRR from sofa experiments 21
2.4 Computational domain and fuel items used in the FDS simulations . . 24
2.5 Comparison of results with different grid sizes at 140 s 25
2.6 Addition of the blanket to the HRR measured in Set 1 to obtain Set 1b. 26
2.7 Predicted average hot layer temperatures 27
2.8 Temperature vs. height distribution at different locations in the compartment 28
2.9 Wall temperature vs. height and Heat flux vs. height distributions . . . 29
2.10 Heat flux to the ceiling 30

3.1 Dalmarnock layout 37
3.2 Input HRR and resulting upper layer temperature 42
3.3 Effect of fire area – gas phase and surface temperature 43
3.4 Effect of waste paper basket – gas phase and surface temperature . . . 44
3.5 Effect of surface $\rho\delta c$ on the predicted bookshelf temperature 46
3.6 Effect of the surface emissivity on the predicted bookshelf temperature 47
3.7 Effect of the radiative fraction on the predicted bookshelf temperature 48
3.8 Effect of the smoke layer built-up in the predicted temperature evolution of the bookshelf 49

3.9 Effect of the soot yield parameter in the predicted temperature evolution of the bookshelf 49

4.1 Data assimilation process 56
4.2 CFD compartment fire used for data generation 63
4.3 Spread rate and entrainment coefficient – medium fire 64
4.4 Lead time – medium fire 65
4.5 Forecast at 42 s after five data points are assimilated 65
4.6 Forecast at 66 s after nine data points are assimilated 66
4.7 Forecast at 90 s after 13 data points are assimilated 66
4.8 Spread rate and entrainment coefficient – slow fire 67
4.9 Lead time – slow fire 68
4.10 Forecast at 160 s after 12 data points are assimilated – slow fire 68
4.11 Spread rate and entrainment coefficient – fast fire 69
4.12 Lead time – fast fire 70
4.13 Forecast at 40 s after 8 data points are assimilated – fast fire 70

5.1 Data assimilation process 77
5.2 Different stages of the fire 79
5.3 Inverse modelling procedure 88
5.4 Set up for the numerical experiment 89
5.5 Sensor Layout 90
5.6 Sensor measurements recorded from the true fire 91
5.7 1–dimensional parameter estimation 92
5.8 The spread rates of 2 independent fires 93
5.9 Estimation of burning rate and spread rate of the fuel 94
5.10 The spread rates of 2 independent fires – 9 sensors 95
5.11 The spread rates of 2 independent fires – 30 sensors 95
5.12 The spread rates of 2 independent fires – sensors away from fire 96
5.13 Estimation of the spread rate and soot yield 96
5.14 Estimation of the spread rate and soot yield – obscuration 97
5.15 Characterization of a compartment fire 98
5.16 Spread rate as a function of the growing assimilation window. 100

5.17 Forecast after 150 s of assimilated data 101
5.18 Forecast after 330 s of assimilated data 101
5.19 Spread rate as a function of the growing assimilation window with unknown fuel load. 102
5.20 Forecast after 330 s of assimilated data with no prior knowledge of the fuel load 103

6.1 Curve fit-forecast 111
6.2 HRRs for sofa as measured in laboratory experiments 112
6.3 Quadratic Fit of HRR curves 113
6.4 Computational domain and fuel items used in the FDS simulations . . 114
6.5 Convergence of Spread Rate 116
6.6 Forecast 200 s 117
6.7 Forecast of the temperature at Rack 1 117
6.8 Forecast of the temperature at Rack 19 118
6.9 Forecast of the temperature at Rack 7 119

A.1 Newton–Raphson method vs. linearization 137

List of Tables

2.1 Time line of main events 20

3.1 Flame heights 45

A.1 Forward algorithmic differentiation example 141

A.2 Reverse algorithmic differentiation example 143

Preface

This thesis has been written in manuscript format. The material has been presented in the following form:

- Chapter 1 is a general introduction to the research. Although this chapter is not a manuscript on its own, it is loosely based on the following published papers:

  A. Cowlard, W. Jahn, C. Abecassis-Empis, G. Rein, J.L. Torero. Sensor Assisted Fire Fighting. *Fire Technology*, in press, 2008. DOI:10.1007/s10694-008-0069-1.

  G. Rein, J.L. Torero, W. Jahn, J. Stern-Gottfried, N.L. Ryder, S. Desanghere, M. Lazaro, F. Mowrer, A. Coles, D. Joyeux, Alvear D., J. Capote, A. Jowsey, C. Abecassis-Empis, and P. Reszka. Round–Robin Study of *a priori* Modelling Predictions of the Dalmarnock Fire Test One. *Fire Safety Journal*, **44**(4):590–602, 2009. DOI:10.1016/j.firesaf.2008.12.008

- Chapter 2 consists of a manuscript that illustrates the complexity of using numerical modelling to match the physical evidence in a real fire scenario. This is intended for the fire engineering community, and has been submitted for publication in a relevant Journal and is currently in the peer review process.

- Chapter 3 consists of a manuscript where the sensitivity of a fire field model to its input parameters is discussed. The work related to this manuscript was presented at the 9th International Symposium on Fire Safety Science, and the manuscript is published as:

  W. Jahn, G. Rein, J.L. Torero. The Effect of Model Parameters on the Simulation of Fire Dynamics. *Fire Safety Science*, Vol. 9, pp: 1341–1352, 2008. DOI:10.3801/IAFSS.FSS.9-1341.

- Chapter 4 consists of a manuscript that illustrates the inverse modelling methodology using a zone modelling approach. This manuscript has been submitted for publication in a relevant Journal and is currently under review.

- Chapter 5 consists of a manuscript where the application of the inverse modelling to a fire field model is demonstrated. This manuscript has been submitted for publication in a relevant Journal and is currently under review.

- Chapter 6 consists of a manuscript where the inverse modelling methodology presented in chapters 4 and 5 is applied to a full scale fire test in order to establish the growth rate of the fire. This manuscript has been submitted for publication in a relevant Journal and is currently under review.

The main body of this document can be divided in two parts:

- In chapters 2 and 3 a 'trial and error' approach to inverse modelling of enclosure fire dynamics is described using data from a real fire. Here the main focus is on the thorough understanding of fire dynamics and the associated modelling process. In the context of forecasting fire dynamics it became evident from this first part that a simple and robust fire growth model is needed.

- In chapters 4 and 5 an automated inverse modelling process is proposed and illustrated by means of a simplified virtual fire scenario (data are generated by a fire model). Finally, in chapter 6 the presented methodology is put to trial using real data of a complex fire scenario.

The first part justifies the transition from the real fire scenario (Dalmarnock) to a idealized and simplified scenario in order to establish a methodology that can robustly forecast fire growth, while the second part presents the methodology. The inverse modelling is illustrated using firstly generated data, and then the real fire data from the Dalmarnock Tests, thus closing the circle by returning to the initial set of data.

Declaration

This thesis and the work described within have been completed solely by Wolfram Jahn at the BRE Centre for Fire Safety Engineering at the University of Edinburgh, under the supervision of Dr Guillermo Rein and Prof José Luis Torero. Where others have contributed or other sources are quoted, references are given.

Wolfram Jahn,
May 2010

This research was funded by
Alβan Programme High level Scholarships for Latin America , Grant
N^{o}E06D100038CL
and the UK Technology Strategy Board's Collaborative Research and Development
programme through FireGrid
which is greatfully acknowledged.

Acknowledgments

I would like to thank my supervisor Dr Guillermo Rein for his patience, encouragement and guidance during the past years. In many, sometimes philosophical, sometimes desperate discussions we little by little set the basis for the work described in this thesis and found a way to put the very theoretical idea of this project into practice. With his contagious optimism and zest for action he many a time convinced me to try the (in my opinion) impossible, and taught me never to surrender.

I would also like to thank Professor José Luis Torero for encouraging me to take this huge step, to leave family and friends behind and cross the ocean to do a PhD. He is the original artificer behind this work, and although we only had a few thesis related meetings, all of them proved to be crucial in the development of my research. I would also like to thank him for his constant concern about the well-being of the PhD students in the Firelab, which made the dealing with administrative matters so much easier.

A special 'Thank You' to all my colleagues at the Firelab and their families, not only for the many fruitful conversations and discussions about research related issues, but also for their friendship and for making the years in Edinburgh such a pleasant period that I will always dearly remember. Thanks to Francesco and Nicolas for all those late evening dinners and for always keeping the doors of their flat open for me to stay. To Thomas for many long conversations where we discussed and fixed the problems of the world in general and of fire safety engineering in particular. To Cecilia, Adam and Hubert for providing a home away from home on my final trips to Edinburgh. To Paolo for being an oasis of quietness and tranquility in that many times all too noisy up-stairs office. To Pedro for sharing his experience and expertise with me and for including us in the social life of postgraduate Edinburgh. To my office mates Koo, Kate and Rory for making work fun. To Angus, David, Joanne, Holy, Aitor, Aida, Alan, Albert, Jamie and all those who would offer me a smile and have a wee talk with me on my rounds through the lab whenever I needed a break.

Thanks to all the master students I had the pleasure to work with, for putting their

trust in me and for involving me in their work. I hope our discussions were as useful to you as they were to me. Thanks to David, Steffen, Luca, Cristián and Phil for not being just visitors, but companions and friends.

I would like to thank my family, especially my mother, who has always insisted that we invest in our education, as it is the one thing nobody can take away from us. Thanks for sowing the seed. Thanks to my sister for taking care of my affairs back home, and for always being there for me.

Finally, and most specially, I would like to thank my wife Marcela for leaving her family behind and going on this huge adventure with me. Thanks for having come into my life and for being there for me whenever I need you. Your support and encouragement during these years have been the most important ingredients to the successful completion of this thesis. Without you I would never have done this. THANK YOU!!

1

Introduction

The human attraction for the prediction of future events permeates deep into science and technology, where some disciplines have emerged to provide the scientific knowledge capable of forecasting the dynamics of non-trivial systems. Astronomical objects, tides and weather are the most popular examples.

Forecasting enclosure fire dynamics is a subject of central interest in fire safety engineering. While the first line of response to a fire event is part of the design process of a building in the form of compartmentation of open spaces, smoke barriers, egress paths, suppression and detection systems etc., fires that overcome these measures may occur, and it is necessary to prepare for that case. If a fire escalates and the building and occupants are unable to terminate the threat by the time fire fighters arrive, then intervention should take place and management of the scene will be delegated to the fire service. The fire fighting strategy to follow during a potential fire is currently based mostly on the experience and the intuition of commanding officers of the fire service on duty, but it would be life saving if fire fighting strategies could be decided upon based on short and medium term forecasts of the development of the fire. Not only would this allow for more efficient strategies, it would also assure the safety of fire fighters who enter the emergency scenario in order to attack the fire and rescue the occupants.

The state-of-the-art of fire safety engineering does currently not provide the tools

to forecast fire events, and limited, experience based predictions that can be made are assisted only by minor technological input such as smoke detectors or sprinkler systems.

In 1984 Howard Emmons, giving in to the aforementioned attraction, made a prediction of a different nature. He ventured a forecast of the future development of fire safety sciences, succeeding with surprising accuracy regarding the main activities of fire research in the 1990's, the dual characteristic of fire modelling (practical zone models on one hand and highly complex field models for research on the other) until the first quarter of the 21st century, and conjecturing a series of developments during the centuries to come that are to be corroborated in the future [1]. For the decade of 2050 Emmons predicts the development of an integrated system that would provide commanding fire officers with backup computed information to aid him in his critical decisions.

The goal of this research is to take a first step into that direction by developing a conceptual framework and a mathematical methodology that allows for forecasting of fire events based on combining observations of physical quantities from the fire scenario with numerical modelling. Data collected from the fire are used to feed a numerical model with information of the evolving emergency, and thus to steer the computations.

1.1 FireGrid

Despite advances in the understanding of fire dynamics over the past decades and despite the advances in computational capacity, our ability to predict the behaviour of fires in general and building fires in particular using numerical models remains very limited. From a fire fighting point of view, forecasting of fire events only makes sense if it occurs with a positive lead time, i.e. if the prediction is based on current information of the state of the system, and can be completed faster than the fire is evolving. Current computational fluid dynamics (CFD) based fire models generally demand heavy resources and computational time periods that are far greater than the time associated with the processes being simulated (hours to model seconds). If comprehensive computational models are ever to be used to estimate, forecast and understand fire growth in support of emergency response, the computational time has to be shorter than the event itself. This problem is being addressed in the FireGrid

project [2], and a full justification of this project together with an introduction to sensor assisted fire fighting is presented by Cowlard et al. [3]. A summary of the key points is presented in the rest of this section.

Modern buildings provide some useful information about an ongoing fire emergency, including emergency management plans, security camera footage and security panels which can indicate in a crude manner the origin and magnitude of the event. This information will be included in the decision making process of commanding officers, who then can deploy people and equipment more effectively. The current density and nature of information, however, makes reliance on experience and intuition unavoidable.

Although more detailed information about the emergency could be of great value, it would have to be provided to commanding officers in a synthesized and summarized manner in order to avoid information-overload. Sensors that track the evolution of physical variables such as temperatures, gas concentrations, light intensity and mechanical stress have to be interpreted to provide relevant information. Security cameras can be used to count people or to assess the magnitude of a fire. There are some examples in the literature where different cameras have been used for this purpose [4], but while good results have been obtained in isolated cases, generalization has always been proven difficult. Other sensors, like thermocouples or strain gauges provide point measurements of physical variables that in isolation provide information of little value or could mislead conclusions. Higher sensor density can portray a clearer picture of the nature of the event, but as mentioned before, a large flow of data becomes difficult to interpret and can rapidly result in information-overload. Tracking of the evolution of physical variables *per se* is therefore not a useful option to assist an intervention in a fire.

An alternative approach is to use the output of computational fire models in order to obtain an insight into the evolving fire. Fire models are based on the numerical solution of equations of energy, mass, momentum and species conservation, and their output can reach from average temperatures of the hot layer of the fire compartment in the case of zone models, to detailed field distributions of all kind of physical quantities such as temperature, flow velocities, species concentration etc. in the case of field models. The main limitation of computer fire models is that is it not possible to solve the underlying physics accurately enough to actually predict fire development. Most complex fire

models, based on Computational Fluid Dynamics (CFD), can reproduce simple fire scenarios satisfactorily, but it takes several hours and even days to run them in order to simulate a few minutes [5]. The state-of-the-art of fire modelling does not even allow for those models to predict fire growth on a scale relevant to compartment fires, and they must rely, just as simpler zone type models, on a previously defined heat release rate as input. While technological and scientific progress could eventually make fire models fast and precise enough, given the inherent uncertainty of the input parameters that would need to be defined, it is questioned whether the output of fire models could ever be robust enough. Fire dynamics are inherently transient with timescales ranging from a few seconds to several hours, and they are governed by strong coupling between the gas phase (movement of hot gases, combustion) and the solid phase (heating of surface, pyrolysis, fire spread) [6].

Although a recent attempt of modelling flame spread from first principles has shown good agreement with experimental observations [7], this can only consider scenarios of very limited size (flame length in the order of 10 cm) due to the very extensive computational time it requires. Natural fires in real-size enclosures involve mechanisms that develop in length-scales ranging from micrometres (flame thickness) to metres (compartment size), and time-scales from milliseconds (chemistry) to minutes (burnout) [5]. Thus, coupled computational simulations from first principles of fire growth would demand extensive computational times far greater than the time associated with the phenomenon itself.

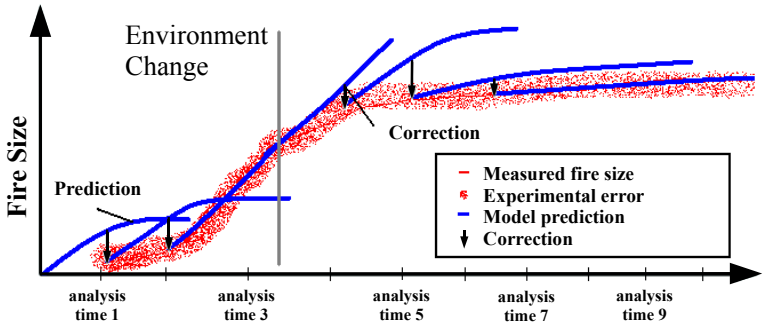

Figure 1.1: Conceptual representation of the data assimilation process and the sensor steering of model predictions even when fundamental changes take place in an evolving emergency scenario.

Even if all the mechanisms could be solved correctly in an acceptable time, their chaotic nature imposes a maximum possible lead time to the forecast, as has been

shown for other dynamical systems (e.g. weather [8]). It is thus suggested that fire modelling cannot be used for emergency response without feedback information from the evolving fire scenario [3]. Nevertheless, in conjunction with sensor data it has the potential to achieve required speed, precision and robustness. Sensor data can be used as a substitute for detailed models enabling simpler approaches to provide fast and well-informed outputs. Continuous correction of the model output by means of sensor data can allow for steering of the models to account for uncertainty in the input variables and for changes in the environment of an evolving fire scenario that modify the fire dynamics (window breakage, door opening etc). This concept is illustrated in Fig. 1.1, where sensor data is assessed and then continually reassessed to recreate the fire environment and steer the computations. The model output can thus be used to forecast the evolution of the event with some lead time. The information can then be summarized and delivered to the fire service in the most useful form.

FireGrid thus aims to provide predictions of fire growth and fully developed fire behaviour by feeding numerical models with information of the evolving fire scenario. The philosophy behind it is to use measured data to provide the information that cannot be obtained from the models, thus accelerating the modelling predictions by being able to use relatively coarse grids and simplified models instead of highly complex models. To further increase computational speed and to allow for escalation High Performance Computers (HPC) are proposed to be used within a Grid configuration. HPC will allow running parallelized versions of the models at increased speed and the Grid will enable to use off-site computational resources on demand, combined with databases of pre-computed scenarios.

The predictions would be used to produce a series of potential outcomes given different intervention strategies. The outcomes are then optimized and a preferred intervention strategy is defined by a Command & Control unit. The forecasts would be presented in a succinct form that is compatible with the training and knowledge of emergency responders, thus making interpretation of the output effective and reliable. Continuous updating of the predictions would enable changes of strategy on the basis of the evolution of the event.

As envisioned by Emmons [1], FireGrid will not be commercial at full scale within the next decade. At this stage it is a concept under development, and the work presented

in this thesis represents but one step towards an operational forecast system for fire emergencies.

1.2 Dalmarnock Fire Tests

A series of real scale tests were conducted in a housing estate in Dalmarnock (Glasgow, UK) in order to illustrate the concept of FireGrid, and to assess simple Command and Control (C&C) procedures based on information from the fire that had been synthesized in a crude manner. Detailed information of the experimental setup and outcome of the Dalmarnock Fire Test can be found in [9, 10].

Three tests were conducted, two compartment fire tests (Test One and Test Two) and a smoke filling test (Test Three) in the staircases. The compartment fire tests were set in two identical flats in different floors of the building, both flats having the same layout, furniture and sensors installed in order to assure the repeatability of the test. The impact of changing the ventilation conditions in Test Two while the fire was evolving was assessed comparing the outcome to Test One, where the fire was left to burn without interaction from C&C.

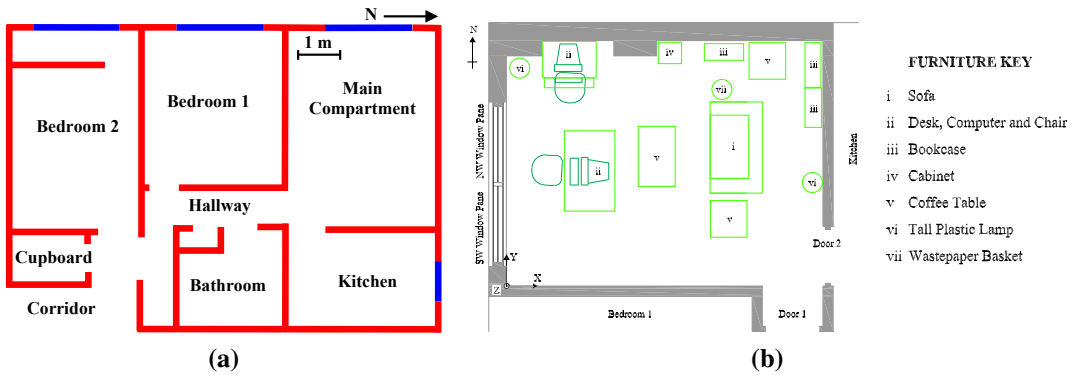

Figure 1.2: Dalmarnock Fire Test layout [9, 10]: (a) Flat compartments, vents and basic dimensions (to scale), (b) Furniture in the main compartment.

Figure 1.2 shows the geometry and layout of the flat where Tests One and Two where carried out. The compartments of the flat and their distribution are shown in Fig. 1.2a. The main compartment, where the fire was started, is in the upper right corner. A detailed layout of the test compartment and its furniture is given in Fig. 1.2b.

The main compartment, where the fires started, was heavily instrumented. Twenty

thermocouple trees, with 12 vertically arranged thermocouples each, were spread throughout the compartment. Five further trees of thermocouples were placed along the window sill. Twenty nine thin-skin calorimeters were used to measure heat fluxes on ceiling and walls. Eight laser emitter-receiver pairs were used to measure smoke obscuration at different heights. Three bidirectional velocity probes were placed in both compartment doors, and a further eight were placed outside the compartment window. All sensors were connected to a set of central data loggers recording at a frequency of 0.5 Hz. Additionally, several early warning fire alarm systems and CCTV cameras were installed in the compartment.

The fire was started in a waste paper basket located next to a sofa. A blanket that was thrown over the armrest of the sofa and was hanging partially into the waste paper basket allowed the fire to spread over the fire barriers in the armrest and ignite the seating area of the sofa. After about 275 s the bookshelf next to the sofa ignited and was rapidly engulfed in fire. Within 25 s after ignition of the bookshelf the fire had flashed over.

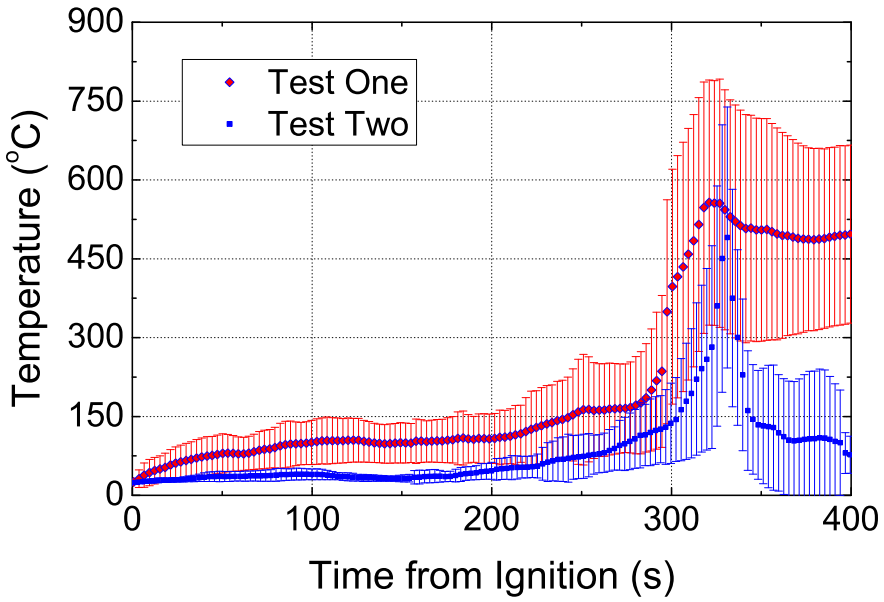

Figure 1.3: Comparison of the experimental average room temperature (^{o}C) variation in time (s) with experimental error of Dalmarnock Test One and Test Two [9, 10]. Data is only presented until extinction of Test Two (400 seconds).

Figure 1.3 shows the average temperature of the gas phase measured in Test One and Test Two during the first 400 s of the tests. Although the temperature is significantly lower in Test Two, it is clear that the onset of flashover occurs at about the same time in

both tests (around 300 s). The interaction of the C&C with the fire development could influence the average temperatures in the compartment, but it could not delay or prevent flashover. This reflects the repeatability intended for this set of experiments.

1.3 *A priori* Fire Modelling

The large amount of data collected in the Dalmarnock Fire Tests has been used for assessment of fire modelling procedures (both *a priori* and *a posteriori*) and for the identification of relevant parameters in the fire modelling process.

Before the Dalmarnock Tests were carried out, a round-robin study of blind predictions was conducted in order to explore the *a priori* predictive capabilities of fire modelling in realistic scenarios [11]. The aim of the exercise was to forecast the fire development as accurately as possible and compare the results. The participating teams were asked to forecast the test results as accurately as possible, and avoid engineering analysis with conservative assumptions of safety factors, as is common for use in fire safety design. All teams were given access to a common pool of information about the experimental test set up and initial conditions. The information available to the teams included geometry and dimensions of the flat, room layout and information about furniture, photographs of the test compartment and the results of a laboratory experiment were the same sofa that acted as ignition source in the Dalmarnock Tests had been burnt.

Ten simulations were submitted, eight simulations using CFD (FDSv4 [12]) and two simulations using zone models (CFAST [13]). Comparison of the modelling results showed a large scatter and considerable disparity among the predictions, and between predictions and experimental measurements.

Figure 1.4 shows large scatter in the outcome of the simulations. The predicted HRR varies between less then 500 kW to over 8 MW, with the estimated HRR from the experiments somewhere in the middle (around 3 MW).

Fig. 1.5 shows the evolution of the average hot layer temperature (Fig. 1.5a) and the hot layer height (Fig. 1.5b) as predicted by the round-robin teams. The experimental values are averaged over the entire layer assuming that during the growth phase the interface is at the 100^{o}C isotherm or at the height of the largest temperature gradient

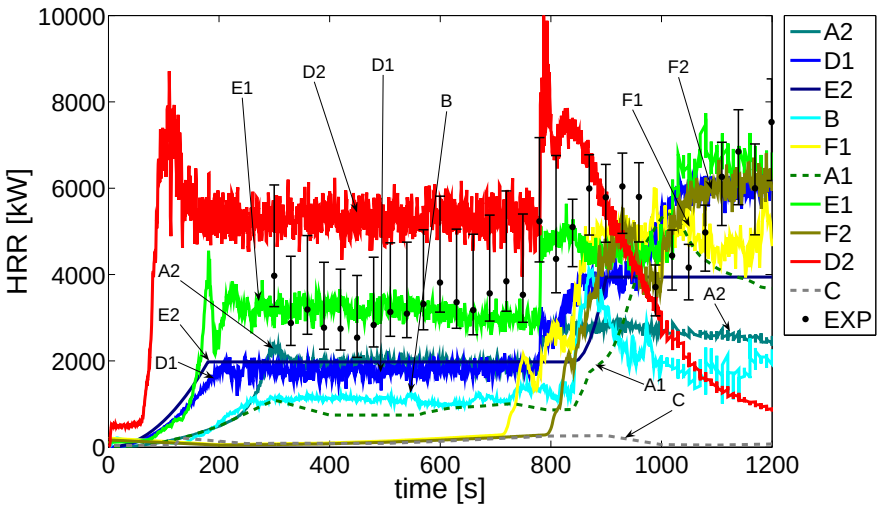

Figure 1.4: HRR as predicted by the various teams that participated in the round-robin study.

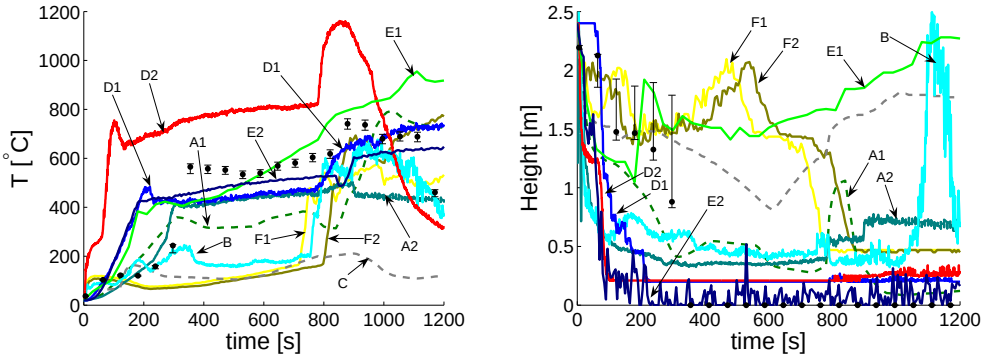

(a) Mean temperature **(b)** Smoke layer height

Figure 1.5: Evolution of the hot layer in the compartment:(a) average temperature and (b) height to the interface from compartment floor. Experimental values derived assuming the smoke layer interface at the 100°C isotherm. The legend in Fig. 1.4 applies.

when below 100°C at the very beginning of the test. The sensitivity of the height to the smoke layer to variations of the assumed isotherm value is also presented in Fig. 1.5 for the range from 90 to 250°C. The smoke height calculations agree with visual estimates of the smoke layer height, during the fire growth stage, obtained from the camera footage [9, 10]. During the post-flashover stages, the video cameras confirm that the smoke layer engulfed the whole compartment and thus the height to the smoke layer is zero.

There is a wide scatter of modelling results shown in Fig 1.5. Most simulations under-predicted the hot layer temperature. Four simulations fell within a 10-40% under-prediction range and the others were above the 50% range of over- and under-predictions.

The very wide range of behaviours predicted reflects the influence of the difference in overall assumptions used for the input. It is worth highlighting that the simulation that performed the best at predicting the HRR (E1), predicting it within a 10% range, predicted the average hot layer temperature within a 30% range but differs greatly from the experimental measurements of smoke layer height.

The results of this study indicate large scatter and considerable disparity regarding the evolution of the HRR, both amongst the predicted fires and between the predicted fires and the experimental data. The scatter of the simulations is much larger than the estimated experimental error. Moreover, comparison between the range of predicted hot layer temperatures (seen in Fig. 1.5a) and the differences between Test One and Test Two (seen in Fig. 1.3) further demonstrates that the scatter is also much larger than the expected experimental variability. The study emphasized on the inherent difficulty of modelling fire dynamics and particularly fire growth in complex fire scenarios like Dalmarnock, and showed that the accuracy to (blindly) predict fire growth (i.e. evolution of the heat release rate) is, in general, poor. However, since good predictions of the effects of a fire in the far field can be achieved, once the fire growth is known [14], it can be suggested based on the results of this study that forecasts of fire development are possible, if they take into account feedback information from the evolving fire scenario.

1.4 Data Assimilation and Inverse Modelling

A deterministic prediction of any physical process is done by solving (numerically or analytically) the system of differential equations that govern the process with a certain set of initial and boundary conditions. In a complex dynamical system, such as a compartment fire, the boundary conditions for the coupled sub-systems that compose the overall dynamical system are complicated to obtain, as they depend on the interaction between those systems. The release of combustible gases from a burning object is a boundary condition to the transport of energy and mass in the gas phase. Similarly, the heat radiated from the flame to the surface of the burning object is a boundary condition to the transport of energy into the solid, and thus for the pyrolysis. While an overall solution to this problem is in principle possible, it would require a large amount of computational resources (fine grid in the order of 1 mm in order to resolve all the spatial

variations of importance). Furthermore, the non-linearity of the underlying physics would result in a theoretical limit to the predictability of the dynamics of the system due to error propagation and subsequent divergence at large time scales [8].

Measurements from the fire compartment can assist the model calculations in two different, although related, ways when assimilated into the model. On one hand collected data can provide the details that cannot be obtained from a simplified fire model, but would be necessary to produce a forecast. For example, it would be possible to model fire growth using a field model with a grid much too coarse to reproduce the interactions between gas and solid phase accurately, since the observations of temperature at some point within the compartment can be used to recover the boundary conditions without the need of solving the coupled systems explicitly. On the other hand observations from the fire can be used to update ongoing simulations and thus extend the limit of predictability, as suggested in Fig. 1.1.

The process of using observation from the dynamical system that is being modelled in order to infer information about the boundary and initial conditions and other parameters is known as inverse modelling (or solving an inverse problem).

In numerical weather predictions (NWP) the inverse modelling is a fundamental part of the forecasting system, taking an important part of the computational resources [15, 16], and is given the name of 'data assimilation'. In order to initialize the numerical models that are used to forecast the state of the atmosphere, weather observations from all over the planet are collected and then assimilated into the model. Observations are assimilated by initializing a new forecast based on a previous forecast (several hours back), and correcting it according to the difference between the previous forecast and the observations [17, 18]. Most modern NWP systems assimilate observations during a certain period of time (assimilation window) before starting the forecast, in order to account for the dynamical coupling of the involved processes [19]. The assimilation algorithm typically involves a linearization of the NWP system around the previous forecast and the subsequent solution of a quadratic minimization problem [15, 20]. Since the problem of NWP is fundamentally the same as the problem addressed in this work, a similar strategy is proposed and implemented and the name of data assimilation is adopted for the inverse modelling, although the concept is extended somewhat to comply with the particularities of the problem of fire event forecasting.

In the modelling of the early stages of a compartment fire the details of the initial conditions are of less importance than the details of the boundary conditions. It is generally enough to assume ambient temperature homogeneously distributed over all the gas phase, since temperatures of the combustion gases are four to five times higher, so that local deviations from the ambient temperature in the initial condition become negligible.

For the early stages of the fire we will thus focus on correctly establishing the boundary conditions. It is proposed in this document to replace the highly complicated interaction between gas and solid phase by a simplified fire growth model that is input into the gas phase model as a boundary condition, and is based on a set of parameters that do not depend on the feedback from the fire and are thus constant (at least for a certain amount of time). The assumptions of the model and its implications and validity are discussed in chapters 4 and 5.

Once the fire has passed the growing stage and flashover has occurred in the compartment (the transition from a localized fire to a fire that engulfs the entire compartment), ventilation conditions become very important. A change in the geometry (window breakage, door opening etc.) can influence the development of the fire greatly. Such changes can often not be predicted, and starting a new simulation, that includes this information, from the beginning of the fire can be impractical. However, if a new simulation is to be started after flashover has occurred, the initial conditions for that simulation will be drastically different from ambient. The exact state of the system at the time the simulation is started has to be obtained from measurements in the fire compartment.

1.5 Review of Inverse Modelling of Fire Dynamics

Parameter estimation and inverse modelling are an important area within the engineering and scientific community. In fire engineering, several studies have been undertaken. Richards et al. [21] use a database of pre-run zone-type models to estimate fire location and fire growth. They use the same zone model to generate the data for comparison, and analyze the influence of measurements and modelling errors. Leblanc and Trouvé use a zone model to predict the heat release rate (HRR) time-history based on observations

generated using the same model [22]. While they are able to closely reproduce the HRR past history, their work does not address how to produce a forecast of future events. Koo et al. [23] used measurements from a fire test experiment to progressively steer fire simulations towards the effective value using a Monte Carlo approach with a set of parameters that was used for random generation of scenarios. While they were able to reproduce past observations of temperature, they could not link the parameters of the model to the physics of the full scale fire test, which limits the forecast of future events to statistical considerations. Cowlard et al. [24, 25] estimate the upward flame spread rate of PMMA based on visual recordings of the flame height and temperature measurements at the PMMA. Their method was able to re-adjust the estimated parameters in order to account for the transition from laminar to turbulent flow. In chapter 2 of this thesis a trial and error approach to inverse modelling of enclosure fire dynamics is presented. An upper and lower bound HRR curve is established based on comparison of the model output to measurements of a real scale fire scenario.

As mentioned at the end of the previous section (section 1.4), the parameters that have to be estimated for the fully developed fire are fundamentally different from the parameters associated to the fire growth stage. The core of the work presented in this thesis focuses on the forecasting of fire growth, and thus on the estimation of the associated parameters. The fully developed fire, and the corresponding data assimilation technique, is discussed only in the last chapter of this document (chapter 7), and only an overview is presented.

References

[1] H. Emmons. The Further History of Fire Science. *Combustion Science and Technology*, 40(1):167–174, 1984.

[2] R. Upadhyay, G. Pringle, G. Beckett, S. Potter, S. Han, S. Welch, A. Usmani, and J.L. Torero. An Architecture for an Integrated Fire Emergency Response System for the Built Environment. *Fire Safety Science*, 9:427–438, 2008. DOI:10.3801/IAFSS.FSS.9-427, http://www.era.lib.ed.ac.uk/handle/1842/2703.

[3] A. Cowlard, W. Jahn, C. Abecassis-Empis, G. Rein, and J.L. Torero. Sensor

Assisted Fire Fighting. *Fire Technology*, in press, 2008. DOI:10.1007/s10694-008-0069-1.

[4] L. Audouin, G. Kolb, J.L. Torero, and J.M. Most. Average Centerline Temperatures of a Buoyant Pool Fire Obtained by Image Processing of Video Recordings. *Fire Safety Journal*, 24(2):167–187, 1995.

[5] G. Cox and S. Kumar. Modelling Enclosure Fires using CFD. In P. DiNenno, editor, *SFPE Handbook of Fire Protection Engineering*, chapter 3–8, pages 3–194–3–218. National Fire Protection Association, Quincy, MA 02269, 3 edition, 2002.

[6] D. Drysdale. *An Introduction to Fire Dynamics*. ISBN 0-471-97290-8. Wiley & Sons, New York, 2nd edition, 1998.

[7] W. Xie and P. DesJardin. An Embedded Upward Flame Spread Model using 2D Direct Numerical Simulations. *Combustion and Flame*, 156(2):522–530, 2009. DOI:10.1016/j.combustflame.2008.11.011.

[8] E. Lorenz. Deterministic Nonperiodic Flow. *Journal of the Atmospheric Sciences*, 20(2):130–141, 1963.

[9] Rein, Abecassis-Empis, and Carvel, editors. *The Dalmarnock Fire Tests: Experiments and Modelling*. ISBN 978-0-9557497-0-4. The University of Edinburgh, Accesible at www.era.lib.ed.ac.uk/handle/1842/2037, 1st edition, 2007.

[10] C. Abecassis-Empis, P. Reszka, T. Steinhaus, A. Cowlard, H. Biteau, S. Welch, and G. Rein. Characterisation of Dalmarnock Fire Test One. *Experimental Thermal and Fluid Science*, 32(7):1334–1343, 2008. http://www.era.lib.ed.ac.uk/handle/1842/2513.

[11] G. Rein, J.L. Torero, W. Jahn, J. Stern-Gottfried, N.L. Ryder, S. Desanghere, M. Lazaro, F. Mowrer, A. Coles, D. Joyeux, Alvear D., J. Capote, A. Jowsey, C. Abecassis-Empis, and P. Reszka. Round–Robin Study of *a priori* Modelling Predictions of the Dalmarnock Fire Test One. *Fire Safety Journal*, 44(4):590–602, 2009. DOI:10.1016/j.firesaf.2008.12.008, http://www.era.lib.ed.ac.uk/handle/1842/2704.

[12] K. McGrattan. Fire Dynamics Simulator (Version 4) – User's Manual. NISTIR 6784, 2003.

[13] W. Jones, R. Peacock, G. Forney, and P. Reneke. CFAST – Consolidated Model of Fire Growth and Smoke Transport, Version 6. Technical report, 2005.

[14] K. McGrattan. Fire Modelling: Where Are We? Where Are We Going? *Fire Safety Science*, 8:53–68, 2005. DOI:10.3801/IAFSS.FSS.8-53.

[15] E. Kalnay. *Atmospheric Modeling, Data Assimilation and Predictability*. ISBN 978-0-521-79629-3. Cambridge University Press, Cambridge, 1st edition, 2003.

[16] J.M. Navon, X. Zou, and J. Derber. Variational Data Assimilation with an Adiabatic Version of the NMC Spectral Method. *Monthly Weather Review*, 120(7):1433–1446, 1992.

[17] T. Schlatter. Variational Assimilation of Meteorological Observations in the Lower Atmosphere: A Tutorial on How it Works. *Journal of Atmospheric and Solar–Terrestial Physics*, 62(17):1057–1070, 2000.

[18] J. Hoke and R. Anthes. The Initialization of Numerical Models by a Dynamic–Initialization Technique. *Monthly Weather Review*, 104(12):1551–1556, 1976.

[19] D. Harms, S. Raman, and R. Madala. An Examination of Four–Dimensional Data Assimilation Techniques for Numerical Weather Prediction. *Bulletin Amercian Meteorolical Society*, 73(4):425–440, 1992.

[20] F. Bouttier and P. Courtier. Data Assimilation Concepts and Methods. Technical report, European Centre for Medium-Range Weather Forecasts, 2001.

[21] R. Richards, B. Munk, and O. Plumb. Fire Detection, Location and Heat Release Rate Trough Inverse Problem Solution. Part I: Theory. *Fire Safety Journal*, 28(4):323–350, 1997. DOI:10.1016/S0379-7112(97)00005-2.

[22] M. Leblanc and A. Trouvé. Inverse Modeling of Enclosure Fire Dynamics. In *Proceedings of the 6th U.S. National Combustion Meeting*, 2009.

[23] S. Koo, J. Fraser-Mitchell, and S. Welch. Sensor-steered fire simulation. *Fire Safety Journal*, 45(3), 2010. DOI:10.1016/j.firesaf.2010.02.003.

[24] A. Cowlard, L. Auersperg, J.B. Richon, G. Rein, S. Welch, A. Usmani, and J.L. Torero. A Simple Methodology for Sensor Driven Prediction of Upward Flame Spread. *Turkish Journal of Engineering and Environmental Sciences*, 31(6):403–413, 2007.

[25] A. Cowlard. *Sensor and Model Integration for the Rapid Prediction of Concurrent Flow Flame Spread*. PhD thesis, The University of Edinburgh, 2009. http://www.era.lib.ed.ac.uk/handle/1842/2753.

2

The Challenge of *A posteriori* Modelling of the Growth Phase of Dalmarnock Fire Test One

2.1 Introduction

Modelling of compartment fires using computational fluid dynamics (CFD) has been a research topic since the introduction of computational techniques in fire science in the 1980's [1]. Only in the last decade the available computational power and knowledge on fire dynamics have grown sufficiently to carry out simulations of fire development in real-size building enclosures, using grids that are fine enough to reproduce fire-driven flows reasonably well [2]. CFD has since been extensively used to model fire dynamics [3, 4, 5]. A common engineering application of CFD is the reconstruction of accidental fires as part of forensic investigations. Recent examples are the 2001 WTC [6] and the 2003 Station Nightclub [7] investigations.

The state of the art of fire modelling is such that given a fire of a certain size and power, CFD can be used to calculate the resulting temperature and smoke concentration

fields. The fire source is therefore treated as a input into the model by means of a prescribed heat release rate (HRR) as a function of time [8]. This poses a problem in the study of accidental fires where the HRR is generally unknown. Predicting the evolution of the fire (i.e., spread rate and pattern), and calculating the HRR instead of measuring it, is a more challenging task that is still part of fundamental research [9, 10]. The complex interaction between flames, hot gases and the solid phase requires a thorough understanding of the different physical processes of combustion, radiation and solid degradation.

Most modelling work in the literature corresponds to simple fire sources, like pool fires or a single burning item, and avoids the more complex processes of flame spread and fire growth. Little research has been done comparing simulations with real-scale fire tests that use realistic fuel loads. Three examples are presented here. Reneke et al. [11] simulated fire tests involving crib fires in a full scale single compartment with a zone model obtaining reasonable agreement with the measured average temperatures when the measured HRR is used as an input. Miles et al. [12] obtain good results in average temperatures when performing simulations of a series of fire tests involving wood cribs, but they do not compare results at the field level. Pope et al. [8] simulated the 1999-2000 BRE large compartment test series [13] using the CFD code FDS. The simulations provided reasonable agreement with the measured temperature field within the context of structural fire safety.

This paper reports a series of CFD simulations conducted *a posteriori* to reproduce the large-scale Dalmarnock Fire Test One that involved real burning items leading to a complex fire spread process. The HRR of the growth phase was not measured directly, but the compartment was densely instrumented thus providing a very rich set of data that could be used to aid defining the HRR of the fire source and to reproduce the main features of the fire. Many different simulations were conducted and many parameters were readjusted to achieve acceptable agreement at the compartment average and field level. The work can be seen as attempting to solve a large and complex inverse problem by trial and error.

A key difference between previous modelling studies of large-scale tests and the present work is that the heavily instrumented full-scale Dalmarnock Fire Tests provided measurements at sufficient spatial resolution to be suitable for comparison with field

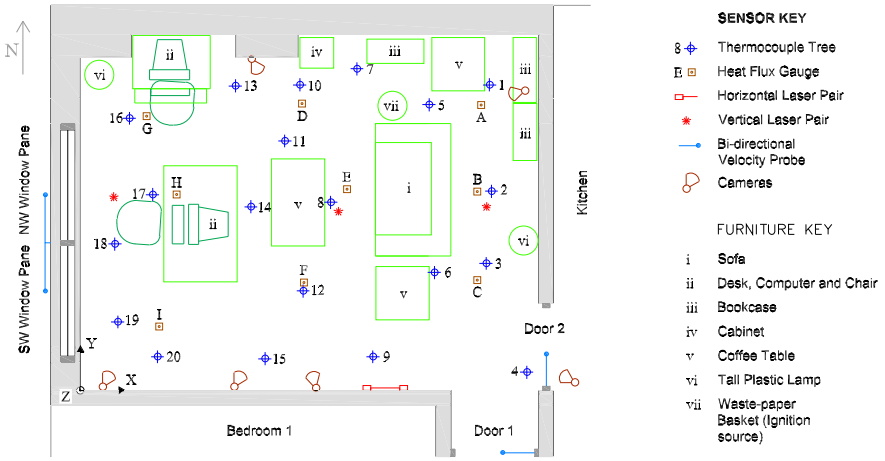

Figure 2.1: Room layout with fuel load and location of sensors [14].

models at the grid size level [14].

2.2 Dalmarnock Test One

Detailed information about the experimental set-up and the chain of events that occurred during the Test One can be found elsewhere [15, 14], but a short summary is given here. Test One was held in a two-bedroom single family flat, with the living room set up as the main experimental compartment. This compartment was 3.50 m by 4.75 m wide and 2.45 m high with a 2.35 m by 1.18 m two-pane window as shown in Fig. 2.1. While the main source of fuel was a two-seat sofa stuffed with flexible polyurethane foam, the compartments also contained two office work desks with computers, each with its own foam-padded chair, three tall wooden bookcases, a short plastic cabinet, three small wooden coffee tables, a range of paper items and two tall plastic lamps. A plastic wastepaper basket filled with crumpled newspaper and 300-500 ml of heptane was the ignition source. The fire spread to a blanket on the sofa hanging into the basket, igniting the seating area of the sofa. After about 275 s the bookshelf next to the sofa ignited and was rapidly engulfed in fire. Within 25 s after ignition of the bookshelf the compartment reached flashover conditions (see Table 2.1 for a time line of the events).

The HRR in the fire tests was estimated by the principle of oxygen depletion, using the measurements from the gas velocity probes at all the ventilation openings and assuming total O_2 consumption [15]. An estimation for the post-flashover fire results in about 3 MW before the first window breakage, and about 5 MW after the second

Table 2.1: Time line of main events during Dalmarnock Test One. [14]

Event	Time from ignition (s)
Ignition	0
Cushions ignite	9
Bookcase ignites	275
Fire engulfs bookcase (flashover)	300
Compartment window breakage (NW Pane)	800
Compartment window breakage (SW Pane)	1100
Extinction	1140

breakage as shown in Fig. 2.2a. During the growth phase the assumption of total O_2 consumption does not hold, as the fire is not ventilation controlled, thus the evolution of the HRR during fire growth is unknown.

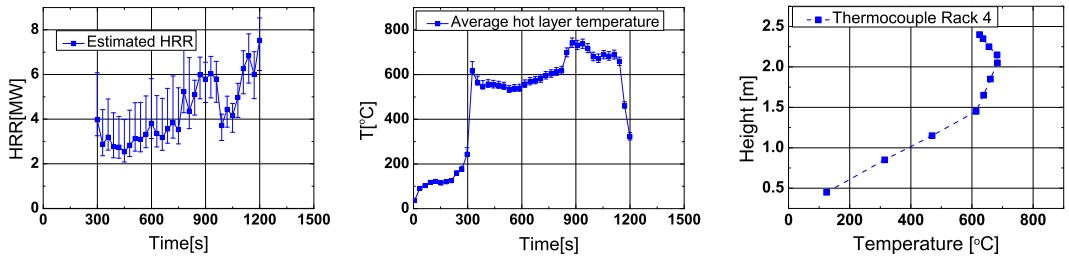

(a) Estimated HRR **(b)** Average Temperature **(c)** Temperature vs. Height

Figure 2.2: Measurements from the Dalmarnock Test One: a) estimated HRR (using oxygen consumption), b) average temperature of the hot layer in the main compartment (corrected for radiation) and c) vertical temperature distribution in front of the compartment door at 600 s[14] (rack 4, see Fig 2.1).

Figure 2.2b shows the average temperature of the hot layer measured in Test One and Fig. 2.2c the vertical distribution of temperatures along one specific thermocouple rack. A detailed presentation of the data can be found in [15, 14].

Prior to Test One, laboratory experiments were conducted in order to determine the HRR curves for the sofa and the bookshelves inside the furniture calorimeter (using an exact replica of those used in Test One) [14]. A second series of laboratory experiments was conducted after Test One in order to analyze variations to the ignition protocol [16]. These two sets of experiments were the only direct source of information on the HRR in Test One.

Figure 2.3 shows the evolution of the HRR of the sofa and the effect of variations to the ignition source. The experiment conducted prior to Test One (referred to as Set 1)

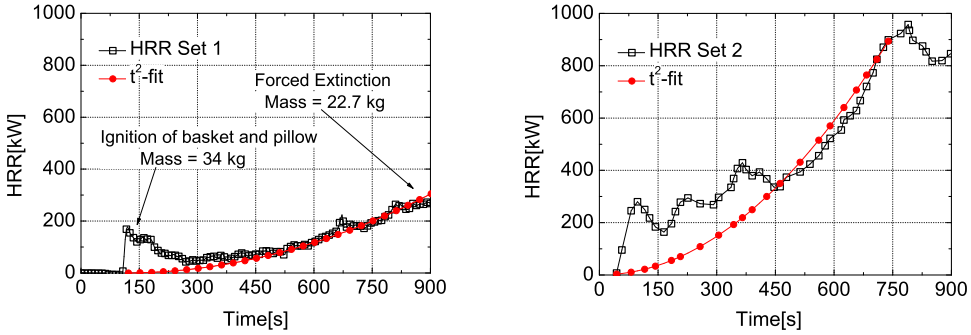

(a) Sofa without blanket **(b)** Sofa with blanket

Figure 2.3: Measured HRR for variations to the ignition source and equivalent t-squared fires: a) measured in the laboratory prior to Test One including sofa and waste basket (Set 1); and b) after Test One including the sofa, waste basket and blanket (Set 2).

(Fig. 2.3a) consisted of a sofa with two cushions, and a waste paper basket located next to the sofa. Accelerant was poured into the paper basket and the basket was ignited. The fire then spread over the armrest to the sofa and was stopped about 800 s after ignition when approximately one third of the sofa had been burnt. In the experiments conducted after Test One (referred to as Set 2, Fig. 2.3b), the exact ignition protocol of Dalmarnock Test One was replicated, which was like Set 1 but including a blanket that had been placed over the armrest of the sofa, and the accelerant distributed between basket and blanket. The presence of the blanket in Set 2 allowed the fire to bypass the armrest fire barrier and led to a faster growth rate involving the cushions. The fire growth rate for Set 2 is equivalent to a t-squared fire with growth constant 0.0016 kW/s^2 (a medium fire [17]). The constant in Set 1 is 0.0005 kW/s^2 (corresponding to a slow fire [17]). The two tests show that the uncertainty in the growth rate of the sofa fire during the early stages is significant and varies between a slow and a medium fire.

Figure 2.3a suggests two patterns in the burning behaviour; an initial peak that rapidly decreases is followed by a growing fire that resembles a t-squared curve. A similar behaviour can be seen in Figure 2.3b for Set 2. It is conjectured that the initial peak corresponds to the waste paper basket, accelerant and the blanket (in the case of Set 2), while the t-squared fire corresponds to the sofa itself.

By measuring flame heights from visual recordings, it can be established that the sofa's HRR in Set 1 grew slower than the observed fire in Test One. Flashover in Test One occurred at 300 s. According to Set 1, this is only 100 s after the period when the

basket fire dominated the HRR. Comparison of the fire development using the video available of both fires confirms this. At the initial laboratory experiment no blanket was used, so that the fire could not spread across the armrest to the cushions as fast. The fire in Dalmarnock Test One spread quickly from the basket over the armrest to the sofa, whereas in Set 1, the flames took considerably longer to spread over the armrest.

2.3 *A priori* vs. *A posteriori* Modelling

Before the Dalmarnock Tests were carried out, a round-robin study of blind predictions [9] was conducted in order to explore the *a priori* predictive capabilities of fire modelling in realistic scenarios. The aim of the exercise was to forecast the fire development as accurately as possible and compare the results. Comparison of the modelling results showed a large scatter and considerable disparity among the predictions, and between predictions and experimental measurements. The scatter of the simulations was much larger than the error and variability expected in the experiments. The study emphasized on the inherent difficulty of modelling fire dynamics in complex fire scenarios like Dalmarnock, and showed that the accuracy of blind prediction of fire growth (i.e. evolution of the heat release rate) is poor.

The present work revisits the modelling of the Dalmarnock Fire Test One, this time using the large set of measurements available. That is, the work is conducted *a posteriori*. Many different simulations are conducted and many parameters are (re-)adjusted until acceptable agreement is reached. Work is focused only on the growth phase of the Dalmarnock fire Test One.

As mentioned before, during the growth phase of Test One the evolution of the HRR is unknown. Moreover, the laboratory experiments of the sofa and similar ignition sources show significant uncertainty. Indeed, this is one of the most important issues addressed in this chapter. The challenge is to be able to reproduce the HRR such that the fire environment (temperature and smoke) is simulated correctly. The work solves a large and complex inverse problem by trial and error.

2.4 Computational Domain

The code Fire Dynamics Simulator v4.07 [18, 19], one of the most commonly used fire CFD codes, is used here. FDS solves a form of the Navier-Stokes equations adequate for low-speed thermally driven flows. While large eddies are solved directly, turbulences at subgrid scale are modelled using Smagorinsky's approach [20].

The computational domain (Figure 2.4) includes the main test compartment with its vent openings (two pane windows to the exterior), the nearby kitchen (with another window to the exterior) and hallway. It was considered that the other rooms of the apartment did not contribute to the fire dynamics and they were therefore not included. The fuel load in the main compartment was reduced to the most important fuel elements involved in the growth phase; the sofa, the ignition source and two bookshelves in the corner behind the sofa. The other fuel items, the computers, coffee table, chairs and desks also contributed to the fuel load, but this occurred only after flashover, and are therefore outside the scope of this work. The FDS default reaction (propane) was used for combustion chemistry. The fire area on the sofa was assumed constant in time (2/3 of the seating area) and the time variation of the HRR was imposed as a ramp of the fuel injection. The compartment walls and ceiling were modelled as 10 cm thick concrete, whereas the compartment floor was assumed to be covered with a carpet. This simplification of the more complex composition of the real walls is justified by the inherent inaccuracies of the heat transfer modelling from the hot gases to the walls. Open boundary conditions were used at the exterior of the compartment. All other parameters were left with the default values in FDS.

The grid size is one of the most critical parameters in numerical simulations. In the scope of this work a large number of simulations had to be run in order to converge toward good agreement with the measured data and it was therefore necessary to use a sufficiently coarse grid allowing for an efficient use of computational resources. However, too coarse a grid could induce significant numerical errors in the solution. It has been proposed [21, 22] that to resolve the fire plume properly, the ratio between the characteristic fire diameter, D^*, and the grid size should be at least 5 to 10. D^* is defined as:

$$D^* = \left(\frac{\dot{Q}}{\rho_\infty c_p T_\infty \sqrt{g}} \right)^{2/5}. \tag{2.1}$$

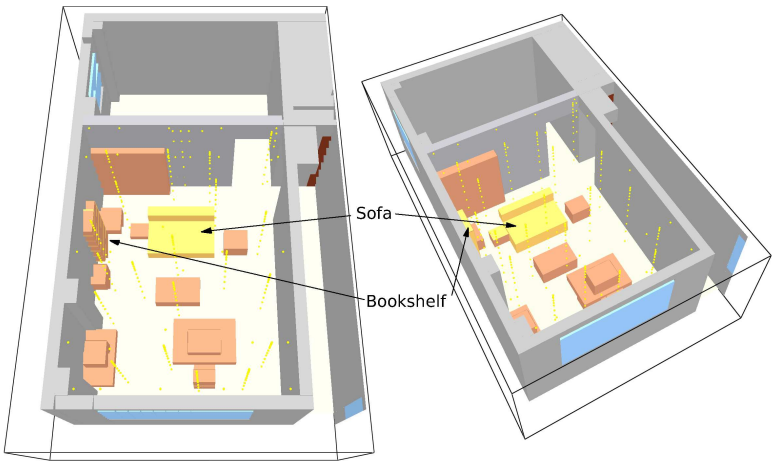

Figure 2.4: Computational domain and fuel items used in the FDS simulations

During the growth phase, the order of magnitude of the HRR is 300 kW, and the characteristic diameter of the sofa is around 0.6 m. Hence the grid size should be smaller than 11 cm for an adequate plume resolution. This value is used as an order of magnitude reference. In order to select an adequate grid size, simulation were run with a wide range of different grid sizes: 5 cm, 10 cm, 15 cm and 20 cm edge cubes. The HRR was prescribed according to the laboratory experiment Set 1.

Figure 2.5 shows the temperature vs. height distribution at two different locations in the experimental compartment, one near the burning sofa, and one near the window away from the fire. See Figure 2.1 for rack locations. The time of comparison is 140 s, although data are averaged in time (10 s) in order to account for local differences due to turbulences. The simulations using coarser grids (15 and 20 cm) actually showed better agreement when compared to the measured data, both qualitatively and quantitatively than the finer grids (5 and 10 cm). Near the fire (Figure 2.5a), the 20 cm and 15 cm grids are in agreement between them and reproduce well the lower zone temperatures and the smoke layer height, but overpredict the temperatures of the smoke layer by 17%. The 10 cm grid underpredicts the smoke layer height by around 15%, but is in good agreement regarding the smoke layer temperature. The 5 cm grid underpredicts the measurements by more than 35% at all heights. Away from the fire (Figure 2.5b), the 10, 15 and 20 cm grids are in reasonable agreement to the measurements, while the 5 cm grid shows divergence both quantitatively (>30%) and qualitatively.

While it is generally accepted for numerical integration that a smaller grid yields more accurate results, FDS results depend on the size of the numerical grid due to

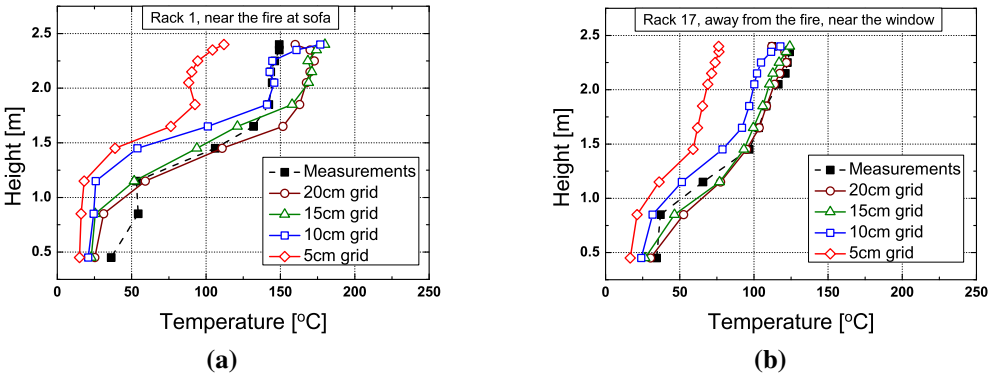

Figure 2.5: Comparison of results with different grid sizes at 140 s: a) distribution at the north wall next to the bookshelf (rack 1); and b) distribution near the window (rack 17).

the LES approximation [23], and also because other approximations depend on the grid size (radiation and combustion mechanisms, geometry and buoyancy induced turbulence [22]). This could explain why relatively coarser grids in this case provide better results. Moreover, the LES Smagorinsky constant used by default in FDS was calibrated to predict smoke movement in large scale applications where boundary layers are not well resolved [24] and thus for scenarios different from the one studied here.

Based on the grid dependency study, the 10 cm grid was chosen because it showed good comparison to the experiments, allowed for fast computations and complied with the recommendation associated to the characteristic fire diameter [21, 22]. Given the present results, there are no good reasons to choose a finer grid.

2.5 Hot Layer Average Temperatures

Two distinct levels of detail are analysed. This section predicts the average hot layer temperature while the next section looks at the distribution of local field temperature and wall heat fluxes. Comparison at detailed level requires a good agreement at averaged level first.

As seen in the Set 1 and Set 2 experiments, the blanket significantly modifies the HRR. A possible HRR of the blanket alone can be estimated assuming quadratic growth and decay phases. The blanket, made of cotton, weighed 1 kg, hence the total combustible energy stored in the blanket including 100 ml of accelerant can be estimated to be around 21 MJ (see chapter 3 or [25]), assuming a heat of combustion

of 16.5 MJ/kg for the cotton. The resulting peak HRR would be 150 kW. This is not negligible compared to the measured HRR of the sofa in the early stages, and should therefore be included in the input HRR for the model. Figure 2.6 shows the reconstruction HRR of the blanket alone and its addition to the HRR measured in Set 1. The resulting HRR is referred to as Set 1b. Note that here the data is shifted by 150 s compared to Fig. 2.3a, so that the ignition occurs at 0 s.

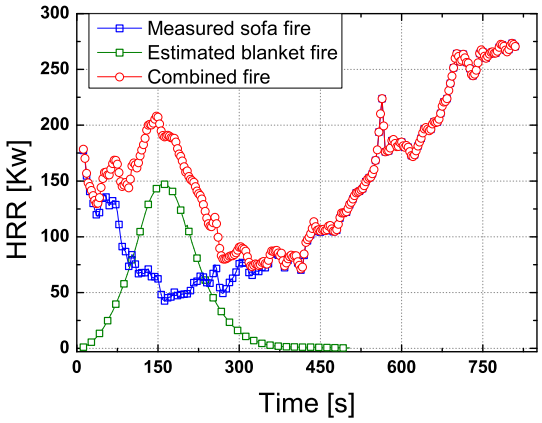

Figure 2.6: Addition of the blanket to the HRR measured in Set 1 to obtain Set 1b.

The predicted hot layer average temperature using different HRR and comparison to measurements are shown in Figure 2.7. For the Set 1 HRR, the simulated hot layer temperature rise agrees with the measured temperature during the first 100 s, but the decrease in the input HRR between 0 s and 150 s (see Fig 2.3a) results in much lower (up to 50%) simulated average temperatures after about 100 s compared to the measurements (Fig. 2.7a). For Set 2, the average hot layer temperature is overpredicted by about 50% between 25 s and 100 s, and by about 35% between 150 s and 250 s (Fig. 2.7c). For the Set 1b HRR, the simulated hot layer temperatures are in good agreement with the measured temperatures (within the instrumental uncertainty) until 200 s into the fire. After that the simulated temperature decreases in contrast to the measured temperature which rises continually until flashover.

Based on the resulting hot layer average temperature, Set 1 showed to result in unrealistically low temperatures (which was anticipated by the comparison of the burning behaviours of Set 1 and Set 2). Set 1b provides a lower bound to the HRR curve during pre-flashover, while Set 2 proved to be an upper bound. The uncertainty in the average temperature predictions using HRR bounds is between 0 and 50%, which is

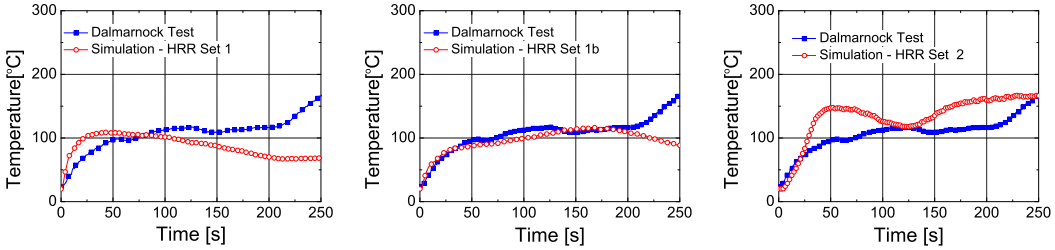

(a) Set 1 **(b)** Set 1b **(c)** Set 2

Figure 2.7: Predicted average hot layer temperatures; a) Set 1; b) Set 1b and c) Set 2.

relatively low. The results presented confirm that if the HRR is well characterized, the average temperatures can be reproduced with reasonable agreement and without major effort in small compartments.

2.6 Comparison of Field Variables

The density of measurements in Test One present an opportunity to assess field level simulations. Figure 2.8 shows the temperature vs. height distributions at different locations in the experimental compartment using the two bounding HRR curves Set 1b and Set 2 established as input. Two times, 150 s and 200 s, are chosen arbitrarily for illustration purposes. In general the simulations are in reasonable agreement with the measurements, although it can be seen that the further away from the burning sofa the better the agreement between measurements and simulations.

As expected the lower and upper bound HRR curves result in an upper and lower bound for the hot layer average temperatures. In the cold layer FDS tends to underpredict the temperatures even for the upper bound HRR curve. This indicates that the Dalmarnock fire had a less sharply defined hot layer than estimated by FDS. In accordance with this, it can be observed that the thickness of the hot layer is not significantly affected by the higher HRR. It only produces higher temperatures in the hot layer.

At thermocouple rack 7, roughly 1.5 m away from the fire, the temperatures are underpredicted by around 45% at 150 s (Figure 2.8a) using the lower bound HRR (Set 1b), and by around 40% using the upper bound HRR (Set 2). At rack 11 and 150 s into the fire the simulations with both input HRR curves are in good agreement with the measured data (Fig. 2.8b), lying within the experimental error in the hot layer,

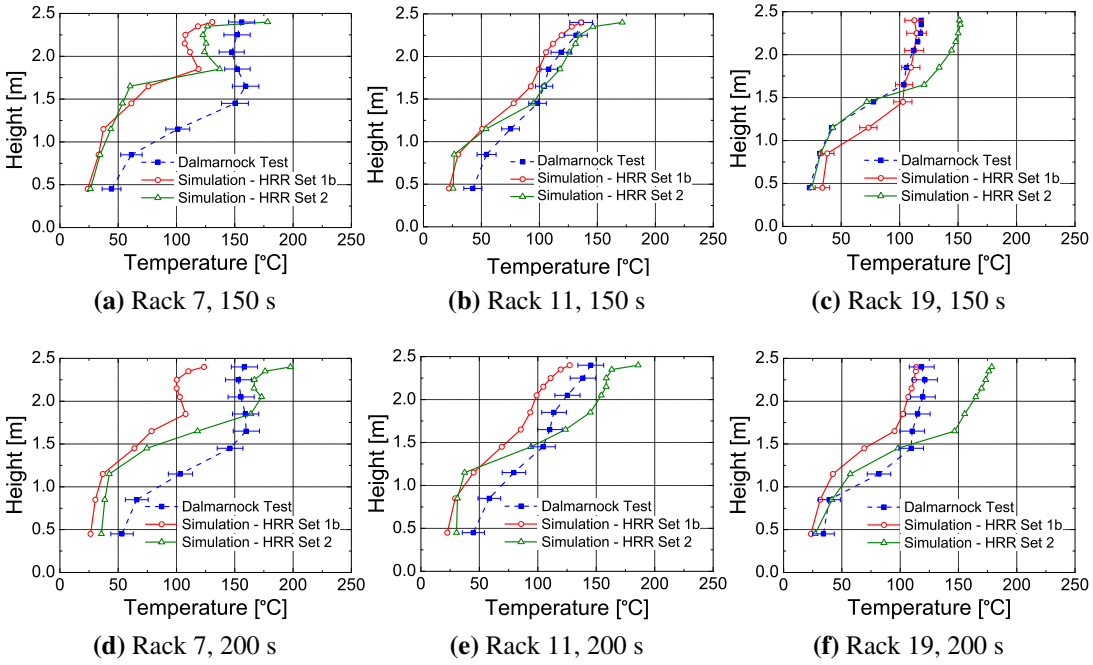

(a) Rack 7, 150 s **(b)** Rack 11, 150 s **(c)** Rack 19, 150 s

(d) Rack 7, 200 s **(e)** Rack 11, 200 s **(f)** Rack 19, 200 s

Figure 2.8: Temperature vs. height distribution at different locations in the compartment at 150 s (a,b and c) and 200 s (d, e and f). Rack 7 (a,d) is located near the fire, rack 11 (b,e) is located next to the centre table and rack 19 (c,f) is located near the window. See Fig. 2.1 for rack location.

and underpredicting the temperatures in the cool layer by about 40%. At rack 19 and 150 s (Fig. 2.8c), the lower bound HRR curve produces temperatures that lie within the experimental error in the upper layer, while the upper bound HRR curve results in overprediction of the hot layer temperature by about 30%. Both HRR curves predict the hot layer to be about 0.5 m higher than the measured hot layer. At 200 s the upper layer temperatures at rack 7 are overestimated (although very close to the experimental error, Fig. 2.8d) when using the upper bound HRR, and underestimated by around 35% when using the lower bound HRR curve. The lower layer temperatures are underestimated by around 50% for both input HRR curves. At rack 11 temperatures simulated with the lower bound HRR curve are underpredicted by less than 20% in the hot layer (Fig. 2.8e), having almost identical shape as the measured distribution. With the upper bound HRR curve as input, the temperatures at rack 11 are overpredicted by about 25% in the hot layer, but underpredicted by about 35% in the cool layer, thus indicating higher temperature differences between hot and cool layer. Near the window, at rack 19 (Fig. 2.8f), the temperatures (specially of the hot layer) are in good agreement with the lower bound HRR as input, although the predicted hot layer height is around 0.5 m

higher than that observed. Using the upper bound HRR curve for the simulation, the hot layer temperature is overpredicted by about 40%, which is in accordance to the overprediction by around 40% of the hot layer average temperature resulting from the upper bound HRR curve at 200 s.

In addition to gas phase temperatures, the simulated wall temperatures and wall heat fluxes are compared to the measurements. Figures 2.9a and 2.9c show the distribution of wall temperature at the back wall that separated the fire compartment from the kitchen at 150 s and 200 s, respectively. Figures 2.9b and 2.9d show the distribution vs. height of heat fluxes at the same wall.

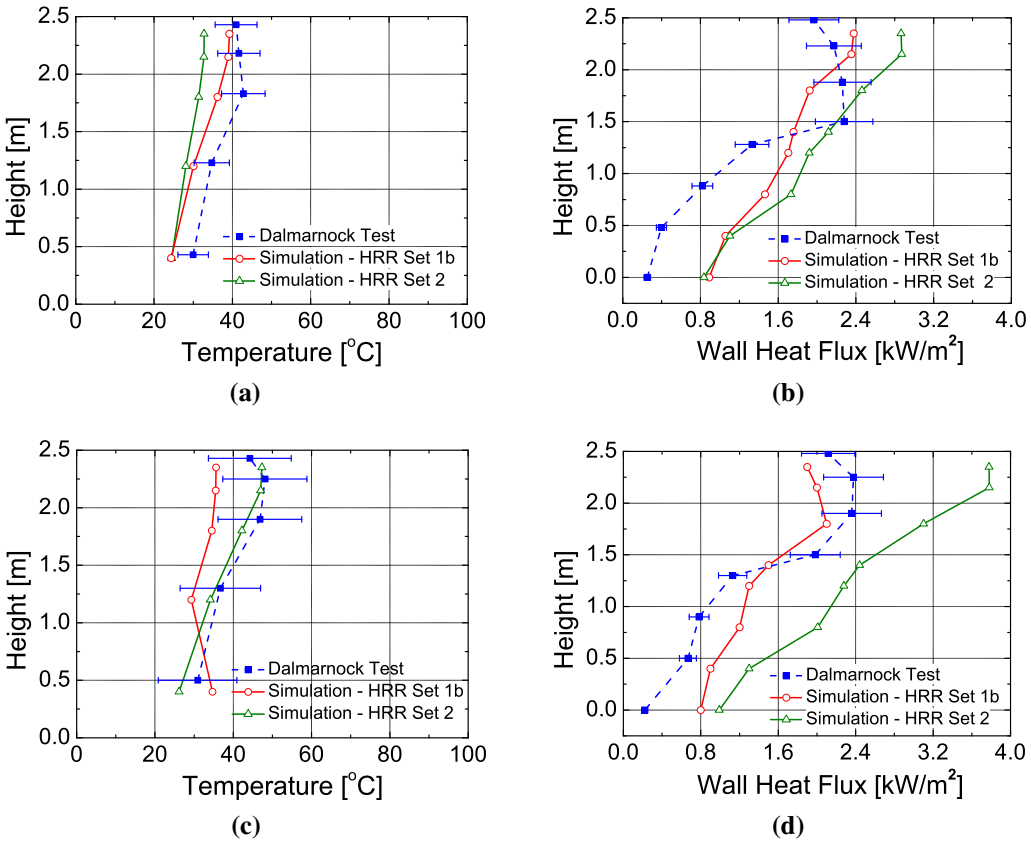

Figure 2.9: Wall temperature vs. height (a and c) and Heat flux vs. height (b and d) distribution on the back wall of the fire compartment.

Using the lower bound HRR curve, the wall temperature is underpredicted by about 20% at 150 s, and within or very close to the uncertainty induced by the experimental error at 200 s. For the upper bound HRR curve the simulated wall temperature lies within the experimental error at both times. This apparent advantage of the upper bound HRR curve is contradictory to the corresponding results for heat fluxes to the wall.

While the lower bound HRR curve produces heat fluxes in the upper layer close to the bounds of experimental error at 150 s, the upper bound HRR curve overpredicts heat fluxes in the upper and lower layer. Figure 2.9d shows that at 200 s the heat flux predicted with the lower bound HRR curve is in reasonable agreement with the measurements, both qualitatively and quantitatively with the hot layer predictions almost within the experimental error. The upper bound HRR curve produces overpredictions of the heat fluxes by more than 90%.

Figure 2.10 shows the comparison of the distribution of heat fluxes on the ceiling. The vertical axis is the heat flux, and the horizontal axis corresponds to the distance across the main compartment. In Figs. 2.10a and 2.10c, the measurements are taken between the bedroom wall (south) and the northern wall of the experimental compartment. In Figs. 2.10b and 2.10d, the measurements are taken between the window (west) and the kitchen wall (east) in the middle of the room.

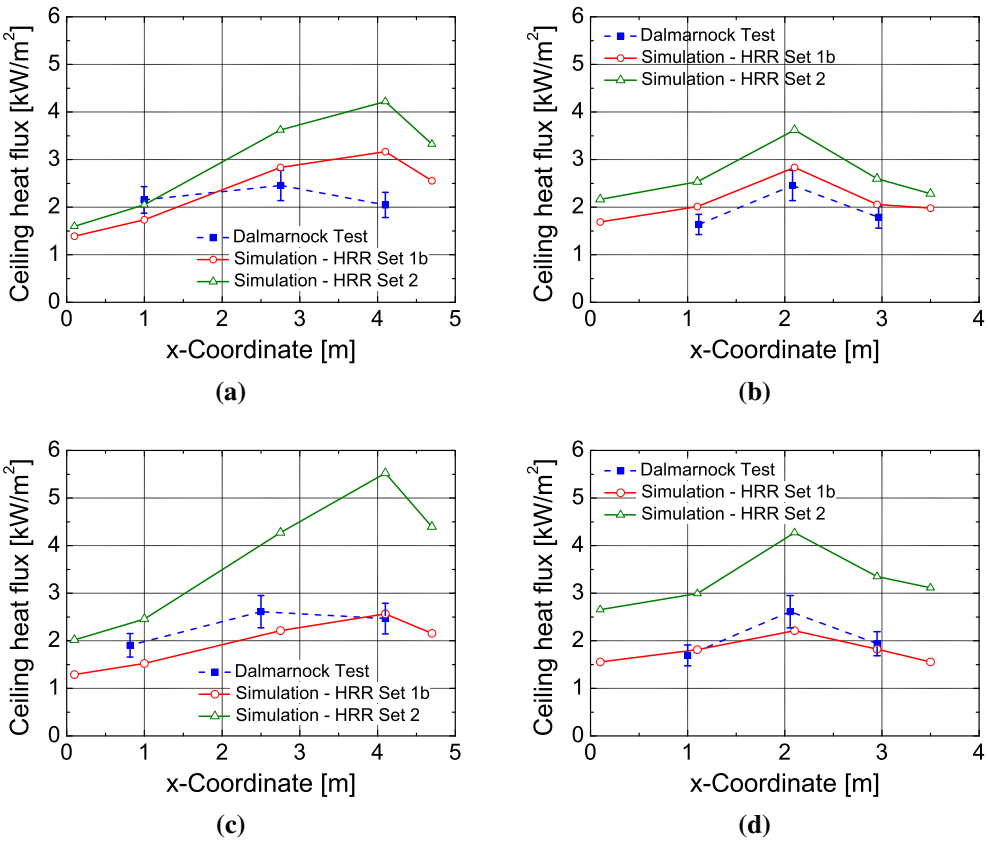

Figure 2.10: Heat flux to the ceiling; a) and c) heat flux vs. the distance across the main compartment from the window to the kitchen wall in the middle of the room at 150 s and 200 s respectively. b) and d) transversal distribution of the heat flux from the bedroom wall to the north wall of the experimental compartment at 150 s and 200 s.

The simulated heat flux to the ceiling agrees well with the measured heat flux when using the lower bound HRR curve. At 200 s half of the compared locations the simulations were within the error bounds, and at the remaining locations the heat flux was underpredicted by less than 20%. At 150 s the comparison between bedroom wall and northern wall (Fig. 2.10a) shows overprediction of less than 20%, and the shape of the distribution agrees well with the measurements. Using the upper bound HRR curve, the heat fluxes to the ceiling are largely overpredicted (over 80%). The better quantitative results compared to the heat flux to the kitchen wall (Fig. 2.9b) when using the lower bound HRR curve could be explained by the fact that the radiation from the flame to the ceiling is damped by the smoke layer, so that the inaccuracy of modelling the flame geometry and flame emission has a smaller effect on the heat flux.

The difficulty of modelling the near field of the fire on one hand, and the relatively good agreement of the results away from the fire is consistent with the trend throughout the chapter and with previous work [9].

2.7 Conclusions

In the present work a detailed account of the *a posteriori* modelling of Dalmarnock Test One has been given. Available information was used together with possible HRR curves. Simulations were then compared against detailed measurements, and input parameters were adjusted in order to fit the results. It was shown that even with full access to the measured data it is not easy to satisfactorily reproduce the course of the fire. Although averaged quantities were in reasonable agreement with the measurements (<10% error for Set 1b and <50% for Set 2), matching of the simulations with the measurements at a detailed level provided larger errors (differences between 25% and 50% in the gas phase temperature and around 20% for wall temperatures and heat fluxes).

Comparison of the field temperatures in the experimental compartment suggested that far away from the fire FDS is capable of capturing the temperature vs. height distribution of the gas phase (provided an acceptable HRR has been input), while close to the fire important differences between simulations and measurements were detected, both quantitatively (35 to 50%) and qualitatively for both explored HRR inputs. Hot layer temperatures were consistently overpredicted when using an upper bound HRR

curve (25 to 40%), and underpredicted when using a lower bound HRR curve (less than 20%). However, it was observed that the cold layer temperatures were underpredicted by both upper and lower bound HRR inputs. The higher HRR input raised the hot layer temperatures without significantly increasing the cool layer temperatures, and thus predicting a more sharply defined hot layer than measured in Dalmarnock Test One.

Although it was possible to construct a range of suitable HRR curves that provided an upper and lower bound for field temperatures, secondary ignition could not be achieved robustly and the resulting incapability of predicting fire growth was shown to be a fundamental constraint to fire modelling.

References

[1] H. Emmons. The Further History of Fire Science. *Combustion Science and Technology*, 40(1):167–174, 1984.

[2] K. McGrattan. Fire Modelling: Where Are We? Where Are We Going? *Fire Safety Science*, 8:53–68, 2005. DOI:10.3801/IAFSS.FSS.8-53.

[3] T. Ma and J. Quintiere. Numerical simulation of axi-symmetric fire plumes: accuracy and limitations. *Fire Safety Journal*, 38(5):467–492, 2003.

[4] R. Hasib, R. Kumar, Shashi, and S. Kumar. Simulation of an Experimental Compartment Fire by CFD. *Building and Environment*, 42(9):3149–3160, 2007.

[5] B. Lattimer, S. Hunt, M. Wright, and U. Sorathia. Modeling fire growth in a combustible corner. *Fire Safety Journal*, 38(8):771–796, 2003.

[6] K. McGrattan, C. Bouldin, and G. Forney. Computer Simulation of the Fires in the World Trade Center Towers (Draft). Technical report, NIST, 2005.

[7] W. Grosshandler, N. Bryner, and D. Madrzykowski. Report of the Technichal Investigation of The Station Nightclub Fire. Technical report, NIST, 2005.

[8] N. Pope and C. Bailey. Quantitative Comparison of FDS and Parametric Fire Curves with Post-flashover Compartment Fire Test Data. *Fire Safety Journal*, 41(2):99–110, 2006.

[9] G. Rein, J.L. Torero, W. Jahn, J. Stern-Gottfried, N.L. Ryder, S. Desanghere, M. Lazaro, F. Mowrer, A. Coles, D. Joyeux, Alvear D., J. Capote, A. Jowsey, C. Abecassis-Empis, and P. Reszka. Round–Robin Study of *a priori* Modelling Predictions of the Dalmarnock Fire Test One. *Fire Safety Journal*, 44(4):590–602, 2009. DOI:10.1016/j.firesaf.2008.12.008, http://www.era.lib.ed.ac.uk/handle/1842/2704.

[10] J.W. Kwon, N. Dembsey, and C. Lautenberger. Evaluation of FDS v.4: Upward Flame Spread. *Fire Technology*, 43(4):255–284, 2007. DOI:10.1007/s10694-007-0020-x.

[11] P. Reneke, M. Peatross, W. Jones, C. Beyler, and R. Richards. A Comparison of CFAST Predictions to USCG Real-Scale Fire Tests. *Journal of Fire Protection Engineering*, 11:43–68, 2001. DOI:10.1106/HH4D-0CKM-J53X-FQK1.

[12] S. Miles, S. Kumar, and G. Cox. Comparisons of Blind Predictions of a CFD Model with Experimental Data. *Fire Safety Science*, 6:543–554, 2002. DOI:10.3801/IAFSS.FSS.6-543.

[13] S. Welch, A. Jowsey, S. Deeny, and J.L. Torero. BRE Large Compartment Fire Tests – Characterising Post-flashover Fires for Model Validation. *Fire Safety Journal*, 42(8):548–567, 2007.

[14] Rein, Abecassis-Empis, and Carvel, editors. *The Dalmarnock Fire Tests: Experiments and Modelling*. ISBN 978-0-9557497-0-4. The University of Edinburgh, Accesible at www.era.lib.ed.ac.uk/handle/1842/2037, 1st edition, 2007.

[15] C. Abecassis-Empis, P. Reszka, T. Steinhaus, A. Cowlard, H. Biteau, S. Welch, and G. Rein. Characterisation of Dalmarnock Fire Test One. *Experimental Thermal and Fluid Science*, 32(7):1334–1343, 2008. http://www.era.lib.ed.ac.uk/handle/1842/2513.

[16] T. Steinhaus and W. Jahn. Full-Scale Furniture Tests. Internal Publication BRE Centre for Fire Safety Engineering, 2007.

[17] D. Drysdale. *An Introduction to Fire Dynamics*. ISBN 0-471-97290-8. Wiley & Sons, New York, 2nd edition, 1998.

[18] K. McGrattan. Fire Dynamics Simulator (Version 4) – Technical Reference Guide. NISTIR 6783, 2003.

[19] K. McGrattan. Fire Dynamics Simulator (Version 4) – User's Manual. NISTIR 6784, 2003.

[20] J. Smagorinsky. General Circulation Experiments with the Primitive Equations. i. The Basic Experiment. *Monthly Weather Review*, 91(3):99–164, 1963.

[21] J. Dreisbach and K. McGrattan. Verification and Validation of Selected Fire Models for Nuclear Power Plant Applications, Volume 6: FDS. Technical report, U.S. Nuclear Regulatory Commission, Office of Nuclear Regulatory Research, 2006.

[22] K. McGrattan, R. Rehm, and H. Baum. Large Eddy Simulations of Smoke Movement. *Fire Safety Journal*, 30(2):161–178, 1998.

[23] S. Pope. 10 Questions Concerning the Large-Eddy Simulation of Turbulent Flows. *New Journal of Physics*, 6(35), 2004.

[24] K. McGrattan, S. Hostikka, J. Floyd, H. Baum, and R. Rehm. Fire Dynamics Simulator (Version 5) – Technical Reference Guide. NIST Special Publication 1018–5, 2008.

[25] W. Jahn, G. Rein, and J.L. Torero. The Effect of Model Parameters on the Simulation of Fire Dynamics. *Fire Safety Science*, 9:1341–1352, 2008. DOI:10.3801/IAFSS.FSS.9-1341, http://www.era.lib.ed.ac.uk/handle/1842/2696.

3

The effect of model parameters on the simulation of fire dynamics

3.1 Introduction

The central aspect of fire protection engineering is to understand the dynamics of compartment fires in order to design built environments where the likelihood of a fire event is minimized and the protection of its people, content and structure from fire damage is maximized. Fire safety aims at constantly improving and developing new response systems for these emergencies. A possibility currently being explored in new emergency response systems is to combine live sensor monitoring and forecast of fire development [1]. It is envisioned that the forecasting of fire dynamics in enclosures will imply a paradigm shift in the response to emergencies, providing the fire service with essential information about the fire ahead of time [1, 2].

There is an inherent difficulty in predicting fire behaviour since it involves complex dynamics driven by critical events, such as the ignition of secondary items, flashover, window breakage, sprinkler activation, etc. Moreover, fires involve mechanisms that develop in length scales ranging from millimetres to metres, and time scales from

milliseconds to minutes. Coupled computational simulations of these phenomena (i.e. CFD) demand extensive computational times that are far greater than the time associated with the phenomena themselves. Thus, a forecasting emergency response technology is currently non-existent because, putting aside the level of accuracy attained, the best available fire simulations predict with a negative lead time, i.e. the fire evolves at a much faster rate than forecasts can be produced. If comprehensive computational models are to be used to estimate, forecast and understand fire growth in support of emergency response, a simple, robust and effective approach is required.

The most promising technology for fire forecasts involves the constant update from live-recorded data to assist the simulations. If available in real time, sensor data could in principle be used to train and correct the simulation output. One of the current main limitations for this technology is in the large number of parameters that are required in fire models. Many of these parameters are scenario dependent, poorly defined or unphysical and the majority is associated to large uncertainties. Thus, for the concept of fire forecast to work and in order to be able to actually predict fire dynamics ahead of time, it is essential to identify the parameters to which fire modelling is most sensitive, so that these become the centre of attention of the forecast process.

3.2 Large-Scale Tests and Simulations

Only a few real-scale fire tests in enclosures have been conducted and very few of them had the required level of instrumentation for field model comparison; the BRE large compartment test series [3], NIST's experiments for the World Trade Center (WTC) [4] and The Dalmarnock Fire Tests [5] to name the most important. All these have been the objective of fire modelling. The BRE test series were modelled by Pope et al. [6] with FDS and a reasonable agreement was reached within the context of structural fire safety, although their post flashover simulations underpredicted the measured temperatures. The NIST experiments of fire growth were primarily conducted to validate their WTC simulations with FDS [7]. The Dalmarnock Tests, the most recent, have been modelled *a priori* [8] and *a posteriori* [9] and are the focus of the simulations in this chapter.

The Dalmarnock Fire Tests involved two flats in a 23-storey reinforced concrete tower in Glasgow (UK) and were conducted in July 2006. Test One was held in a

two-bedroom single family flat, with the living room set up as the main experimental compartment as shown in Fig. 3.1. Extensive information on the layout, experimental setup and outcome of the Dalmarnock fire tests can be found elsewhere [5, 10], but an overview is included here for quick reference.

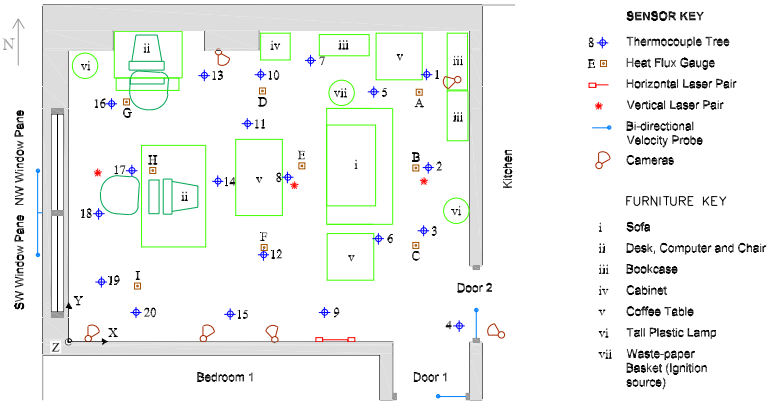

Figure 3.1: Layout and sensor distribution of the flat used in the Dalmarnock Fire Tests.

The main experimental compartment was the living room 2.45 m high, 3.50 m by 4.75 m in area, with a window and connected to another room and the hallway. It was furnished as a mixed regular living room/office. The general layout was such that most of the fuel was concentrated towards the back wall of the compartment, away from the window, with a fairly even fuel loading throughout the rest of the room.

A large number of sensors were installed throughout the flat in order to monitor in detail the fire development [5, 10]. Dalmarnock is the only fire test to date with an instrumentation density high enough to provide measurements with spatial resolution suitable for comparison with field models. More than 270 thermocouples were distributed in the main compartment to measure gas temperatures. 20 video cameras produced visual recordings which allowed monitoring of the fire development. Other measurements include light extinction, gas velocities at the opening, smoke detectors, temperature and heat fluxes on the walls and monitoring of the structural response of the building.

The fire in the Dalmarnock Test One was initiated at the sofa near the corner away from the window of the fire compartment (see Fig. 3.1). The sofa fire grew and after 275 s ignited the plastic boxes on a bookshelf standing about 1 m away. Once the bookshelf caught fire and flames spread vertically, the smoke layer descended rapidly to the ground and flashover took place at 300 s. At 800 s the compartment window was

purposely broken from outside and led to a change in the ventilation conditions. Finally, 1140 s into the fire, the fire brigade intervened and extinguished it.

Two sets of CFD simulations have been carried out regarding the Dalmarnock Fire Tests. Before the tests actually took place, a round robin-study was conducted with the objective of assessing the capability of blind predictions of real fire scenarios [11]. The output from the simulations of the participating teams scattered over a wide range of values and no consistency between simulations and the measurements was established beyond mere qualitative trends. The results showed that blind *a priori* simulations of complex scenarios are not accurate and thus that fire forecasts using these tools alone are not reliable. *A posteriori* simulations using FDS version 4 aided by the experimental measurements were carried out after the tests [9]. These show that even when full access to measurements is given, it is remarkably difficult to reproduce the spatial patterns and the different stages of fire development to a satisfactory level of accuracy.

In this work, further *a posteriori* simulations using FDS version 4 have been carried out using the experimental measurements. The objective is to find a set of model parameters that allow good reproduction of the pre-flashover fire. In the process of attaining accurate results, it is possible to identify the variables to which the output is sensitive and those parameters that have a minor effect in the result. This sets a framework for the development of simpler models that could potentially achieve positive lead times within the required levels of precision.

3.3 Fire Dynamics Forecast and Model Parameters

Fire dynamics are fundamentally different during the pre- and post-flashover phases of a fire. The dynamics of each phase is thus associated to different modelling parameters. This difference suggests splitting the problem in two parts.

3.3.1 Pre-flashover Fire

During the pre-flashover period the fire is growing and localized, i.e. only a few items within the compartment are burning and the production of pyrolyzates is the limiting step [12]. Fire growth is generally driven by flame spread over the initially burning

item or secondary ignitions of surrounding objects. Eventually, if sufficient objects are burning, flashover could take place. From the point of view of fire forecast, knowing the flame spread and which of the items in the room will ignite next, and the time of this ignition allows predicting the time to flashover. Secondary ignition is controlled by the heating of material surfaces by the flame and the hot layer. Thus, if the location of the fire and the rate of heat release could be estimated based on sensor data (e.g. from thermocouples and heat flux gauges on the walls and ceiling of the compartment) then once the flame location and height is known, the heat fluxes to surrounding surfaces and their temperature evolution could be calculated. This would allow prediction of the time to ignition of different items. This work studies the sensitivity of simulated surface temperatures and incident heat fluxes during the growing fire phase to different parameters.

3.3.2 Post-flashover Fire

Once flashover has occurred the fire is no longer localized, and combustible gases fill the entire compartment. They will burn when they find the right conditions of oxygen concentration and temperature.

Post-flashover fires are ventilation controlled, and thus from the point of view of fire forecast, knowing the ventilation conditions is essential for accurate predictions. One of the most challenging parts is that the fire could lead to window breakage that could modify substantially the fire behavior but are difficult to predict with current tools. The effect of fire parameters during post-flashover stage are beyond the scope of this work and will be subject of future studies.

3.3.3 Model Parameter

The most important input variable to fire simulations is the evolution of heat release rate (HRR) with time [13, 14]. However, in real fires the HRR is seldom available and can only be estimated at best. Only experiments conducted under controlled laboratory conditions provide measurements of HRR evolution. Current fire modelling tools provide good predictions of the thermal effects of a fire (e.g. the resulting thermal environment) but the predictions of the fire development are poor (e.g. flame spread and

fire growth). The proper prediction of the HRR evolution is therefore among the first priorities of a fire modeller studying real fire development. The effect of the modelling parameters to predict the HRR evolution is studied here.

In general terms, there are three different types of parameters that can be varied in a CFD simulation. The first type consists of parameters related to the boundary conditions, such as geometry, openings and the location of solid items. These parameters are the basis of any simulation and in principle are determined by the fire scenario that is to be modelled. Thus their uncertainty is related directly to the confidence in the known details from the scenario geometry. The second type consists of the parameters related to physical properties of the fuel packages and other solid surfaces such as thermal inertia, ignition temperature, heat of combustion, surface emissivity, etc. In theory, these parameters can be experimentally measured or determined via empirical correlations, but in practical terms the associated uncertainty can be very large creating a wide range of possible values. Mathematical and computational parameters comprise the third type of parameters and generally depend on the model being used. In the case of LES, the grid size, the Smagorinsky constant and others belong to this group of parameters [15]. These parameters are related to mathematical approximations and the solution method of the particular model. Nevertheless, variation of those parameters affects the outcome of the computations. In principle, their values should be determined based on computational and mathematical criteria alone and calibration. These parameters have been the focus of many studies, e.g. Wen [16].

This paper focuses mainly on the effect of the second type of modelling parameters, the material properties, but the other types are also investigated.

3.4 Results of Sensitivity to Model Paramters

The results of simulating the Dalmarnock Fire Test One are presented in this section. Simulated gas phase temperatures are compared to the measurements from ignition to 250 s (before flashover), and surface temperatures on the bookshelf next to the sofa obtained from simulations for different parameter values are presented.

3.4.1 Ignition Source

A typical love-seat sofa acted as an ignition source for the Dalmarnock Fire Test. It was ignited using a waste paper basket standing adjacent to it. A cotton blanket was placed over the armrest of the sofa with one part hanging inside the basket. Over both the basket and blanket, 300 ml of heptane were poured to ensure ignition.

Prior to the large-scale test, a sofa replica was burned under laboratory conditions in a furniture calorimeter [17]. Figure 3.2a shows the HRR measured during the laboratory test. This test provides an estimation of the initial fire evolution in the Dalmarnock Test and the measured HRR is used as a first step towards the characterization of the ignition source. The main difference between the laboratory test and the actual Dalmarnock fire was that in the laboratory the heptane soaked blanket was not included. The HRR resulting from the burning blanket and the heptane was modelled following a fast t-squared behaviour (see Fig. 3.2a) and then added to the experimental HRR. In addition to the fast fire assumption, the total energy released by the blanket is forced to match the energetic value according to Eq. (3.1):

$$\int \mathrm{HRR}_{blk}\,\mathrm{d}t = m_{blk}\Delta h_{c,blk} + m_{hep}\Delta h_{c,hep}, \tag{3.1}$$

where m_{blk} is the initial mass of the blanket (estimated at 1.2 kg), $h_{c,blk}$ its heat of combustion of cotton (16.5 MJ/kg [18]), m_{hep} is the mass of the heptane added to the blanket (0.07 kg for the estimated 100 ml poured over the blanket [5]) and $h_{c,hep}$ is the heat of combustion of heptane (44.5 MJ/kg [19]). A decay function of the form $(t - t_0)^2$ was introduced to complete the consumption of the blanket mass, where t_0 is the burnout time and set to 400 s. The resulting fast t-squared fire for the blanket alone can be seen in Fig. 3.2a.

Camera footage of the Dalmarnock Test can be used to estimate the peak value of the HRR and support these approximations. The Dalmarnock fire spread quickly to the blanket and flames of about 1 m in length were observed at the location of the blanket. Using Heskestad's correlation, the HRR of a fire can be calculated from its size [20] as,

$$\dot{Q} = \left(\frac{L + 1.02D^*}{0.23}\right)^{5/2} \tag{3.2}$$

where $\dot{Q}$ is the HRR, L the flame length and D^* the equivalent fire diameter. The blanket occupied an area with an equivalent diameter of 0.6 m. The HRR of a fire of this diameter corresponding to the observed 1 m high flames is of the order of 150 kW, in accordance with the peak HRR resulting from the fast t-squared assumed here.

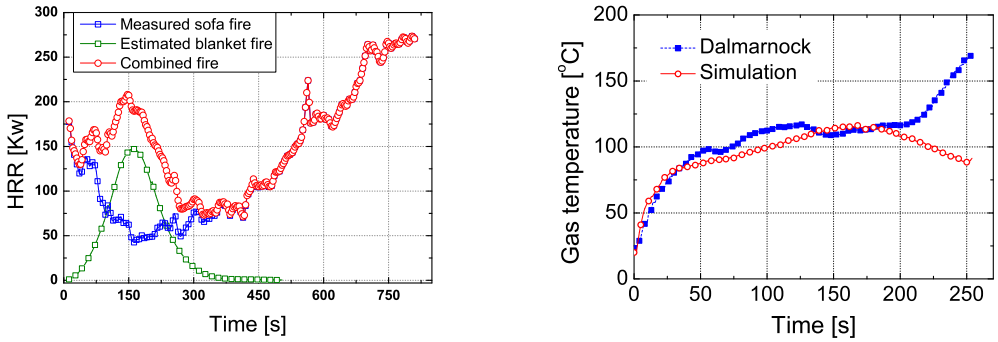

Figure 3.2: a) Laboratory measured HRR of the basket and sofa fire, next to the approximated calculation for the blanket fire. b) Upper layer temperature during the growing phase (with blanket) comparing simulations and Dalmarnock measurements [5].

Using the combined measured and blanket HRR and applying it over the sofa area, the predicted average temperature of the upper layer in the room is in reasonable agreement with the measurement. A comparison between the simulated and measured gas temperatures is presented in Fig. 3.2b. The agreement lasts up to 200 s, then the simulated temperature decreases due to the predicted burnout of the basket and blanket fires and raises rapidly at 250 s when the bookshelf ignition and subsequent flashover is predicted (the rise is not shown in the figures). This dip was not observed in the Dalmarnock experiment itself. Thermocouples located between the basket and the bookshelf next to the sofa at a height of 0.5 m show considerably higher temperatures (approx. 200^{o}C higher) than those obtained in the simulations. This suggests that some fuel in the area was burning at that time, but there is no evidence to support this, since the area was not covered by CCTV cameras.

3.4.2 Fire location, fire area and heat of combustion

The total HRR is an important variable but the fire location and flame size and shape are as well important to predict the ignition of secondary objects and the growth phase. The diameter and height of the flame have a direct influence on the radiative heat fluxes

to surrounding objects and on the air entrainment and thus on the convective heating of objects in the upper layer. For a given HRR, the pyrolyzate production rate per unit area affects the flame height by directly changing the buoyant strength of a fire and thus affecting air entrainment, burning rate and heating [12]. The HRR $\dot{Q}$ can be expressed as,

$$\dot{Q} = \Delta h_c \cdot A \cdot m''_f, \tag{3.3}$$

where Δh_c is the heat of combustion of the fuel, A is the fire area, and m''_f is the pyrolyzate mass flow per unit area. For a fixed HRR, the mass flow increases either due to a decrease in the area or due to a decrease in the heat of combustion.

As seen in visual recordings during the growth phase of the Dalmarnock fire, the flames were not distributed over the entire sofa, but stayed predominantly in one third of the sofa near to the basket. Decreasing the fire diameter, but maintaining the imposed HRR, will then give rise to prediction of a higher flame according to Eq. (3.2). This increase in the flame height and the concentration of released heat on a smaller area changes the relationship between flame and surfaces from an optical point of view. Figure 3.3 shows the effect of changing the fire area (while keeping the HRR the same) on the upper layer temperature and the surface temperature of the nearby bookshelf. It is seen that the effect of the fire area is important on the surface temperature of the surrounding objects (Fig. 3.3b) while the effect is minor for the average temperature of the upper layer (Fig. 3.3a).

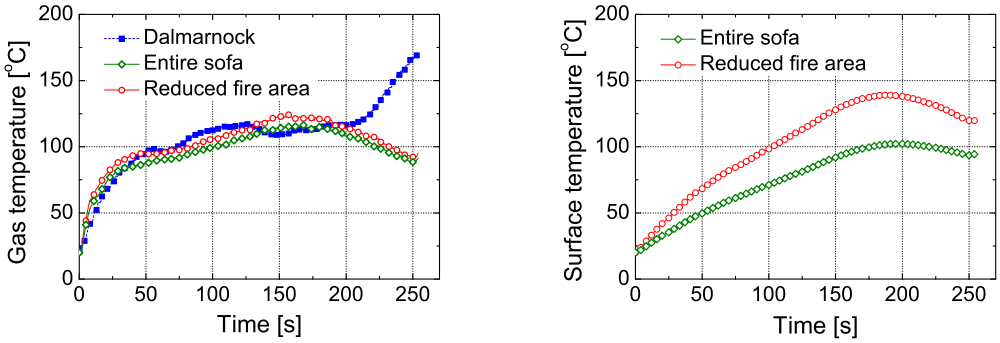

Figure 3.3: Effect in the predictions of changing the fire area while keeping the HRR the same. a) average upper layer temperature with comparison to Dalmarnock measurements [5] b) bookshelf surface temperature of the bottom part of the bookshelf.

Given the importance of locating the origin of the HRR, the effect of separating the

HRR measured in the laboratory between the basket and sofa portions and applying them in their respective locations was investigated. The decay from initial conditions to the growth inflection at 150 s seen in Fig. 3.2a is attributed to the burn-out of the basket. If this HRR is deducted from the measurement what is left fits well to a t-squared fire of slow growth. This is attributed to the burning of the sofa alone. The basket HRR can be separated from the measurement and be distributed over a small area on the right side of the sofa representing the basket location. The blanket fire is added to the sofa fire and both are applied over an area of 1/3 of the sofa's total horizontal surface. Figure 3.4 shows the effect of separating the HRR between the basket and the sofa on the upper layer temperature and the surface temperature of the nearby bookshelf. The separation of the two fires provides temperature predictions in the upper layer 20°C higher during the first 30 s, which is not a significant change. However, the difference is 40°C higher in the surface temperatures of the bookshelf which is important for the predictions of the ignition time of the bookshelf material. The significant effect of separating the basket fire is due to the small area of the basket and the relatively high HRR peak contributing to produce flames up to 1.3 m and so changing the geometry of the flame.

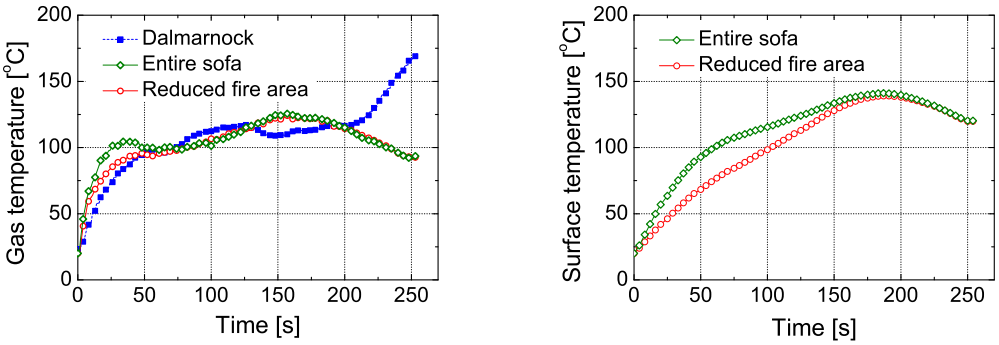

Figure 3.4: Effect of separating the total HRR into the basket and the sofa fires: a) temperature of the upper layer and comparison to Dalmarnock measurements [5] and b) surface temperature of the bookshelf.

Another parameter that affects the flame height and the fire environment is the heat of combustion of the fuel, Δh_c, used in the simulation. Decreasing the heat of combustion while keeping the HRR and the fire area fixed, results in an increase of the pyrolyzate mass flow per unit area (and vice versa), as expressed in Eq. (3.3). However, the Froude number, and thus the buoyant strength of the fire, is only affected weakly

Table 3.1: Predicted flame heights on the sofa for different fires while keeping the HRR constant. Comparison with the observed values in the Dalmarnock Test One.

Simulations	**60 s**	**150 s**	**250 s**
	flame height (m)	flame height (m)	flame height (m)
Fire over entire sofa area	0.4	0.6	0.4
Fire over 1/3 sofa area	0.9	1.1	0.7
Fire over 1/3 sofa area and separated basket	0.8	1.1	0.6
Fire over 1/3 sofa area and lower h_c	1.3	1.3	0.8
Observed in Dalmarnock	~ 1	~ 0.8	~ 0.8

by the heat of combustion and thus a small effect is expected. The effect of changing this and also the fire area has been explored and the results are presented in Table 3.1 which shows the predicted flame heights for different sofa fire scenarios keeping the HRR fixed. The effect of changing the heat of combustion by more than 100% increases the predicted flame height by approx. 20-30%. Simulation with the lower heat of combustion shows that the change in the heat of combustion does not translate into a significant change in the time to ignition of the bookshelf.

3.4.3 Thermal and ignition material properties

The objects receiving incident heat flux from the fire will heat up according to their material properties [21]. In the Dalmarnock experiments, the bottom shelf of the bookshelf next to the sofa contained plastic boxes. Due to the small thickness of their walls the boxes can be considered as thermally thin, and therefore the parameter of interest for ignition predictions is the product of the thickness (δ), density (ρ) and specific heat (c) [22]. The rate of change in the temperature of the object is proportional to the incident heat flux [22]:

$$\rho \delta c \frac{\mathrm{d}T}{\mathrm{d}t} = \dot{q}''_{net} \tag{3.4}$$

where the net heat flux is the difference between the incident heat flux and the re-radiation:

$$\dot{q}''_{net} = \alpha \dot{q}''_{in} - \sigma \varepsilon T_w^4. \tag{3.5}$$

Equation 4 can be integrated over time yielding the expression for the surface temperature as a function of time. The larger the thermal inertia $\rho\delta c$ is, the longer it takes for the surface to respond to the heating, and the peak temperature is not as high as it is for lower thermal inertias.

Figure 3.5 shows the surface temperature for different thermal inertia ($\rho\delta c$). It shows that varying this parameter by 50% (from 1 to 0.5 kJ/m^{2}K) can produce important differences in the temperature of the surface (up to 40%). Since the material properties of nearby objects or fuel packages are normally not known accurately, the sensitivity to this parameter is very important.

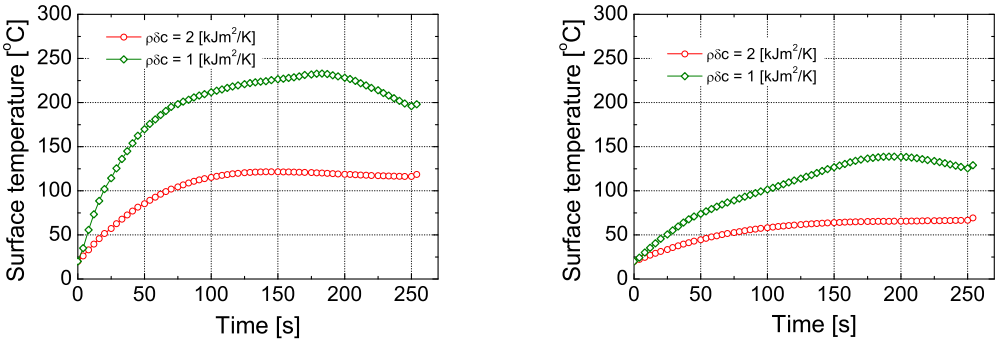

Figure 3.5: Effect of surface $\rho\delta c$ on the predicted bookshelf temperature at different heights a) 0.1 m above floor b) 1.5 m above floor.

Under Kirchhoff's law [22], the emissivity of a surface represents the fraction of the total radiative power that the surface emits and absorbs. For relatively cold surfaces heated by a nearby fire, the absorption component dominates. Thus, this parameter has a double effect on the surface temperature, by establishing the fraction of incident radiation absorbed and the fraction re-radiated back into the gas phase.

A comparison of surface temperature for different emissivities is presented in Fig. 3.6. Near the flame, at 0.5 m above the floor, the variation of the emissivity from 0.4 to 1 changes the surface temperature by more than 60% during the entire growth phase.

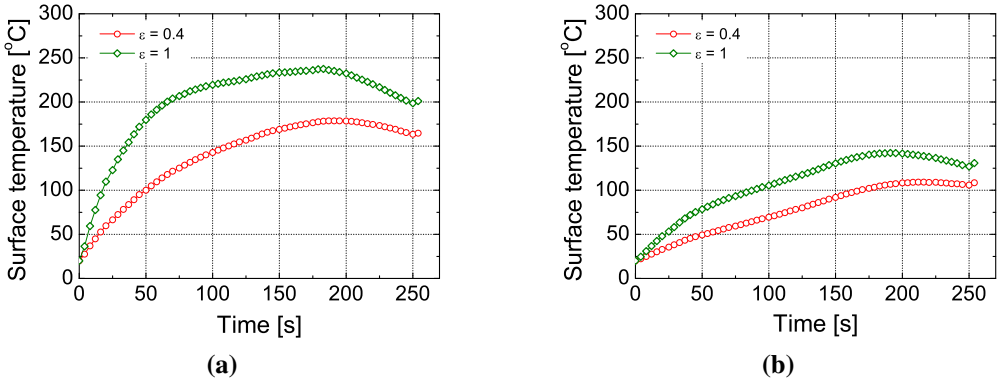

Figure 3.6: Effect of the surface emissivity parameter on the predictions of the bookshelf temperature at different heights: a) 0.1 m above floor b) 1.5 m above floor.

3.4.4 Flame radiative fraction

In LES calculations the local temperatures are averaged over the entire volume element, which could produce an important underprediction of the flame temperature when the elements are not small enough [15]. To avoid the subsequent strong underprediction of heat losses by radiation, in FDS (and other CFD codes) the flame radiation is calculated as a fixed fraction of the HRR. Although values around 35% are generally accepted to be the radiative fraction, this is an empirical finding and significant deviations from this value are abundant. Figure 3.7 shows the impact that a variation of this parameter has on the surface temperature of the bookshelf. As the radiative fraction is decreased from 0.35 to 0.0, the predicted peak temperature decreases from 225 to 150°C. When the radiative fraction is increased from 0.35 to 0.7, the predicted peak temperature increases from 225 to 330°C. Although the range considered for variation of this parameter (0.0 to 0.7) is somewhat extreme and includes all physically possible values, these results imply that the parameter has a significant effect for the prediction of the time to ignition.

3.4.5 Heating from the smoke layer

Radiation and convection from the smoke in the upper layers of the compartment heat up the objects in the room. Convective heating is largely restricted to the upper layers but radiation can heat up objects at lower layers. The heat feedback from the smoke layer might not be negligible and is investigated here in the context of the Dalmarnock fire.

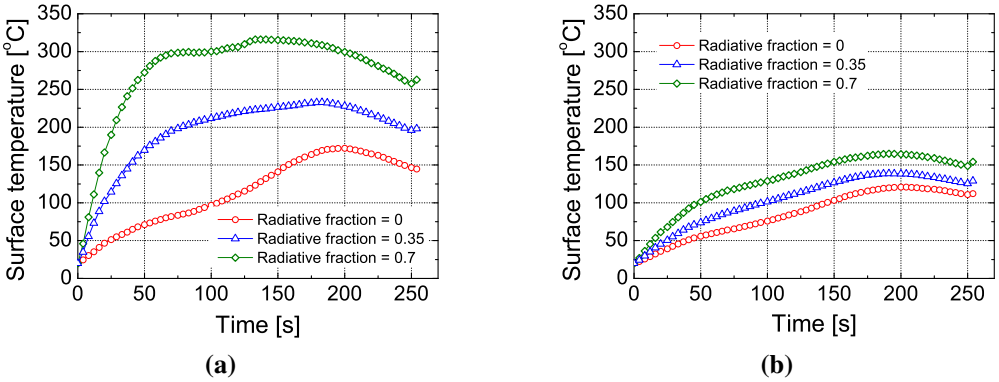

Figure 3.7: Effect of the radiative fraction parameter in the predicted temperature evolution of the bookshelf at different heights. a) 0.1 m above floor b) 1.5 m above floor.

In order to study the effect of the smoke layer on the heating of surrounding objects, a simulation was conducted where the smoke easily escapes the compartment through a hole on the ceiling. This is not a realistic scenario but allows studying the case where all the smoke is removed. The predicted surface temperature is compared to the case where smoke accumulates. Figure 3.8 shows the surface temperature of the bookshelf at 0.5 and 1.5 m above the floor with smoke layer and without smoke layer. At 0.5 m, i.e. the height of the basket, there is no perceivable difference between the two cases, whereas at 1.5 m above floor the temperatures differ approximately 10%. Since the bookshelf is tall and its upper parts are in direct contact with the hot smoke at 1.5 m, part of that difference can be attributed to convective heating from the smoke. It can be concluded that radiative heat feedback from the smoke layer during growth is not important in the Dalmarnock scenario for the ignition of objects outside the smoke layer, but that the convective part accounts for a significant increase in temperature of objects within the smoke layer.

Considering that in FDS the radiation from the flame is modelled as a fraction of the HRR and thus it is decoupled from the radiative properties of the flame, it seems natural that soot production would not affect considerably the predicted incident heat flux. Figure 3.9 confirms this by showing that surface temperatures on the bookshelf do not vary by more than 7% while varying the soot yield produced in the combustion reaction in a range between 0.1 and 0.3.

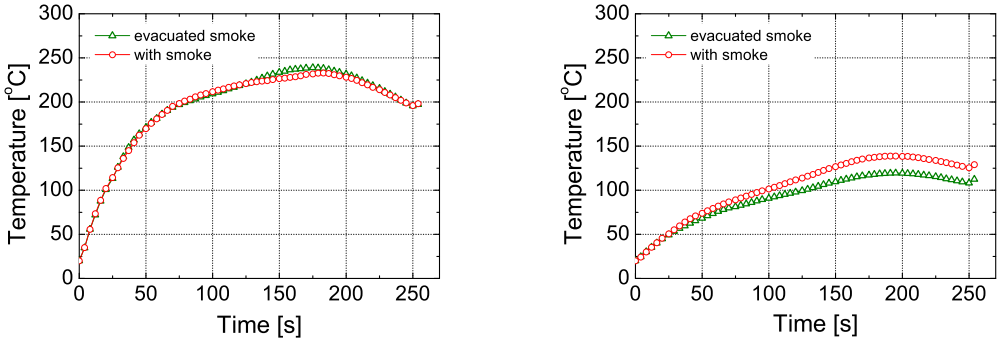

Figure 3.8: Effect of the smoke layer built-up in the predicted temperature evolution of the bookshelf. a) 0.1 m above floor b) 1.5 m above floor.

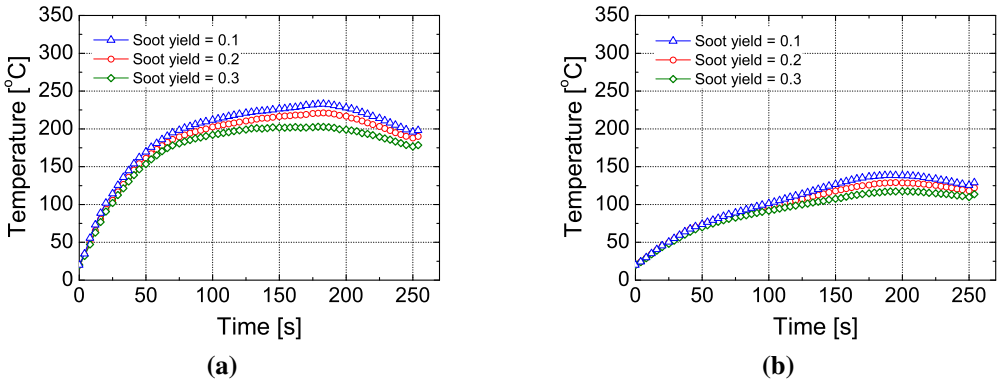

Figure 3.9: Effect of the soot yield parameter in the predicted temperature evolution of the bookshelf. a) 0.1 m above floor b) 1.5 m above floor.

3.5 Conclusions

It is widely accepted that the HRR is an essential variable in fire simulations. However, its value and evolution are rarely known beforehand in accidental fires. Then, the HRR must be estimated using fire dynamics, the lay-out of the scenario and material properties. When these parameters are studied, other parameters become also important in predicting fire dynamics. During the growth phase, the time to ignition of secondary items is important for predictions of fire spread and time to flashover. Radiation from the flame is to be one of the most important mechanisms for the ignition of nearby objects. The location and area where the heat is released, and the height of the flame, are important for flame radiation calculations. A smaller fire area and a higher pyrolyzate production rate for the same HRR will produce longer flames.

The associated sensitivities of the upper layer temperature and surface temperature

predictions have been quantified for the scenario of the large-scale Dalmarnock Test One. The results show that the global HRR in the compartment is a good input to predict the average temperatures in the compartment but produced poor prediction of the time to flashover. Simulations of the fire growth are significantly sensitive to the location of the HRR, fire area, material thermal properties, surface emissivity and flame radiative fraction, whereas the simulations are relatively insensitive to changes of the heat of combustion (while keeping the HRR constant), the soot yield and the heating from the smoke layer.

Since the material properties of nearby objects, surfaces and fuel packages are normally not known accurately, the sensitivity to this parameter is very important. Predictions of secondary ignition, fire spread and thus of time to flashover can depend strongly on the appropriate estimation of these material and fire parameters.

The development of fire forecasting methodologies in support of the emergency response must focus on the variables identified here as important. The live sensor data could be used to update and provide somehow best estimates of these parameters and to reduce the associated uncertainty. These parameters could then be used in the computational predictions. Since heat feedback from the smoke layer during fire growth is not significant for objects outside the smoke layer, the results here suggest that for predictions of secondary ignition and flashover, fire CFD modelling may not be justified in terms of accuracy, and other, simpler and computationally cheaper models could be used to accelerate computational fire forecasts.

References

[1] R. Upadhyay, G. Pringle, G. Beckett, S. Potter, S. Han, S. Welch, A. Usmani, and J.L. Torero. An Architecture for an Integrated Fire Emergency Response System for the Built Environment. *Fire Safety Science*, 9:427–438, 2008. DOI:10.3801/IAFSS.FSS.9-427, http://www.era.lib.ed.ac.uk/handle/1842/2703.

[2] A. Cowlard, W. Jahn, C. Abecassis-Empis, G. Rein, and J.L. Torero. Sensor Assisted Fire Fighting. *Fire Technology*, in press, 2008. DOI:10.1007/s10694-008-0069-1.

[3] S. Welch, A. Jowsey, S. Deeny, and J.L. Torero. BRE Large Compartment Fire Tests – Characterising Post-flashover Fires for Model Validation. *Fire Safety Journal*, 42(8):548–567, 2007.

[4] A. Hamins, A. Maranghides, K. McGrattan, E. Johnsson, T. Ohlemiller, M. Donelly, and J. Yang. Experiments and Modeling of Structural Steel Elements Exposed to Fire. Technical report, NIST, 2005.

[5] C. Abecassis-Empis, P. Reszka, T. Steinhaus, A. Cowlard, H. Biteau, S. Welch, and G. Rein. Characterisation of Dalmarnock Fire Test One. *Experimental Thermal and Fluid Science*, 32(7):1334–1343, 2008. http://www.era.lib.ed.ac.uk/handle/1842/2513.

[6] N. Pope and C. Bailey. Quantitative Comparison of FDS and Parametric Fire Curves with Post-flashover Compartment Fire Test Data. *Fire Safety Journal*, 41(2):99–110, 2006.

[7] K. McGrattan, C. Bouldin, and G. Forney. Computer Simulation of the Fires in the World Trade Center Towers (Draft). Technical report, NIST, 2005.

[8] G. Rein, J.L. Torero, W. Jahn, J. Stern-Gottfried, N.L. Ryder, S. Desanghere, M. Lazaro, F. Mowrer, A. Coles, D. Joyeux, Alvear D., J. Capote, A. Jowsey, C. Abecassis-Empis, and P. Reszka. Round–Robin Study of *a priori* Modelling Predictions of the Dalmarnock Fire Test One. *Fire Safety Journal*, 44(4):590–602, 2009. DOI:10.1016/j.firesaf.2008.12.008, http://www.era.lib.ed.ac.uk/handle/1842/2704.

[9] W. Jahn, G. Rein, and J. Torero. The Dalmarnock Fire Tests: Experiments and Modelling. In Cecilia Abecassis Empis Guillermo Rein and Richard Carvel, editors, *The Dalmarnock Fire Tests: Experiments and Modelling*, chapter 11. The University of Edinburgh, Edinburgh, 2007. http://www.era.lib.ed.ac.uk/handle/1842/2404.

[10] P. Reszka, C. Abecassis-Empis, H. Biteau, A. Cowlard, T. Steinhaus, I. Fletcher, and A. Fuentes. The Dalmarnock Fire Tests: Experiments and Modelling. In Cecilia Abecassis Empis Guillermo Rein and Richard

Carvel, editors, *The Dalmarnock Fire Tests: Experiments and Modelling*, chapter 2, pages 31–61. The University of Edinburgh, Edinburgh, 2007. http://www.era.lib.ed.ac.uk/handle/1842/2412.

[11] G. Rein, J.L. Torero, W. Jahn, J. Stern-Gottfried, N.L. Ryder, S. Desanghere, M. Lazaro, F. Mowrer, A. Coles, D. Joyeux, Alvear D., J. Capote, A. Jowsey, C. Abecassis-Empis, and P. Reszka. The Dalmarnock Fire Tests: Experiments and Modelling. In Cecilia Abecassis Empis Guillermo Rein and Richard Carvel, editors, *The Dalmarnock Fire Tests: Experiments and Modelling*, chapter 10. The University of Edinburgh, Edinburgh, 2007. http://www.era.lib.ed.ac.uk/handle/1842/2405.

[12] D. Drysdale. *An Introduction to Fire Dynamics*. ISBN 0-471-97290-8. Wiley & Sons, New York, 2nd edition, 1998.

[13] V. Babrauskas and R. Peacock. Heat Release Rate: The Single Most Important Variable in Fire Hazard. *Fire Safety Journal*, 18(3):255–272, 1992.

[14] G. Cox and S. Kumar. Modelling Enclosure Fires using CFD. In P. DiNenno, editor, *SFPE Handbook of Fire Protection Engineering*, chapter 3–8, pages 3–194–3–218. National Fire Protection Association, Quincy, MA 02269, 3 edition, 2002.

[15] K. McGrattan. Fire Dynamics Simulator (Version 4) – Technical Reference Guide. NISTIR 6783, 2003.

[16] J. Wen, K. Kang, T. Donchev, and J. Karwatzki. Validation of FDS for the prediction of medium-scale pool fires. *Fire Safety Journal*, 42(2):127–138, 2007.

[17] T. Steinhaus and W. Jahn. The Dalmarnock Fire Tests: Experiments and Modelling. In Cecilia Abecassis Empis Guillermo Rein and Richard Carvel, editors, *The Dalmarnock Fire Tests: Experiments and Modelling*, chapter 6, pages 111–135. The University of Edinburgh, Edinburgh, 2007. http://www.era.lib.ed.ac.uk/handle/1842/2415.

[18] P. DiNenno, editor. *APPENDIX C*. National Fire Protection Association, Quincy, MA 02269, 3rd edition, 2002.

[19] P. DiNenno, editor. *SFPE Handbook of Fire Protection Engineering–Appendix B*. National Fire Protection Association, Quincy, MA 02269, 3rd edition, 2002.

[20] G. Heskestad. Fire Plumes, Flame Height, and Air Entrainment. In P. DiNenno, editor, *SFPE Handbook of Fire Protection Engineering*, chapter 2–1, pages 2–1–2–17. National Fire Protection Association, Quincy, MA 02269, 3 edition, 2002.

[21] C. Lautenberger, J.L. Torero, and C. Fernandez-Pello. Understanding Materials Flammability. In V. Apte, editor, *Flammability Testing of Materials Used in Construction, Transport and Mining*, pages 1–21. Woodhead Publishing, Cambridge, UK, 2006.

[22] F. Incropera and D. DeWitt. *Fundamentals of Heat and Mass Transfer*. Wiley & Sons, New York, 4th edition, 1996.

4

Forecasting Fire Growth using an Inverse Zone Modelling Approach

4.1 Introduction

The human attraction for the prediction of future events permeates deep into science and technology, where some disciplines have emerged to provide the scientific knowledge capable of forecasting the dynamics of non-trivial systems. Astronomical objects, tides and weather are the most common examples.

It is envisioned that the forecasting of fire dynamics in enclosures will lead to a paradigm shift in the response to fire emergencies in buildings, providing the fire service with essential information about the development of the fire with some lead time (i.e. seconds, minutes or hours ahead of the event) [1]. This technology is currently non-existent because available fire simulation tools cannot predict fire growth in a fast, precise and robust manner.

There is an inherent difficulty in predicting fire behaviour, since it involves complex dynamics driven by critical events such as window breakage, flashover, sprinkler activation, etc., and feedback interactions. Even flame spread over a single burning

item involves closely coupled physical processes both in the gas phase and in the solid phase. Although a recent attempt of modelling flame spread from first principles has shown good agreement with experimental observations [2], this can only consider scenarios of very limited size (flame length in the order of 10 cm) due to the very extensive computational time it requires. Natural fires in real-size enclosures involve mechanisms that develop in length-scales ranging from micrometres (flame thickness) to metres (compartment size), and time-scales from milliseconds (chemistry) to minutes (burnout) [3]. Thus, coupled computational simulations from first principles of fire growth would demand extensive computational times far greater than the time associated with the phenomenon itself.

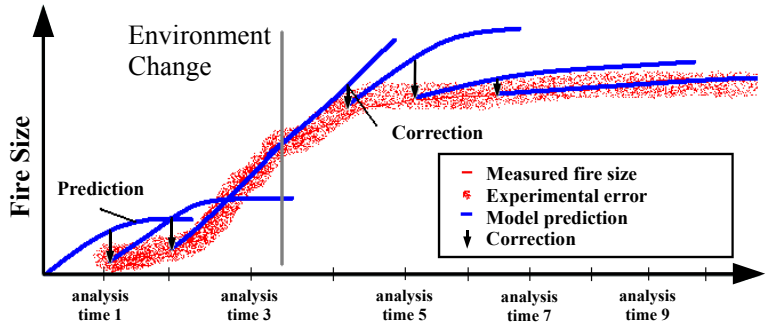

Figure 4.1: Conceptual representation of the data assimilation process and the sensor steering of model predictions even when fundamental changes take place in an evolving emergency scenario.

If comprehensive computational models are ever to be used to forecast fire growth in support of the emergency response, a more simple, robust and effective approach is required. This will result in more approximations and thus in a loss of detailed information about the underlying physical processes. It is thus proposed to incorporate sensor data into the model in order to recover the information lost by the approximations [1]. This is a concept widely used in weather forecasting under the label of data assimilation. The concept of data assimilation basically consists of using computer models of some complexity that are steered by updated sensor observations of the ongoing event as it develops.

The system aims to provide useful predictions even when fundamental, unpredictable, changes take place in the evolving emergency. For example, if a window breaks during a building fire, the flame dynamics are significantly changed, and therefore the model should respond to this change by readjusting within some time its

predictions to the new conditions. This concept is demonstrated in Fig. 4.1, where sensor data is assimilated to steer the simulations of the flame dynamics.

An important step of data assimilation is to find fundamental parameters that govern the dynamics, and that do not change over a certain period of time (these are the invariants of the problem). If these invariants are estimated correctly, it should then be possible to predict fire behaviour until a critical event takes place, when the invariants change and estimations need to be re-adjusted.

Parameter estimation and inverse modelling is widely used in engineering applications, and various examples can be found in the fire science literature. Richards et al. [4] use a database of pre-run models to estimate fire location and fire growth. They use the same zone model to generate the data for comparison, and analyze the influence of measurements and modelling errors. Leblanc and Trouvé use a zone model to predict the heat release rate (HRR) time-history based on observations generated using the same model [5]. While they are able to closely reproduce the HRR past history, their work does not address how to produce a forecast of future events. Wang et al. [6] predicted the fire location using temperature data from several sensor arrays distributed in the fire room. Cowlard et al. used a simple flame spread correlation and assimilated temperature observations and flame front measurements to predict upward flame spread [7]. They were able to estimate input parameters for the empirical correlation and make super real time predictions of upward fire spread. Jahn et al. [8] propose a tangent linear approach to estimate fire growth parameters using a computational fluid dynamics (CFD) fire model. Koo et al. [9] used measurements from a fire test experiment to progressively steer fire simulations towards the effective value using a Monte Carlo approach with a set of parameters that was used for random generation of scenarios. While they were able to reproduce past observations of temperature, they could not link the parameters of the model to the physics of the full scale fire test, which limits the forecast of future events to statistical considerations.

In the present work the problem of estimating invariant parameters for the prediction of fire growth is investigated using data assimilation into a simple zone model. The estimated parameters are then input into the model to produce a forecast. In order to demonstrate the concept, a simple compartment fire is chosen and only the fire growth stage before flashover is investigated. The scenario includes a small fire that ignites

locally at a certain point (e.g., started by an electrical failure or arson) and flames spread radially. A CFD based fire model (Fire Dynamics Simulator version 5.1.6 [10]) is used to generate the observations of the true fire. A simple two-zone model is used to predict the fire based on comparison to the observed temperature and height of the hot layer. Optimization of the estimations uses a gradient-based method and the gradient of the cost function is computed using the tangent linear approach [8].

4.2 Fire Modelling

Fire dynamics in natural fires involves coupled solid phase processes (heating, pyrolysis and burning) and gas phase processes (turbulence, radiation and flame dynamics). Two main types of fire models can be identified, zone and CFD models. Zone models are based on the assumption that the fire compartment can be divided into two homogeneous layers, a hot upper layer and a cold lower layer. While the solution to a zone model is very fast, the accuracy of the results is limited by the simplifying assumptions where a large part of the underlying physics is treated in a simplified manner. Heat and mass transport within a layer is assumed to be much faster than the transport between layers, thus energy and species can be assumed to be homogeneously distributed. The fire and transport of energy and mass from the cold to the hot layer are defined by empirical correlations that are intended to reproduce in a simple manner the complex fluid mechanics involved.

CFD models consider and couple the important fundamental mechanisms. Their main drawback is that when applied to real-size compartments, the computational requirements outsize the available resources. However, both types of fire models are restricted by the need for a prescribed fire growth curve as input.

4.3 Modelling Approach

4.3.1 Two-Zone Model

The fire model used to produce forecasts is based on the two-zone model with floor leak proposed by Zukoski [11]. There are no vents in the compartment. A transient

mass balance is stated for the cold layer, assuming that its temperature does not change significantly,

$$\rho_a \frac{\mathrm{d}V_l}{\mathrm{d}t} + \dot{m}_e + \dot{m}_p = 0, \tag{4.1}$$

where t is time, ρ_a is the air density at ambient temperature, V_l is the volume of the cold layer (lower layer), $\dot{m}_e$ is the mass flow through the floor leak, and $\dot{m}_p$ is the mass flow of the fire plume.

The flow through the floor leak ($\dot{m}_e$) can be obtained from the energy balance of the whole compartment, and is expressed in terms of the mass flow of the fire plume and of the quotient between plume temperature (T_p) and ambient temperature (T_a):

$$\dot{m}_e = \dot{m}_p \frac{T_p - T_a}{T_a}. \tag{4.2}$$

Heskestad's correlation [12] for plume entrainment is used to estimate the mass flow of the fire plume,

$$\dot{m}_p = C \left(\frac{\rho_a^2 g}{c_p T_a} \right)^{1/3} \dot{Q}^{1/3} (H_0 - h(t))^{5/3}, \tag{4.3}$$

with the constant C, the entrainment coefficient, depending on the geometrical relationship between the room boundaries and the fire. $\dot{Q}$ is the HRR of the fire, g is gravity, c_p is the specific heat of air, T_a is ambient temperature, $h(t)$ is the height of the interface between the hot layer and the cold layer measured from the floor at time t, and H_0 is the height of the compartment.

The hot layer temperature was obtained by means of a mass balance of the hot layer (upper layer),

$$\rho_u \frac{\mathrm{d}V_u}{\mathrm{d}t} + V_u \frac{\mathrm{d}\rho_u}{\mathrm{d}t} = \dot{m}_p, \tag{4.4}$$

where ρ_u and V_u are the hot layer density and volume, respectively.

Substituting Eq. (4.1) in Eq. (4.4) and rearranging using the condition $V_l + V_u =$ constant and Eq. (4.2), an expression for the change of the hot layer density in time is obtained,

$$\frac{\mathrm{d}\rho_u}{\mathrm{d}t} = \frac{1}{V_u} \left(\dot{m}_p - \rho_u \frac{\dot{m}_p T_p}{\rho_a T_a} \right), \tag{4.5}$$

where T_p is the plume temperature, which is obtained assuming that all the released energy ($\dot{Q}$) is used to heat the plume. The initial state of the system, $\mathbf{y}_0$, is ambient

temperature in the entire compartment and a hot layer height equal to the height of the compartment.

By integrating Eqs. (4.1) and (4.5) together with (4.3), the temperature and height of the hot layer in time can be obtained for a given HRR curve in time. This is denoted by $\mathscr{M}_i(\mathbf{y}_0, \boldsymbol{\theta})$ which is the forward integration model at time t_i with parameters $\boldsymbol{\theta}$ and initial state $\mathbf{y}_0$.

4.3.2 Heat Release Rate

Although important advances have been made [2], the prediction of fire growth and flame spread are still research topics and the state of the art is not yet satisfactory.

A study published in 2007 investigated the capability of a fire field model (FDS [10]) to predict fire growth using a grid size comparable to grid sizes typically used in fire modelling applications, concluding that the predicted rate of fire growth is not reliable due to the crude approximations in the pyrolysis and combustion submodels [13].

In the present work, fire growth is modelled by decoupling the solid phase processes from the gas phase based on the assumption that the radius of the burning area of an isotropic fuel grows at a constant rate. This is a reasonable assumption for early fire development when flames do not penetrate into the hot layer and heat feedback from the flames will not accelerate flame spread [14]. The heat release rate (HRR) of a fire can be expressed as a function of the spread rate r and time t as follows:

$$\dot{Q} = \Delta h_c \dot{m} = \Delta h_c \dot{m}''_f r^2 \pi (t - t_0)^2, \tag{4.6}$$

where Δh_c is the heat of combustion of the fuel, $\dot{m}''_f$ is the mass flow of fuel per unit area, and t_0 is a time delay. It is common in fire engineering to define a fire growth parameter $\alpha = \Delta h_c \dot{m}''_f r^2 \pi$, in order to write the HRR as a quadratic function of time,

$$\dot{Q} = \alpha (t - t_0)^2. \tag{4.7}$$

This αt^2 dependency has been validated for many different fire scenarios. It can be shown that α is relatively insensitive to changes in Δh_c and $\dot{m}''_f$ compared to changes in r^2, and the range of possible values of r in real fires is much wider. Thus the correct

estimation of α relies on a good estimation of the spread rate.

4.4 Inverse Modelling

4.4.1 Framework

Once a fire has been detected and observations are collected during the assimilation window, the relevant invariants can be estimated and a forecast of the fire development can be made without solving the complex interactions between gas and solid phase. The assimilation window is the period of time where observations are received and considered for the optimization step. As time goes by, new observations come in, providing more information on the history of the fire development, and the invariant parameters can be estimated with higher accuracy. When invariants have converged, the extent of the lead time depends only on when the next critical event will take place. A critical event (e.g. window breakage, flashover) will fundamentally change the invariants governing fire growth (e.g. change in boundary conditions, secondary ignition), and thus constitutes an upper limit to predictability.

The entrainment coefficient (C in Eq. (4.3)) has been shown to vary significantly with the fire characteristics [15], and it is therefore necessary to estimate this parameter for each specific fire scenario. The invariants of interest here are thus the spread rate (implicitly in α in Eq. (4.7)) and the entrainment coefficient. These invariants are separated from the physical variables of the processes involved and will be an input for the forecast zone model. Additionally, a delay time constant t_0 (see Eq. (4.7)) is estimated, in order to account for the time it takes for the hot gases to travel from the flame upwards and to mix in the hot layer. This transport time is not considered in zone models but added here to relax the assumption that combustion products move immediately into the upper layer. Note that t_0 in this context differs somewhat from its traditional definition of time to ignition.

The problem can thus be represented on the basis of these invariants summarized in the vector $\boldsymbol{\theta}$:

$$\boldsymbol{\theta} = [\alpha, C, t_0]\,. \tag{4.8}$$

In order to be useful in a fire scenario, a forecast has to be delivered with a positive lead time, i.e. the forecast has to be ready before the event being predicted takes place. Here, the lead time is defined as the time ahead of the event during which the forecasted temperature is less than 10% off the true temperature.

4.4.2 Cost Function

Data are assimilated into the model by minimizing a cost function that describes the distance between predictions and observations. The invariants are then adjusted until convergence is obtained. The hot layer temperature and height are used in the present work to be assimilated into the model. The cost function $J(\boldsymbol{\theta})$ is then defined as the sum over time of the squares of the differences between the model predictions for a given set of invariants $\boldsymbol{\theta}$ and the physical observations $\mathbf{y}_i$ at time t_i,

$$J(\boldsymbol{\theta}) = \sum_{i=1}^{N} \left[\mathbf{y}_i - \hat{\mathbf{y}}_i(\boldsymbol{\theta})\right]^T \left[\mathbf{y}_i - \hat{\mathbf{y}}_i(\boldsymbol{\theta})\right], \tag{4.9}$$

where $\hat{\mathbf{y}}_i(\boldsymbol{\theta})$ is the output of the forward integration model that predicts the state of the system at time t_i. Data is assimilated during a time period between t_0 and t_i that is discretized in N time steps.

Thus, the inverse problem that has to be solved can be formulated as the following minimization problem:

$$\begin{aligned} \min_{\boldsymbol{\theta}} \quad & J(\boldsymbol{\theta}) \\ \text{s.t.} \quad & \hat{\mathbf{y}}_i(\boldsymbol{\theta}) = \mathscr{M}_i(\mathbf{y}_0, \boldsymbol{\theta}). \end{aligned} \tag{4.10}$$

4.4.3 Optimization

The minimization problem presented in Eq. (4.10) is non-linear and has to be solved using a numerical approach. Although the zone model used as forward model in this case is simple and very fast to run, the methodology presented here is extendable to more complex fire models that can take considerably longer time to run. Thus gradient based optimization [16] was chosen to solve the problem of estimating the invariants, as function evaluations can become very time extensive with more complex forward models, and including information about the gradient can reduce the number of function

evaluations necessary to find a minimum [16]. The computation of the gradient of the cost function (Eq. (4.9)) involves the differentiation of the forward model with respect to $\boldsymbol{\theta}$, as shown,

$$\nabla J(\boldsymbol{\theta}) = -2 \sum_{i=1}^{N} \nabla \mathscr{M}_i(\mathbf{y}_0, \boldsymbol{\theta})^T \left[\mathbf{y}_i - \mathscr{M}_i(\mathbf{y}_0, \boldsymbol{\theta}) \right] \tag{4.11}$$

Algorithmic differentiation [17] of the forward model was used to obtain the derivative, as this method yields the exact derivative and is relatively easy to obtain for any existing code.

4.5 Fire Growth Forecasting

The case considered is a radially growing fire starting in the middle of a closed compartment with leaks at floor level (see Fig. 4.2), in order to prevent pressure rise in the compartment. The compartment is of 4 m by 5 m and 2.5 m high. The fuel is well distributed horizontally over the floor. The true fire grows radially from the initial point at a rate of 3 mm/s for 150 s, thus reaching a peak of 330 kW at the end of the scenario. These are deemed to represent realistic values of a typical residential or office fire. The true fire is simulated using a CFD fire model (Fire Dynamics Simulator version 5.1.6–FDSv5 [10]), which has been shown to provide good predictions of hot layer temperatures and smoke movement in scenarios similar to the one at hand [18].

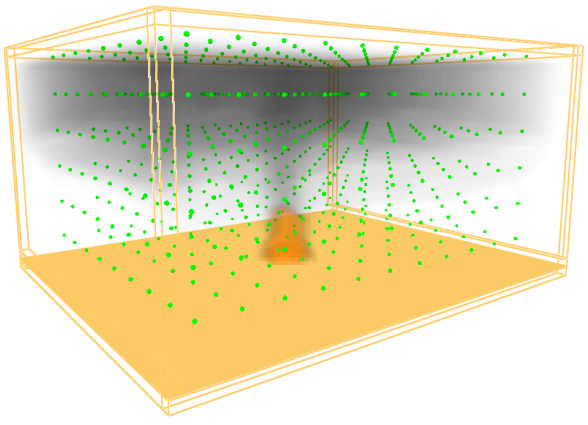

Figure 4.2: Snapshot of the CFD compartment fire used for data generation. The dots represent the sensor locations for temperature.

Temperature sensors were placed uniformly throughout the compartment (at a density of about 11 sensors/m^3). Figure 4.2 shows sensor locations. The 3D observations from the sensors were converted to hot layer variables by vertically integrating the temperature field. The hot layer height is determined by a thermal equilibrium between the continuous temperature distribution and the two zones with average temperatures [10]. The first data considered for assimilation are from 20 s after ignition, and new data are then recorded every 6 s.

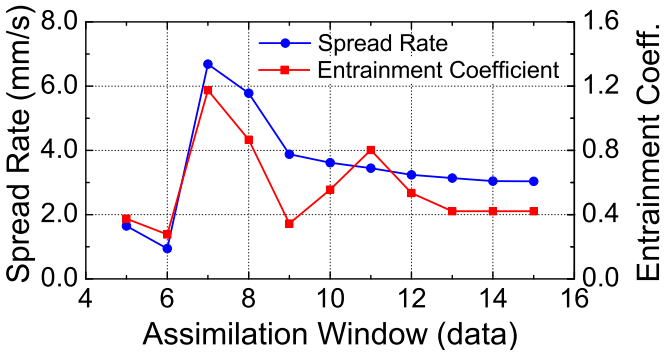

Figure 4.3: Spread rate (blue line) and entrainment coefficient (red line) for increasing number of data points in the assimilation window.

Figure 4.3 shows the convergence of the invariant parameters of the model as a function of the number of observations inside the data assimilation window. The assimilation process is started with 5 data points, yielding the first estimate of the parameters 42 s after ignition. As more data points are considered, the estimated spread rate of the fire converges towards the true value of 3 mm/s. The entrainment constant converges towards 0.4, which is in the same order of magnitude, but higher than the value of 0.21 proposed by Heskestad [12]. However, the presence of walls nearby changes the entrainment flow significantly [15], thus leading to conditions different from those of a free plume.

The predictive capability of the model grows according to the convergence of the spread rate as shown in Fig. 4.4. While the lead time is of less than 15 s with an assimilation window of up to 8 data points, it grows significantly with a wider assimilation window.

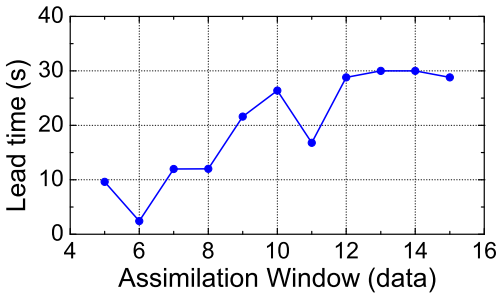

Figure 4.4: Lead time of the forecast for growing assimilation window.

Once the estimated spread rate converges to the spread rate of the observed fire (assimilation window of more than 12 data points), the lead time of the forecast reaches 30 s. At about 130 s the zone model assumptions start to break down, which corresponds to a critical event (transition from growth phase to fully developed phase). This constitutes a limit to the predictability of the fire development. Further incoming data (after 100 s) do not provide new information, and thus do not improve the predictions. A maximum lead time of 30 s is thus reached with an assimilation window of 13 observations. Note that the sharp decrease in the lead time for an assimilation window of 11 observations correlates with the very high estimated plume entrainment for the same assimilation window (Fig. 4.3).

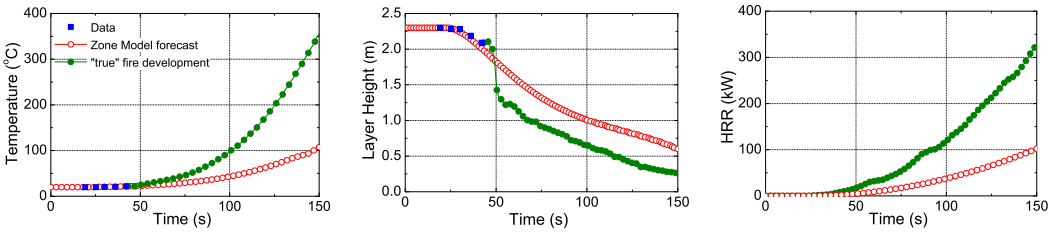

(a) Hot layer temperature **(b)** Hot layer height **(c)** HRR

Figure 4.5: Forecast at 42 s after five data points are assimilated. The observed data is shown together with the future development and the forecast of the fire. a) Hot layer temperature b) Hot layer height c) HRR.

Figure 4.5 shows the forecast of temperature and height of the hot layer and HRR at 42 s. The assimilation window includes five observations evenly distributed in time between 19 s and 42 s. The lead time for the temperature is less than 10 s. Although the prediction at 42 s is similar to the true fire, the forecast diverges rapidly after 50 s and ends up underpredicting the HRR by more than three times at 150 s after ignition. The reduced accuracy is due to the sharp descent of the true hot layer at 50 s, as seen in

Fig 4.5b. As a consequence of the poor forecast of HRR, the temperature and height of the hot layer are poorly forecasted too. Nevertheless, the forecast follows all trends qualitatively.

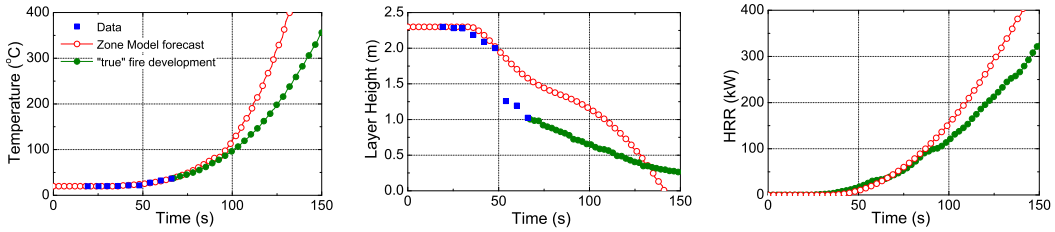

(a) Hot layer temperature **(b)** Hot layer height **(c)** HRR

Figure 4.6: Forecast at 66 s after nine data points are assimilated. The observed data is shown together with the future development and the forecast of the fire. a) Hot layer temperature b) Hot layer height c) HRR.

Figure 4.6 shows the forecast at 66 s with an assimilation window comprising nine evenly distributed observations. The forecast is improved significantly compared to the case with five data points, and the lead time is now 22 s. However, the descent of the hot layer is overpredicted by almost 30% between 50 and 130 s. The HRR is overpredicted by 40% at 150 s after ignition.

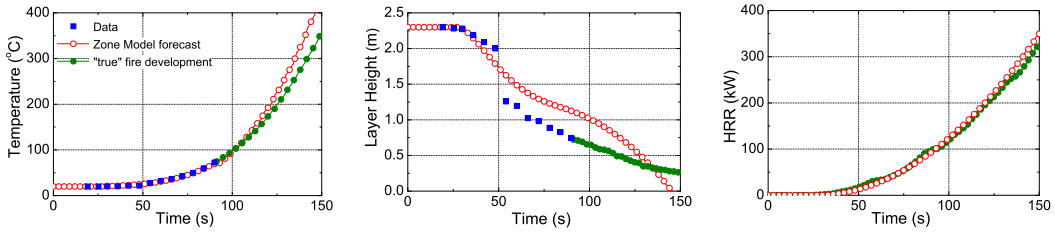

(a) Hot layer temperature **(b)** Hot layer height **(c)** HRR

Figure 4.7: Forecast at 90 s after 13 data points are assimilated. The observed data is shown together with the future development and the forecast of the fire. a) Hot layer temperature b) Hot layer height c) HRR.

Figure 4.7 shows the forecast at 90 s with an assimilation window comprising 13 evenly distributed observations. The growth rate of the fire can be predicted accurately, and thus the forecast for the HRR is close to the actual true fire growth. The lead time is 30 s. The best improvement is seen in the temperature and the HRR. The HRR is overpredicted by only 5% at 150 s after ignition. The descent of the hot layer is still overpredicted by 17%, although to lesser extent than in shorter assimilation windows.

4.5.1 Slow Fire

The observations in the previous case come from a radially growing fire that grows at a rate of 3 mm/s. The corresponding growth factor α of 0.0017 kW/s^2 is in the range of a medium fire as typically occurs with fuel loads such as beds and mattresses [19]. However, the methodology is not limited to a specific case and in the following sections observations from fires with different spread rates were assimilated into the model.

Fires with a growth factor of around 0.003 kW/s^2 are categorized as slow fires. These fires are typically found in scenarios with densely packed paper products. Using the same geometrical layout as in the previous case, a slow fire with a spread rate of 1.3 mm/s ($\alpha = 0.0032$ kW/s^2) was simulated with FDSv5. The output was then used as observations for the assimilation process and the lead times of the resulting forecasts were analyzed. The first data considered for assimilation were from 30 s after ignition, and new data were then recorded every 12 s.

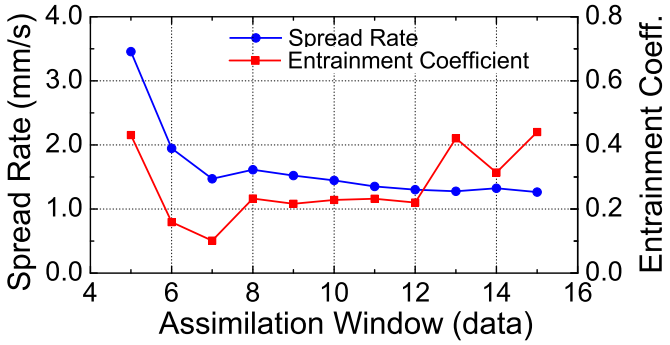

Figure 4.8: Spread rate (blue line) and entrainment coefficient (red line) for increasing number of data points in the assimilation window.

Figure 4.8 shows the convergence of the invariant parameters (spread rate and entrainment coefficient) as a function of the number of observations of the assimilation window. While the spread rate converges to the true value of 1.3 mm/s as the number of observations increases, the entrainment coefficient, which seemed to settle around 0.2, starts oscillating around 0.35 for more than 12 observations, although staying within reasonable bounds (Heskestad suggests 0.21 for a free standing plume [12]).

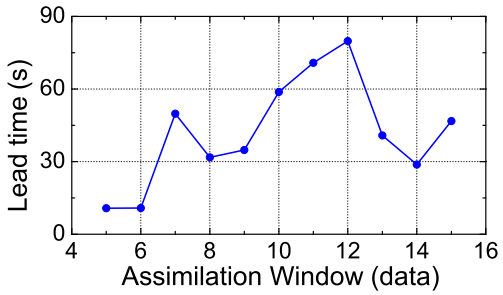

Figure 4.9: Lead time of the forecast for growing assimilation window.

Figure 4.9 shows the lead time of the forecasts as function of the number of observations in the assimilation window. Reasonable lead times are reached with 7 observations or more. The peak value for lead time is 80 s with 12 observations (160 s), allowing for forecasting the compartment conditions until 240 s after ignition. The two zone assumption starts to break down around that point, so that new incoming data (after 160 s) cannot improve the lead time of the forecast.

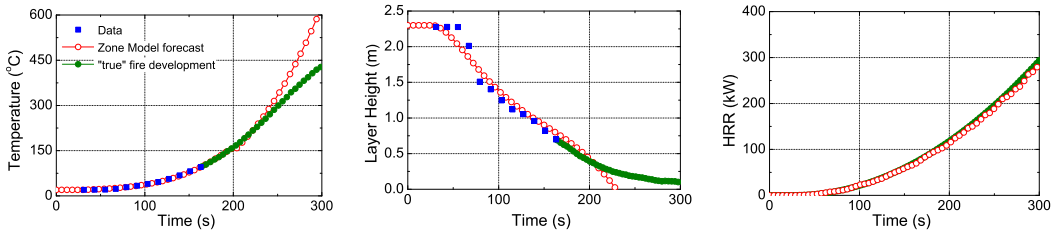

(a) Hot layer temperature **(b)** Hot layer height **(c)** HRR

Figure 4.10: Forecast at 160 s after 12 data points are assimilated. The observed data is shown together with the future development and the forecast of the fire. a) Hot layer temperature b) Hot layer height c) HRR.

The forecasts of smoke layer, average hot layer temperature and HRR are shown in Fig. 4.10 for an assimilation window with observations between 30 s and 160 s. The forecasted temperature (Fig. 4.10a) is within 10% of the observed temperature until about 240 s, yielding a lead time of 80 s as indicated in Fig. 4.9. The smoke height, shown in Fig. 4.10b, is forecasted correctly (within 15% of the observations) for about 45 s. Figure 4.10c shows that the HRR is overpredicted slightly.

It is important to point out that when a zone model is used as forward model, very slow fires, such as the one at hand, are particularly challenging to this methodology. This is due to modelling constraints associated to very small fires in relatively large compartments. While a big fire will release enough energy in order to provide sufficient

information on a global level for the inverse model to estimate the model parameters, a small fire will provide only local observations of higher temperature, which are averaged out on an integrated level. Thus a significant amount of time has to elapse before the observations can provide the necessary information for reliable estimation of model parameters.

4.5.2 Fast Fire

Fires with a growth factor of around 0.047 kW/s^2 are categorized as fast fires [19]. Fast fires are typically found in polyurethane mattresses or polyethylene pallets. Again using the same geometrical layout, a fast fire with a spread rate of 5 mm/s ($\alpha = 0.047$ kW/s^2) was simulated with FDSv5. The output was used as observations for the assimilation process and the lead times of the resulting forecasts were analyzed. The first data considered for assimilation were from 14 s after ignition, and new data were then recorded every 3.5 s.

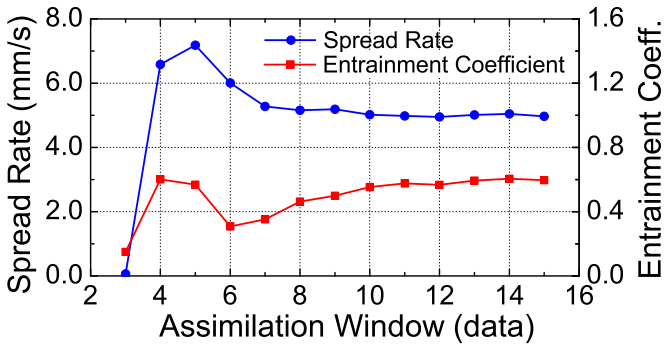

Figure 4.11: Spread rate (blue line) and entrainment coefficient (red line) for increasing number of data points in the assimilation window.

Figure 4.11 shows the evolution of the invariant parameters of the model (spread rate and entrainment coefficient) as a function of the number of observations assimilated into the model. The spread rate converges to the true value of about 5 mm/s after 8 iterations. The entrainment coefficient converges to around 0.6, although it takes about 10 data points to reach convergence. This value is higher than the entrainment coefficient estimated in the case of a medium fire (first case), which can be attributed to

the fact that the relatively bigger fire presents more interaction with the surrounding walls, thus changing the entrainment flow significantly [15].

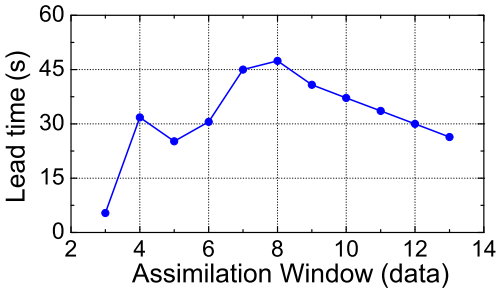

Figure 4.12: Lead time of the forecast for growing assimilation window.

In Fig. 4.12 the lead time of the forecasts as a function of the number of observations assimilated into the model is shown. A maximum lead time of 47 s is reached with 8 observations (40 s), allowing for forecasting of the temperature until about 90 s after ignition. Note that the convergence of the spread rate (Fig. 4.11) is reached with 8 observations, so that new incoming data (9 observations and more) do not improve the forecast, and thus only decrease the lead time.

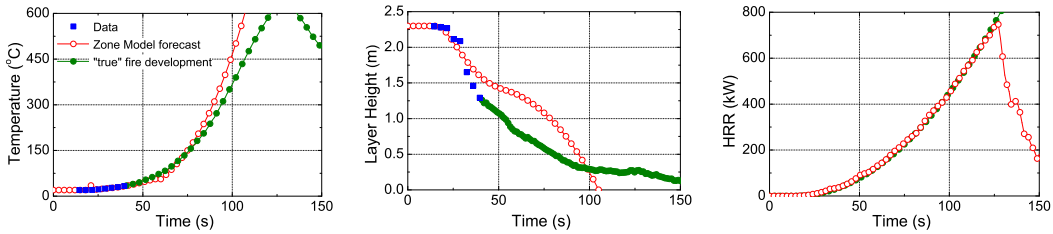

(a) Hot layer temperature **(b)** Hot layer height **(c)** HRR

Figure 4.13: Forecast at 40 s after 8 data points are assimilated. The observed data is shown together with the future development and the forecast of the fire. a) Hot layer temperature b) Hot layer height c) HRR.

Figure 4.13 shows the forecasts of temperature, smoke height and HRR in case of a fast fire for an assimilation window with observations between 14 s and 40 s. Temperatures are within 10% of the observed temperatures until 87 s after ignition, yielding a lead time of 47 s, as suggested in Fig. 4.12. The descent of the hot layer is underpredicted significantly (between 20% and 80%), although the qualitative trend is reproduced correctly. The comparison of the HRRs shown in Fig. 4.13c reflects the good

estimation of the spread rate presented previously. The HRRs of the true fire and the zone model forecast are in very good agreement until about 120 s after ignition, where the fire becomes ventilation controlled, and the fire growth model presented (Eq. (4.6)) no longer holds. The overprediction of the hot layer temperature after 87 s even with a perfect estimation of the growth parameters is explained by the underprediction of the descent of the hot layer, which causes a smaller hot layer volume.

4.6 Concluding Remarks

The current state-of-the-art limitation to forecast fire growth is overcome here using a data assimilation technique. The application is illustrated with a simple compartment fire scenario.

A zone model with a t-squared fire in a compartment was implemented and the growth rate was assimilated based on comparison to hot layer observations generated by a validated CFD model. The results show that the simple mass and heat balances, and plume correlation of the zone model are enough to satisfactorily forecast the main features of the fire. It was possible to estimate the fire growth invariants correctly and to find a physical basis for their values. Moreover, the method provides positive lead times for the growth phase of a fire in the order of 30 s.

It was further shown that the forecast capabilities of the model depend on the amount of data available for comparison. For only a few data points, the forecast is poor, even if the estimated zone model temperatures agree correctly with the observations. As the assimilation window grows, the forecast improves, and the estimated invariants converge towards the true values. With the information of 13 data points the temperature and HRR can be forecasted correctly until the end of the scenario considered here. However, the estimated lead time seems to approach a peak at an assimilation window width near 13 data points.

Data assimilation in real cases is expected to depend on the scenario and model used, but results presented here show that positive lead times are possible and suggest the existence of an optimal assimilation window width that will be of interest for further technological developments. These results are an important step towards the forecast of fire dynamics to assist the emergency response.

References

[1] A. Cowlard, W. Jahn, C. Abecassis-Empis, G. Rein, and J.L. Torero. Sensor Assisted Fire Fighting. *Fire Technology*, in press, 2008. DOI:10.1007/s10694-008-0069-1.

[2] W. Xie and P. DesJardin. An Embedded Upward Flame Spread Model using 2D Direct Numerical Simulations. *Combustion and Flame*, 156(2):522–530, 2009. DOI:10.1016/j.combustflame.2008.11.011.

[3] G. Cox. Turbulent Closure and the Modelling of Fire by Using Computational Fluid Dynamics. *Philosophical Transactions: Mathematical, Physical and Engineering Sciences*, 356(1748):2835–2854, 1998. http://www.jstor.org/stable/55051.

[4] R. Richards, B. Munk, and O. Plumb. Fire Detection, Location and Heat Release Rate Trough Inverse Problem Solution. Part I: Theory. *Fire Safety Journal*, 28(4):323–350, 1997. DOI:10.1016/S0379-7112(97)00005-2.

[5] M. Leblanc and A. Trouvé. Inverse Modeling of Enclosure Fire Dynamics. In *Proceedings of the 6$^{\text{th}}$ U.S. National Combustion Meeting*, 2009.

[6] S. Wang, M. Berentsen, and T. Kaiser. Signal Processing Algorithms for Fire Localization using Temperature Sensor Arrays. *Fire Safety Journal*, 40(8):689–697, 2005. DOI:10.1016/j.firesaf.2005.06.004.

[7] A. Cowlard, L. Auersperg, J.B. Richon, G. Rein, S. Welch, A. Usmani, and J.L. Torero. A Simple Methodology for Sensor Driven Prediction of Upward Flame Spread. *Turkish Journal of Engineering and Environmental Sciences*, 31(6):403–413, 2007.

[8] W. Jahn, G. Rein, and J. L. Torero. Data Assimilation in Enclosure Fire Dynamics - Towards Adjoint Modelling. In T. Burczynski and J. Périaux, editors, *Evolutionary Methods for Design, Optimization and Control*. CIMNE, Barcelona, Spain, 2009.

[9] S. Koo, J. Fraser-Mitchell, and S. Welch. Sensor-steered fire simulation. *Fire Safety Journal*, 45(3), 2010. DOI:10.1016/j.firesaf.2010.02.003.

[10] K. McGrattan, B. Klein, S. Hostikka, and J. Floyd. Fire Dynamics Simulator (Version 5) – User's Guide. NIST Special Publication 1019–5, 2008.

[11] E. Zukoski. Development of a Stratified Ceiling Layer in the Early Stages of a Closed–room Fire. *Fire and Materials*, 2(2), 1978. DOI:10.1002/fam.810020203.

[12] G. Heskestad. Engineering Relations for Fire Plumes. *Fire Safety Journal*, 7(1):25–32, 1984. DOI:10.1016/0379-7112(84)90005-5.

[13] J.W. Kwon, N. Dembsey, and C. Lautenberger. Evaluation of FDS v.4: Upward Flame Spread. *Fire Technology*, 43(4):255–284, 2007. DOI:10.1007/s10694-007-0020-x.

[14] C. Fernandez-Pello. The Solid Phase. In G. Cox, editor, *Combustion Fundamentals of Fire*, chapter 2. Academic Press Ltd., 1995.

[15] E. Zukoski, T. Kubota, and B. Cetegen. Entrainment in Fire Plumes. *Fire Safety Journal*, 3(2):107–121, 1981.

[16] J. Nocedal and S. Wright. *Numerical Optimization*. ISBN 978-0387-30303-1. Springer, USA, 2nd edition, 2006.

[17] A. Griewank. *Evaluating Derivatives – Prinicples and Techniques of Algorithmic Differentiation*. SIAM, Philadelphia, USA, 2000.

[18] Verification and Validation of Selected Fire Models for Nuclear Power Plant Applications, Volume 7: FDS. U.S. Nuclear Regulatory Commission, Office of Nuclear Regulatory Research (RES), Rockville, MD, and Electric Power Research Insititute (EPRI), Palo Alto, CA, NUREG–1824 and EPRI 1011999, 2007.

[19] D. Drysdale. *An Introduction to Fire Dynamics*. ISBN 0-471-97290-8. Wiley & Sons, New York, 2nd edition, 1998.

5

Inverse Modelling of Enclosure Fire Dynamics using a Tangent Linear Approach

5.1 Introduction

Forecasting enclosure fire dynamics is a subject of central interest in fire safety engineering. While the first line of response to a fire event is part of the design process of a building in the form of compartmentation of open spaces, smoke barriers, egress paths, suppression and detection systems etc., fires that overcome these measures may occur, and it is necessary to prepare for that case. If a fire escalates and the building and occupants are unable to terminate the threat by the time fire fighters arrive, then intervention will take place and management of the scene will be delegated to the fire service. The fire fighting strategy to follow during a potential fire is currently based mostly on the experience and the intuition of commanding officers of the fire service on duty, but it would be life saving if fire fighting strategies could be decided upon based on short and medium term forecasts of the development of the fire. Not only would this

allow for more efficient strategies, it would also assure the safety of fire fighters who enter the emergency scenario in order to attack the fire and rescue the occupants.

Modern buildings provide some useful information about an ongoing fire emergency, including emergency management plans, security camera footage and security panels which can indicate in a crude manner the origin and magnitude of the event. This information will be included in the decision making process of commanding officers, who then can deploy people and equipment more effectively. The current density and nature of information, however, makes reliance on experience and intuition unavoidable.

It has been suggested to use of the output of fire models to assist emergency response [1], and it is postulated that the forecasting of fire dynamics in enclosures could imply a paradigm shift in the response to emergencies, providing the fire service with essential information about the emergency development within some lead time.

Despite advances in the understanding of fire dynamics over the past decades and despite the advances in computational capacity, our ability to predict the behaviour of fires in general and building fires in particular using numerical models remains very limited. From a fire fighting point of view, forecasting of fire events only makes sense if it occurs with a positive lead time, i.e. if the prediction is based on current information of the state of the system, and can be completed faster than the fire is evolving. Current computational fluid dynamics (CFD) based fire models demand heavy resources and computational time periods that are far greater than the time associated with the processes being simulated (hours to model seconds). If comprehensive computational models are ever to be used to estimate, forecast and understand fire growth in support of emergency response, the computational time has to be shorter than the event itself. This problem is being addressed in the FireGrid project [2], and a full justification of this project together with an introduction to sensor assisted fire fighting is presented by Cowlard et al. [3]. A summary of the key points is presented here.

Fire dynamics are inherently transient with timescales ranging from a few seconds to several hours, and they are governed by strong coupling between the gas phase (movement of hot gases, combustion) and the solid phase (heating of surface, pyrolysis, fire spread) [4]. A comparative study of blind predictions of a real fire has shown that it is not possible to accurately predict fire growth even when extensive information about the fire scenario is available [5].

5.1.1 Inverse Modelling

Even if all the governing mechanisms could be solved correctly, their chaotic nature imposes a maximum possible lead time to the forecast, as has been shown for other dynamic systems like weather [6]. It is thus suggested that fire modelling can not be used for emergency response without feedback information from the evolving fire scenario. Nevertheless, in conjunction with sensor data it has the potential to achieve required speed, precision and robustness. It is proposed in FireGrid that sensor data can be used as a substitute for detailed models enabling simpler approaches to provide fast and well-informed outputs. Continuous correction of the model output by means of sensor data can allow for steering of the models to account for uncertainty in the input variables and for changes in the environment (window breakage, door opening etc). This concept is illustrated in Fig. 5.1, where sensor data is assessed and then continually reassessed to recreate the fire environment and steer the computations. The model output can thus be used to forecast the evolution of the event with some lead time. The information can then be summarized and delivered to the fire service in the most useful form.

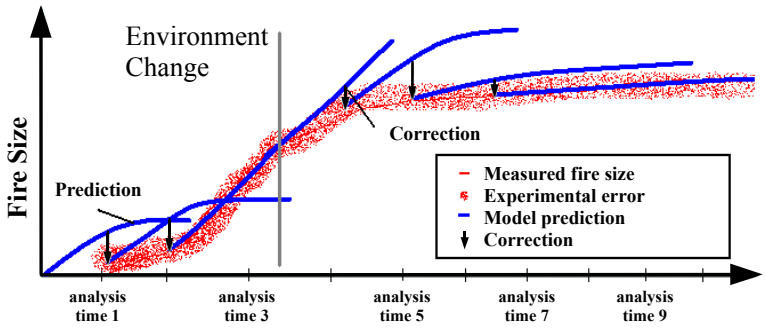

Figure 5.1: Conceptual representation of the data assimilation process and the sensor steering of model predictions even when fundamental changes take place in an evolving emergency scenario.

The use of sensor data to estimate model parameters is generally known as inverse modelling. Parameter estimation and inverse modelling are an important area within the engineering and scientific community.

In numerical weather predictions (NWP) inverse modelling and data assimilation take an important part of the computational resources [7]. In order to initialize the numerical models that are used to forecast the state of the atmosphere, weather ob-

servations from all over the planet are collected and then assimilated into the model. Observations are assimilated by initializing a new forecast based on a previous forecast (several hours back), and correcting it according to the difference between the previous forecast and the observations [8, 9]. Most modern NWP systems assimilate observations during a certain period of time (assimilation window) before starting the forecast, in order to account for the dynamical coupling of the involved processes [10]. The assimilation algorithm typically involves a linearization of the NWP system around the previous forecast and the subsequent solution of a quadratic minimization problem [7]. The basic principles of this methodology, called the tangent linear model (TLM), are applied in this work, adjusted to the specific features of fire dynamics.

In fire engineering, several inverse modelling studies have been undertaken. Richards et al. [11] use a database of pre-run zone-type models to estimate fire location and fire growth. They use the same zone model to generate the data for comparison, and analyze the influence of measurements and modelling errors. Leblanc and Trouvé use a zone model to predict the HRR time-history based on observations generated using the same model [12]. While they are able to closely reproduce the heat release rate (HRR) history, their work does not address how to produce a forecast of future events. Koo et al. [13] used measurements from a fire test experiment to progressively steer fire simulations towards the effective value using a Monte Carlo approach with a set of parameters that was used for random generation of scenarios. While they were able to reproduce past observations of temperature, they could not link the parameters of the model to the physics of the full scale fire test, which limits the forecast of future events to statistical considerations. Cowlard et al. [14] estimate the upward flame spread rate of PMMA based on visual recordings of the flame height and temperature measurements at the PMMA.

In this document a conceptual framework and a mathematical methodology is proposed to allow for forecasting of fire growth. The highly complicated interaction between gas and solid phase are replaced by a simplified fire growth model that is input into the gas phase model as a boundary condition. This growth model is based on a set of parameters that do not depend on the feedback from the fire and are thus constant (at least for a certain amount of time). Observations from the evolving fire provide the information for the estimation of the parameters for the growth model.

(a) Fuel controlled fire **(b)** Ventilation controlled fire

Figure 5.2: Different stages of the fire. a) shows a fuel controlled, localized fire, while b) shows a ventilation controlled fire.

5.2 Enclosure Fire Dynamics

Fire dynamics are governed by complex, strongly coupled physical processes constituting a feedback cycle [4]. Pyrolyzate is produced by chemical decomposition of the fuel source as a result of heat transferred from the flame. The pyrolyzate is then dragged into the flaming region where it mixes with fresh oxygen and burns resulting in flames, which transfer heat back to the fuel source.

Two distinct stages can be observed in an enclosure fire, that have to be treated fundamentally differently: a fuel controlled growth phase and a ventilation controlled fully developed fire (pre- and post-flashover). The difference between both stages is illustrated in the pictures of Fig. 5.2.

5.2.1 Fuel Controlled Fire

During the initial phase of a fire, sufficient oxygen supply is available to feed the fire, and its spread rate does not depend on the ventilation conditions but on fuel arrangement and quantity. During this stage the fire source is localized and modelling emphasis must be on the accurate description of the growth rate of the heat release and the flame geometry. Boundary conditions are important only in the proximity of the flames, and the size and detailed geometry of the compartment does not greatly affect the course of the fire. In this stage fire growth is the most important variable.

This work is focused on the fuel controlled regime, where flame spread is the primary invariant to estimate, since the most important element in fire dynamics is the

fire source, and it is therefore the first objective of a forecast attempt.

5.2.2 Ventilation Controlled Fire

As the fire grows, the compartment geometry and the ventilation conditions start playing a more important role and the fire becomes controlled by the supply of oxygen. At some point flashover will occur, after which flames start coming out of the openings of the enclosure (doors, windows), as shown in Fig. 5.2b. In a ventilation controlled fire the forecasting of temperature distributions and local burning will be of interest, and measured data could be used to assist the model in assimilating new ventilation conditions that can alter flow fields and burning regions.

5.3 Fire Modelling

In fire field modelling, traditional CFD is combined with simplified combustion models, and smoke movement and temperature distributions can be reproduced reasonably if the curve of heat release rate (HRR) of the fire, and the fire dimensions are well characterized [15]. Predicting fire growth however, although theoretically possible, is still subject to ongoing research and has not been implemented satisfactorily at a scale that can be used in fire modelling. The complex physical phenomena involved in the interaction between the flame and the solid fuel result in a large number of degrees of freedom and uncertainties that are difficult to model.

Fire modelling typically handles enclosure length scales of around 10 m. Although depending on the size of the fire, with a LES approach a grid resolution between 1 cm and 10 cm in the gas phase is generally required to obtain sufficient spatial resolution [16]. Thus, the computational cost of modelling fire is considerable.

While flame spread can be reproduced with numerical models to considerable detail for small flames ($\sim$ 10 cm) in restricted computational domains [17, 18], it is much more difficult and computationally expensive to do so in enclosure fire dynamics, as the computationally domain typically consists of several metres, but grid cells of the order of millimetres would be required for the modelling of the flaming and pyrolizing region. A recent study has shown that flame spread modelling with a commonly used fire

modelling tool is not reliable for engineering applications [19], even using a relatively fine grid (2.5 cm).

The limitations in state-of-the-art fire growth modelling are thus an important constraint to the forecast capabilities of fire simulations, as temperatures and smoke production can only be predicted if the time curve of the HRR is provided. It is proposed in this chapter to decouple the gas phase from the solid phase by imposing the fire as a time dependant boundary condition to the gas phase modelling. The interaction between gas and solid phase is replaced by a simplified fire growth model, which is explained in the following section. Temperature measurements in the ceiling can provide information on the governing parameters of the fire growth model, which can then be used to produce a forecast of the future fire development.

5.3.1 Fire Growth

Although the inverse modelling methodology explained in the following sections can be extended to fully developed fires, the present work is focused on the estimation of model parameters related to the growth phase of the fire.

The decoupling of the solid phase processes from the gas phase is based on the assumption that the radius of the burning area of an isotropic fuel grows at a constant rate. This is a reasonable assumption for early fire development when flames do not penetrate into the hot layer and heat feedback from the flames will not accelerate flame spread [20]. The fire source becomes thus a time dependent boundary condition to the gas phase simulation. Assuming a horizontal fire that starts at one point and spreads outwards radially with a spread rate r (m/s), and assuming moreover a constant fuel burning rate per unit area $\dot{\omega}$ (kg/s$\cdot$m^2), the rate of heat release becomes proportional to the area of the fire, which grows as a function of the spread rate and of time,

$$\dot{Q} = \Delta h_c \dot{m} = \Delta h_c \dot{\omega} A(r, t), \tag{5.1}$$

where Δh_c is the effective heat of combustion (in kJ/kg). As long as the fire does not reach the boundaries of the fuel surface the fire area is circular ($A(r, t) = \pi(r(t - t_0))^2$) (or has the form of a fraction of a circle, if the ignition point is e.g. at the wall), and the

resulting HRR follows a quadratic growth.

This is a first approximation to simulate fire growth. It avoids direct coupling of gas and solid phase. This approach is widely used in fire safety engineering, although the governing parameters are summarized into a constant that is tabulated for different materials and leads to what is known as an "αt^2" fire.

For real fuel packages (such as sofas, beds or other furniture), which consist of several finite surfaces each with a potentially different spread rate, this approximation has shown to still hold to a reasonable degree [21], and the constant α corresponds in that case to an equivalent growth rate.

In fire field models the spread rate r can be prescribed, so that adjacent cells are ignited producing a fire area that grows at rate r. This will then result in a fire that evolves according to Eq. (5.1).

5.4 Inverse Modelling

5.4.1 Framework

In order to be able to predict the state of a physical system, it is necessary to identify a set of parameters that characterize the system, and that do not change over time (or change only due to external intervention). These parameters are the invariants of the system. When modelling a physical process from first principles, the initial and boundary conditions constitute the only invariants, and changes of these conditions are only due to external intervention (for example a periodic boundary condition). In that case the invariants are well established. However, physical systems can generally not be modelled from first principles, and approximations have to be introduced, resulting in additional invariants that have to be input into the model. These invariants are normally obtained experimentally (e.g. fire spread rate).

In the present case the pyrolysis process is replaced by a fire growth model which results in a boundary condition that changes over time according to Eq. (5.1). The invariants of interest are the spread rates of the burning item, the corresponding fuel burning rates and other parameters such as soot yield, radiative fraction etc (related to other approximations in the model).

The problem can thus be represented on the basis of these invariants summarized in the vector $\boldsymbol{\theta}$:

$$\boldsymbol{\theta} = \left[r_1, r_2, \ldots, \dot{\omega}_1, \omega_2, \ldots, \chi_{R,1}, \chi_{R,2} \ldots \right]. \tag{5.2}$$

Once a fire has been detected and observations are collected during the assimilation window, the relevant invariants in $\boldsymbol{\theta}$ can be estimated and a forecast of the fire development can be made without solving the complex interactions between gas and solid phase. The assimilation window is the period of time where observations are received and considered for the optimization step. As time goes by, new observations come in, providing more information on the history of the fire development. Note that in the context of FireGrid several different kinds of observations can be recorded and analyzed (e.g. the number of people in a compartment could be obtained from analysis of CCTV recordings), but in the present work the term observation is used as a synonym of a measured quantity (i.e. a measurement) such as temperature, smoke obscuration.

The forward model is a 'black box' in the context of the methodology presented, and thus any model that represents the system to be simulated can be used. For scenarios described in this work and the level of detail required in the approach presented in this chapter, a CFD type fire model is necessary.

5.4.2 Cost Function

Data are assimilated into the model by minimizing a cost function that describes the distance between the model output and the measurements. The governing parameters are then adjusted until convergence is obtained. Many physical observations, such as temperature, smoke obscuration, velocities etc. can be used in the cost function. Temperatures and smoke obscuration are easy to measure and have relatively low experimental error. They are used in the present work to be assimilated into the model. The cost function is then defined as the sum of the distances between model output for a given set of parameters and the measurements:

$$J(\boldsymbol{\theta}) = \sum_{i}^{N} \left[\mathbf{y}_i - \hat{\mathbf{y}}_i(\boldsymbol{\theta}) \right]^T \mathbf{W}_i \left[\mathbf{y}_i - \hat{\mathbf{y}}_i(\boldsymbol{\theta}) \right], \tag{5.3}$$

where $\mathbf{y}_i$ is the set of physical variables that is measured, and $\hat{\mathbf{y}}_i(\boldsymbol{\theta})$ is the output of the forward integration of the numerical model that computes the state of the system at time t_i from the initial state $\mathbf{y}_0$, and $\mathbf{W}_i$ is a weight matrix. The parameters to be estimated are denoted by the vector $\boldsymbol{\theta}$. Data is assimilated during the assimilation window that is discretized according to the output of the numerical model in N time steps.

The inverse problem that has to be solved in order to estimate the parameters $\boldsymbol{\theta}$ can be formulated as the following minimization problem:

$$\begin{aligned} \min_{\boldsymbol{\theta}} \quad & J(\boldsymbol{\theta}) \\ \text{s.t.} \quad & \hat{\mathbf{y}}_i(\boldsymbol{\theta}) = \mathscr{M}_i(\mathbf{y}_0, \boldsymbol{\theta}), \end{aligned} \tag{5.4}$$

where $\mathscr{M}_i(\mathbf{y}_0, \boldsymbol{\theta})$ denotes the forward integration model (a fire specific CFD code in this case).

The CFD code is used to transport the information of the input parameters to the location at the walls where measurements are taken by integrating the governing equations in time and space.

5.4.3 Optimization

Several methods can be used to minimize the non linear cost function $J(\boldsymbol{\theta})$, which can be summarized in two groups: Gradient based and gradient-free methods. While gradient-free methods are heuristic methods that generate a random population of possible minima and evolve towards the global minimum following different laws of selection (for example survival of the fittest in Genetic Algorithms) combined with a stochastic component, gradient methods start from an initial guess relatively close to the minimum and then use information of the gradient to establish a search direction and a step size. One important advantage of gradient-free methods is that they can search over a large parameter space and do not get caught in local minima. They are also very robust regarding the objective function to minimize and do not require smoothness or continuity. However, they tend to need a large amount of function evaluations in each iteration and have slow convergence rates compared to gradient based methods [22]. In minimization problems where the cost function is continuous and an initial guess can assured to be in the vicinity of a global minimum, gradient based optimization methods

outperform evolutionary methods [22, 23].

The continuity of $J(\boldsymbol{\theta})$ and the relatively narrow range of possible parameters (spread and burning rates are within limited ranges) suggest the use of gradient based methods. Furthermore, the high cost of function evaluation (each evaluation of $J(\boldsymbol{\theta})$ involves a forward integration of the fire model) makes evolutionary algorithms unattractive.

The computation of the gradient of the cost function (Eq. (5.3)) involves the differentiation of the forward model with respect to the parameters, as shown in Eq. (4.11).

$$\nabla J(\boldsymbol{\theta}) = -2\sum_{i}^{N} \nabla \mathscr{M}_i(\mathbf{y}_0, \boldsymbol{\theta})^T \mathbf{W}_i \left[\mathbf{y}_i - \mathscr{M}_i(\mathbf{y}_0, \boldsymbol{\theta})\right] \tag{5.5}$$

As a first approximation, a *Finite Differences* (FD) scheme was used to approximate the gradient of the forward model,

$$\frac{\partial \mathscr{M}_i(\mathbf{y}_0, \boldsymbol{\theta})}{\partial \theta_j} \simeq \frac{\mathscr{M}_i(\mathbf{y}_0, \boldsymbol{\theta} + \boldsymbol{\varepsilon}_j) - \mathscr{M}_i(\mathbf{y}_0, \boldsymbol{\theta})}{||\boldsymbol{\varepsilon}_j||}, \tag{5.6}$$

where $\boldsymbol{\varepsilon}_j$ is a vector with a small perturbation in θ_j. While this is very easy to implement, the accuracy of the derivative depends on the size of the perturbation $\boldsymbol{\varepsilon}_j$. Note that this approach becomes computationally expensive when a large set of parameters has to be estimated, as it requires an additional run of the forward model for each parameter. It is, however, computationally cheap for small sets like the one at hand. This approach is also easy to parallelize, as the model integration can be launched with the perturbations on different processors.

5.4.4 Tangent Linear Model

There are a number of gradient based algorithms with different approaches as to how to choose the best search direction and the most suitable step size. In the case of a linear forward model the cost function is quadratic, which can be minimized in one step by solving a linear system. While this is computationally cheap, physical systems tend not to be linear. For a non-linear forward model as the one at hand, the tangent linear model (TLM) can be computed [24, 7]. The TLM method consists in linearizing the forward model $\mathscr{M}_i$ around some initial guess, so that the cost function is approximated as quadratic. A graphical illustration of the TLM is given in Appendix A.

Let us consider a Taylor expansion of the forward model $\mathscr{M}_i$ around some initial guess $\boldsymbol{\theta}_0$,

$$\mathscr{M}_i(\mathbf{y}_0, \boldsymbol{\theta}) \simeq \mathscr{M}_i(\mathbf{y}_0, \boldsymbol{\theta}_0) + \nabla \mathscr{M}_i(\mathbf{y}_0, \boldsymbol{\theta}_0)(\boldsymbol{\theta} - \boldsymbol{\theta}_0) \tag{5.7}$$

The linearized forward model is then inserted into the cost function, yielding a quadratic function $\tilde{J}(\boldsymbol{\theta})$,

$$\tilde{J}(\boldsymbol{\theta}) = \sum_{i=1}^{N} \left(\mathbf{y}_i - \left[\mathscr{M}(\mathbf{y}_0, \boldsymbol{\theta}_0) + \nabla_{\boldsymbol{\theta}} \mathscr{M}(\mathbf{y}_0, \boldsymbol{\theta}_0)(\boldsymbol{\theta} - \boldsymbol{\theta}_0)\right]\right)^T \mathbf{W}_i \left(\mathbf{y}_i - \left[\mathscr{M}(\mathbf{y}_0, \boldsymbol{\theta}_0) + \nabla_{\boldsymbol{\theta}} \mathscr{M}(\mathbf{y}_0, \boldsymbol{\theta}_0)(\boldsymbol{\theta} - \boldsymbol{\theta}_0)\right]\right), \tag{5.8}$$

where $\boldsymbol{\theta}$ is in the vicinity of $\boldsymbol{\theta}_0$.

The gradient of the resulting quadratic cost function (Eq. (5.8)) is then as follows

$$\nabla_{\boldsymbol{\theta}} \tilde{J}(\boldsymbol{\theta}) = -2 \sum_{i=1}^{N} \left[\nabla_{\boldsymbol{\theta}} \mathscr{M}_i(\mathbf{y}_0, \boldsymbol{\theta}_0)\right]^T \mathbf{W}_i \left[\mathbf{y}_i - \left(\mathscr{M}_i(\mathbf{y}_0, \boldsymbol{\theta}_0) + \nabla_{\boldsymbol{\theta}} \mathscr{M}_i(\mathbf{y}_0, \boldsymbol{\theta}_0)(\boldsymbol{\theta} - \boldsymbol{\theta}_0)\right)\right] \tag{5.9}$$

Introducing the following annotation:

$$\begin{aligned} \mathbf{M}_i &= \mathscr{M}_i(\mathbf{y}_0, \boldsymbol{\theta}_0), \\ \mathbf{H}_i &= \nabla_{\mathbf{p}} \mathscr{M}_i(\mathbf{y}_0, \boldsymbol{\theta}_0), \\ \bar{\boldsymbol{\theta}} &= (\boldsymbol{\theta} - \boldsymbol{\theta}_0), \end{aligned}$$

it is possible to write the first order condition for optimality as follows:

$$\sum_{i=1}^{N} \mathbf{H}_i^T \mathbf{W}_i \left[\mathbf{y}_i - \left(\mathbf{M}_i + \mathbf{H}_i \bar{\boldsymbol{\theta}}\right)\right] = 0. \tag{5.10}$$

Equation (5.10) can be rearranged as

$$\sum_{i=1}^{N} \mathbf{H}_i^T \mathbf{W}_i \mathbf{H}_i \bar{\boldsymbol{\theta}} = \sum_{i=1}^{N} \mathbf{H}_i^T \mathbf{W}_i \left(\mathbf{y}_i - \mathbf{M}_i\right), \tag{5.11}$$

which is a linear system of the form

$$\mathbf{A}\bar{\boldsymbol{\theta}} = \mathbf{b},$$

where

$$\begin{aligned} \mathbf{A} &= \sum_{i=1}^{N} \mathbf{H}_i^T \mathbf{W}_i \mathbf{H}_i, \quad \text{and} \\ \mathbf{b} &= \sum_{i=1}^{N} \mathbf{H}_i^T \mathbf{W}_i \left(\mathbf{y}_i - \mathbf{M}_i\right). \end{aligned}$$

By solving this linear system a new estimation of the parameters, $\tilde{\boldsymbol{\theta}}^*$, is obtained. Note that the optimum of this problem is not necessarily equal to the optimum of the original minimization problem (Eq. (4.10)). If the minimum $\boldsymbol{\theta}^*$ of the original minimization problem (Eq. (4.10)) is close enough to the initial guess, the new estimate $\tilde{\boldsymbol{\theta}}^*$ will be equal to $\boldsymbol{\theta}^*$. If not, the procedure is repeated starting from this new point until convergence is obtained.

Figure 5.3 illustrates the inverse modelling process using the TLM approach. A scriptfile calls the forward model (CFD) jobs ($k+1$ in order to compute the k partial derivatives for the gradient of $\mathscr{M}_i(\mathbf{y}_0, \boldsymbol{\theta})$), and, when all of them have finished, calls the executable that computes the TLM. Each CFD job provides an output file with the data for the calculation of the gradient. These files are read by the TLM executable, which then computes $\bar{\boldsymbol{\theta}}$ by minimizing the TLM and provides a new set of input files for the next iteration. The process is repeated until some convergence criterion is met (changes in the parameters from one iteration to the next smaller than a threshold value).

An alternative to the TLM method for unconstrained non-linear problems, the quasi-Newton Broyden-Fletcher-Goldfarb-Shanno (BFGS) method is one of the most widely used as it requires only first order derivative computation, but conserves the good convergence characteristics of the Newton method [23]. The BGFS method is a Newton based optimization algorithm where the second order derivatives are estimated from the first order derivatives instead of calculating them directly. In spite of being computationally less expensive than the traditional Newton method, the computational effort of finding the optimum using the BFGS method is still considerable, as more than

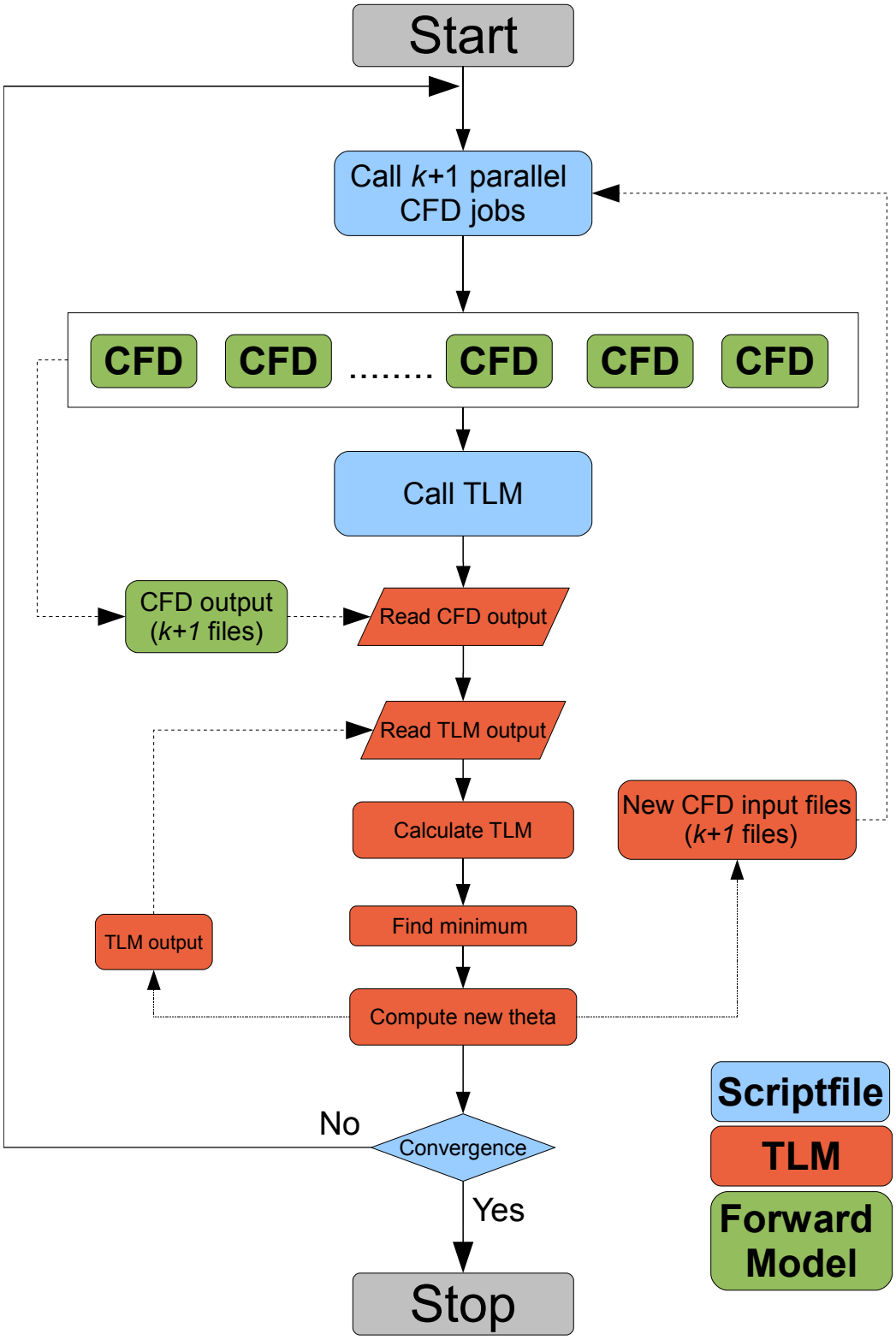

Figure 5.3: Inverse modelling procedure. The blue boxes indicate processes executed by a script file. Red boxes indicate the execution of the TLM method and its output files. Green boxes are the fire model.

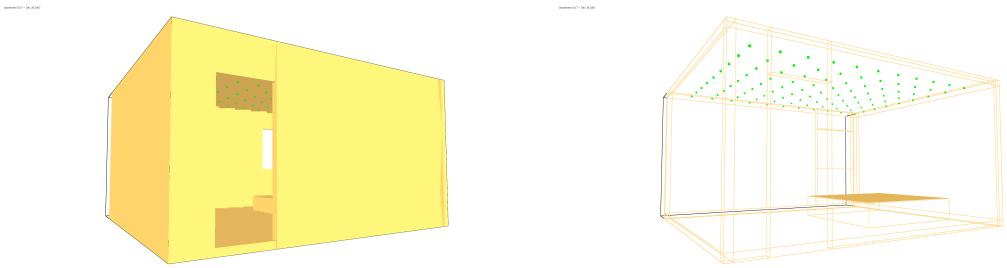

(a) **(b)**

Figure 5.4: Set up for the numerical experiment; a) the compartment as seen through the visualization tool of the CFD solver; b) the same compartment with outlined walls. The thermocouples in the ceiling are shown as dots.

one function evaluation (model run) is required for each iteration in order to find an adequate step size.

The tangent linear model method (TLM) was implemented in this work and its superior performance in this case is shown when compared to BGFS.

5.5 Using the TLM for Parameter Estimation

5.5.1 Scenario

The inverse problem procedure explained in the previous sections is illustrated applying it to a well defined test case. The fire-specific CFD code Fire Dynamics Simulator version 5.1.6 (FDSv5) [16] is used for the fire simulations. FDS solves a form of the Navier-Stokes equations adequate for low-speed thermally driven flows.

The test scenario consists of a compartment of 4m × 5m × 2.5m with a door on one side, and a window on the opposite wall (see Fig. 5.4). The observations are generated using the same CFD model that is used for the inverse modelling (FDSv5) with a set of parameters that will be referred to as true values. The fire is started at the corner of a bed located in the room as shown in Fig. 5.5. It is then allowed to grow over the surface of the bed. Fire spread rates in real fires range from 1 mm/s to 8 mm/s depending on material and geometrical layout of the burning surface [4], and several cases are run with spread rates in that range. A grid size of 10 cm is used and the simulations are run for 300 s. After that the assimilation process is started. The output of the CFD

model consists of wall temperatures measured with thermocouples in the ceiling and smoke obscuration from beam detectors, which is compared to the observations. The white noise option is activated for the generation of observations in FDSv5, which adds a random, zero mean perturbation to the initial condition, in order to account for perturbations and thus simulate real data. The thermocouples that measure wall temperature of the ceiling are distributed uniformly on a 40 cm×40 cm grid throughout the ceiling, resulting in 99 sensor locations as shown in Fig. 5.5. Eleven beam detectors across the compartment, installed 10 cm below the ceiling, provide smoke observation measurements. Their position is shown in Fig. 5.5, where the blue lines represent the laser beams crossing the room. The forward model $\mathscr{M}$ which is used to estimate the

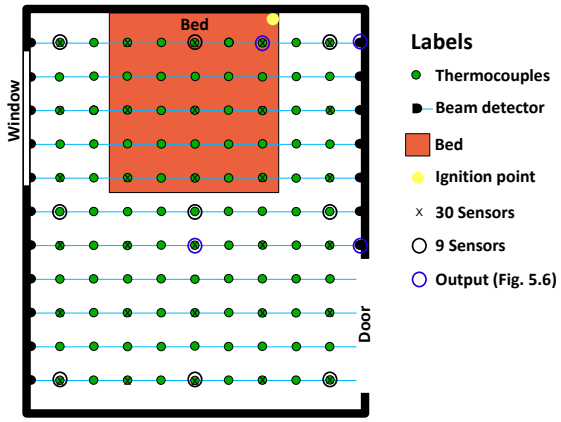

Figure 5.5: Top view of the compartment. The green dots represent the thermocouples in the ceiling, and the blue lines are the beam detectors.

invariants, is initialized with an arbitrary set of parameters $\boldsymbol{\theta}_0$ and consists of the exact same geometry as the model used to simulate the observations, including the position and dimensions of the bed and the grid size.

According to Eq. (5.1) the fire size (HRR) is characterized by the spread and burning rate. Note that Eq. (5.1) only applies as long as the fire does not reach the boundaries of the fuel surface (in this case the bed). Once the fire reaches the boundaries of the fuel surface, the fire growth is not quadratic any more, since the spread rate is not any longer constant in all directions. This is not a problem at this stage, as the geometry of the burning surface is assumed known, and if the spread rate is estimated correctly, it will result in an exact replica of the fire growth curve.

The effective heat of combustion of the fuel is generally a well defined quantity

that depends mostly on the material that is being burnt varying only slightly for similar fuels [25], and a fixed value is assumed in the simulations. It can further be shown that the HRR is relatively insensitive to that parameter [26], so that using an average heat of combustion will not affect the outcome of the modelling significantly. The fuel mass flow rate is a material property that also depends on the incoming heat flux from the flame, and is therefore not independent from the fire.

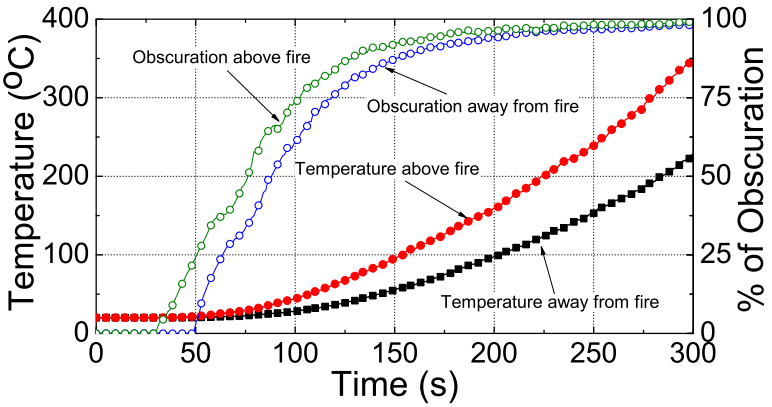

Figure 5.6: Sensor measurements recorded from the true fire.

Figure 5.6 shows a sample of sensor measurements recorded from the true fire. The locations of the considered sensors are indicated by blue circles in Fig. 5.5. The time evolution of the ceiling temperature is shown for a thermocouple above the fire area (close to the ignition point) and for a thermocouple in an area towards the middle of the room, away from the fire. Additionally two examples of the percentage of obscuration as measured by a beam detector close to the ceiling are shown, one above the fire, and another away from the fire.

5.5.2 Single Parameter

As a first approach, only the spread rate of the fire was estimated, and the fuel burning rate was assumed known (1-dimensional estimation). Only thermocouple measurements of ceiling temperatures throughout the ceiling are considered for assimilation. Measurements are compared to model output directly, i.e. without prior data manipulation (averaging, smoothing etc), at the times available from the recordings from the true fire. Figure 5.7 compares the convergence of the spread rate of the bed fire obtained using the TLM to the convergence obtained using the BFGS minimization technique.

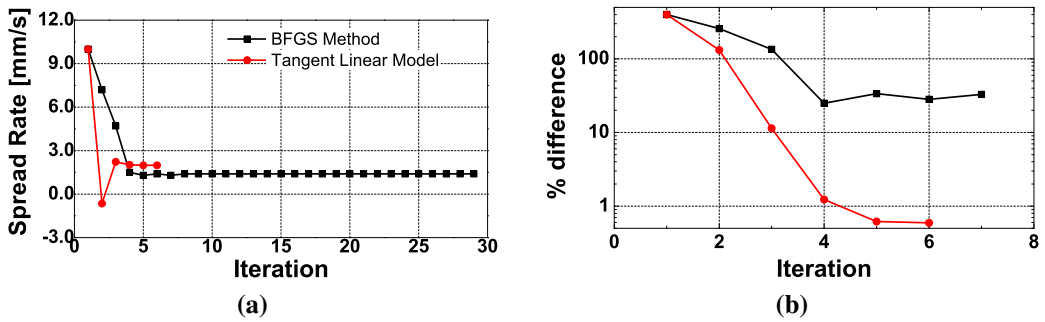

Figure 5.7: 1–dimensional parameter estimation; (a) shows the spread rate at different iterations comparing TLM and BFGS, and (b) shows the difference between the estimated and true value.

Figure 5.7a shows that the BFGS method takes more iterations to converge to a stable value, and the final estimate differs significantly from the true value of 2 mm/s. This is explained by the coarse approximation of the FD differentiation that is used to compute the gradient. If the estimated parameter at iteration n is within a vicinity of the size of the perturbation used to compute the derivative, a descent direction cannot be assured, and the method is thus limited by the accuracy of the differentiation.

Using the TLM the convergence is faster and much more accurate. In this case the approximation of the gradient does not directly affect the precision of the estimation process, as it does not directly search for the zero of the gradient, but estimates the minimum based on assuming that the cost function can be approximated by a quadratic function close to the optimum. An additional advantage is that for the TLM only one model run is required for each parameter per iteration, whereas the BFGS method needs one run for each parameter and a few additional runs in each iteration to determine the step size that assures a descent. Given the superior performance of the TLM, both in accuracy and in computation time, it was decided to concentrate on the TLM and not to develop the BFGS method for multi-parameter estimation.

5.5.3 Two Burning Items

A single burning item is the simplest case of a growing enclosure fire. However, in many situations one item can ignite another close standing object when the flames engulf this object (for example a curtain can catch fire if it is close to a burning bed). The spread rates on both objects are not generally the same, and the capability of simultaneously

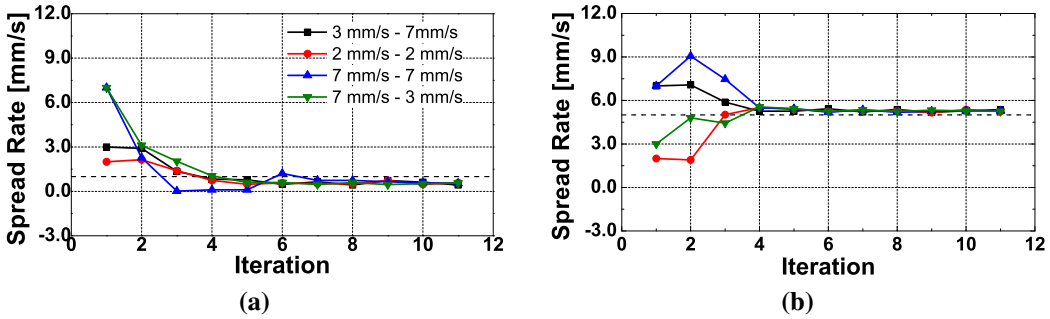

Figure 5.8: The spread rates of 2 independent fires are estimated using TLM for different first guesses. Graph a) shows the convergence of the spread rate on the bed, and b) shows the spread rate of the fire growing vertically on the wall.

estimating both spread rates was investigated.

For this test case the same compartment explained in the previous section was simulated to generate the data, with a fire starting at the same corner of the bed as shown in Fig. 5.5, but simultaneously igniting wall lining material close by. One fire thus spreads over the bed as in the previous case, and a second fire is assumed to grow vertically upwards on the wall. In order to preserve the physical coherence of fire growth, the observations were generated using a faster growth for the vertical fire than for the horizontal (1 mm/s on the bed and 5 mm/s on the wall). Note that a vertical fire will only grow at a constant spread rate as long as the flame is laminar [27]. Once the flame becomes turbulent, the spread rate starts accelerating, and the fire growth model used here (Eq. (5.1)) no longer holds. Within the scope of this work, the vertical fire is for illustration purposes only, and the accelerating growth rate is not discussed.

The forward model was initiated using different first guesses for the parameters. In Figure 5.8 the convergence of the estimated spread rates towards the true spread rates is shown. Each curve represents a pair of first guesses (e.g. black square data was started with a spread rate of 3 mm/s and 7 mm/s respectively). The estimation procedure is shown to be robust regarding the first guess (within the range of physically meaningful values). Figure 5.8a shows that the horizontal spread rate is slightly underestimated. The vertical spread rate on the other hand is overestimated by around 7%, as shown in Fig. 5.8b. Although the spread rates do not agree exactly with the spread rates from the true fire, the difference remains within reasonable bounds. This demonstrates the overall robustness of the estimation method, as it could correctly differentiate between

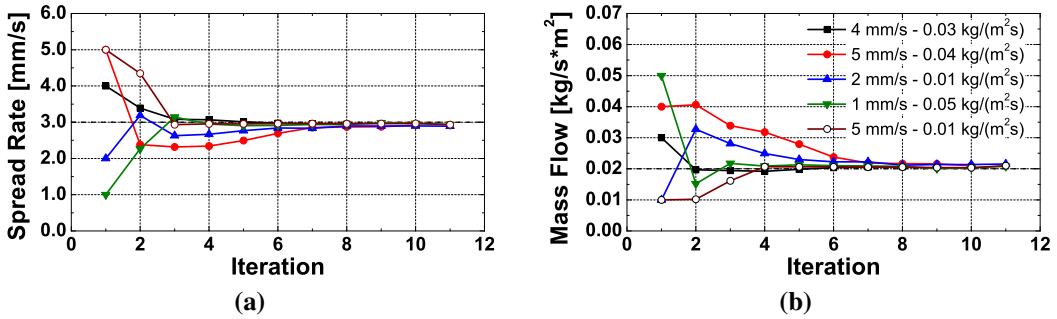

Figure 5.9: Estimation of burning rate and spread rate of the fuel. Graph a) shows the convergence of the burning rate, and b) shows the spread rate of the fire on the bed.

the two fires, even though the fire areas were very close to each other resulting in a single flame.

5.5.4 Estimation of fuel burning rate

In this example it is attempted to estimate the fuel burning rate together with the spread rate for a single burning fire growing over the bed as in the first example. The observations used for assimilation are generated using a true spread rate of 2 mm/s and a true fuel burning rate of 0.02 $kg/s \cdot m^2$ (typical of residential fuels [25]). The estimation process is initiated using different values ranging between 0.01 and 0.05 $kg/s \cdot m^2$ for the fuel burning rate, and values between 1 mm/s and 5 mm/s for the spread rate.

The convergence of the spread rate and of the fuel burning rate of a single burning item is shown in Fig. 5.9. While good convergence is obtained for most first guesses after 4 iterations, in some cases the convergence is noticeably slower (8 iterations). The final difference between the true values and the estimations is of less than 3% for all initial guesses.

5.5.5 Sensitivity to Sensor Locations

Inverse problems by definition cannot assure a unique solution. The more information about the state of the system that can be obtained from the observations, the better the estimations of the parameters, since more information will rule out more ‘wrong’ solutions. It was thus investigated how the density and distribution of sensors affects the outcome of the parameter estimation.

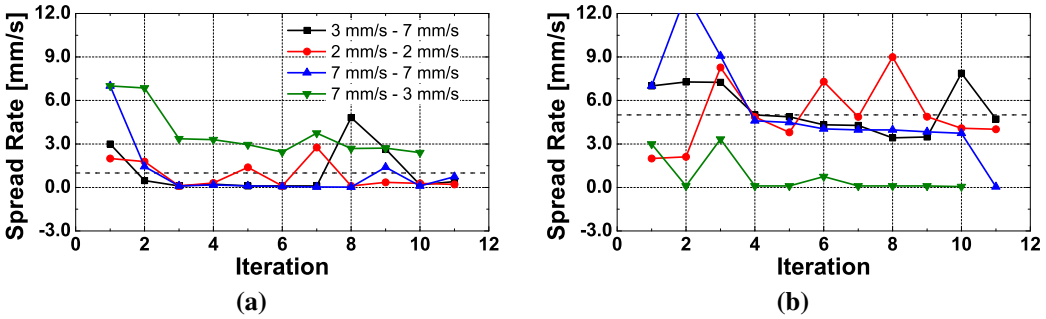

Figure 5.10: The spread rates of 2 independent fires are estimated with only 9 sensors. Graph a) shows the spread rate on the bed, and b) shows the spread rate of the fire growing vertically on the wall as a function of the iteration.

Figure 5.10 shows the estimation process for the parameters using the test case as presented in section 5.5.3, with a fire on the bed and a second, vertically growing fire on the wall. Only 9 sensor locations were used for assimilation, distributed uniformly throughout the ceiling as indicated in Fig. 5.5, where the thermocouples that are considered are enclosed in a circle. It is clear from Fig. 5.12 that 9 sensors are not enough to differentiate between the two spread rates. Convergence of parameters is not generally obtained.

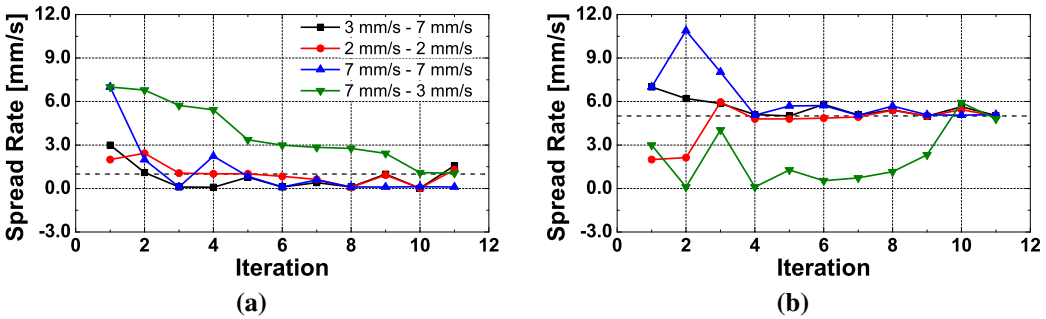

Figure 5.11: The spread rates of 2 independent fires are estimated with only 30 sensors. Graph a) shows the spread rate on the bed, and b) shows the spread rate of the fire growing vertically on the wall as a function of the iteration.

Using 30 uniformly distributed sensor locations (the thermocouples marked with a cross in Fig. 5.5) for assimilation results in a better estimation of the parameters as shown in Fig. 5.11, although convergence cannot be obtained for all first guesses in less than 10 iterations. For those first guesses, where the parameters can be considered to converge, the estimations are within 15% of the true values.

Figure 5.12 shows the convergence history for the parameters in the case that only

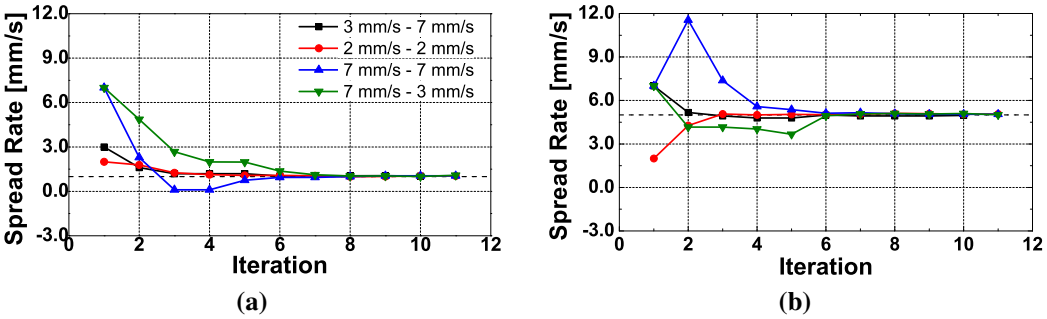

Figure 5.12: Estimation of spread rates using sensors close to the fire and discarding sensors far away from the fire location; a) shows the convergence of the spread rate on the bed, and b) shows the spread rate of the fire growing vertically on the wall.

the sensors in the back part of the compartment, where the bed is located, are considered for the assimilation. The parameters are estimated more accurately than in the case where all sensors are considered (Fig. 5.8). This is explained by the sensors away from the fire not providing useful information, but rather blurring the information provided by sensors closer to the fire and thus making the overall estimation process less accurate.

5.5.6 Alternative sensors

Additionally to the parameters related to the boundary conditions, other model parameters can be of interest and may have to be estimated. Soot production in fires is subject to ongoing research, and state-of-the-art fire modelling tools cannot accurately predict the soot concentration even for simple pool fires [28]. In FDSv5 the soot yield is not computed as a result of combustion, but is an input parameter for the simulation. A global soot yield is therefore estimated alongside with the fire growth rate.

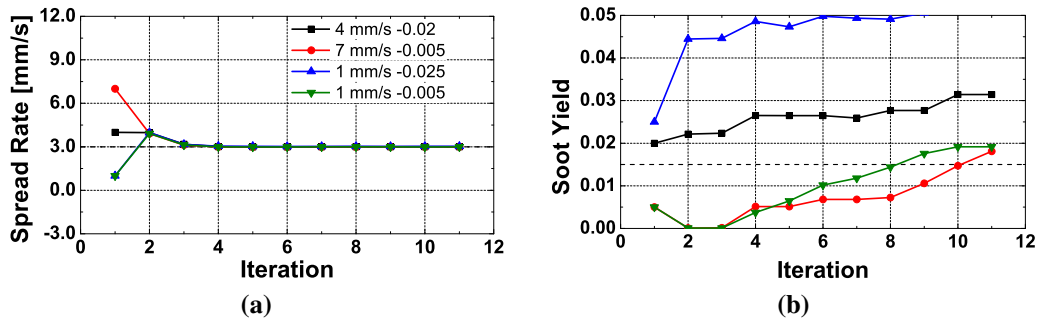

Figure 5.13: Estimation of the spread rate and soot yield in a compartment fire; a) shows the convergence of the spread rate on the bed, and b) shows the soot yield.

Figure 5.13 shows that while the spread rate can be estimated correctly after 4 iterations, the soot yield cannot be obtained by assimilating temperature data. The influence of differences in the soot yield on the temperature distribution is minimal due to the decoupling of soot production from the combustion. Therefore the temperature data alone will not help to differentiate between different soot yields.

Other data will have to be used in order to estimate the soot yield of the fire. Beam detectors are widely used as smoke detectors in industrial facilities. They consist of a laser emitter on one side, and a receiver on the other side across the compartment. The incoming light at the receiver is compared to the intensity emitted, and a percentage of obscuration is calculated. When a certain threshold is passed due to obscuration of smoke, an alarm is triggered. Although beam detectors are currently only used in a binary mode (fire/no fire), it is possible to extract the value of obscuration and use it for comparison to models.

The previous test case is repeated estimating the spread rate of a single burning fire alongside the soot yield of the fire. This time, instead of the ceiling temperature, obscuration measurements are assimilated into the model. The location of the beam detectors is indicated in Fig. 5.5.

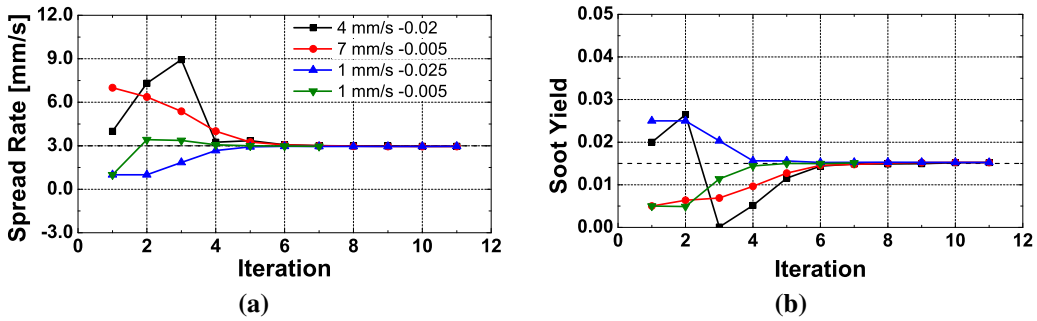

Figure 5.14: Estimation of spread rate and soot yield in a compartment fire using beam detectors as observations for comparison. Graph a) shows the convergence of the spread rate; b) shows the convergence of the soot yield towards the "true" value.

Figure 5.14 shows the convergence behaviour for the spread rate and the soot yield. The obscuration due to the smoke of the fire provides enough information for the accurate estimation of these two parameters.

When adding the fuel burning rate as a parameter to estimate, the obscuration data alone could not pick up the joint contributions of spread rate and fuel burning rate to

the overall HRR. For the full characterization of a compartment fire, including spread rate, fuel burning rate and the soot production, the beam detectors were therefore used in conjunction with thermocouples in the ceiling.

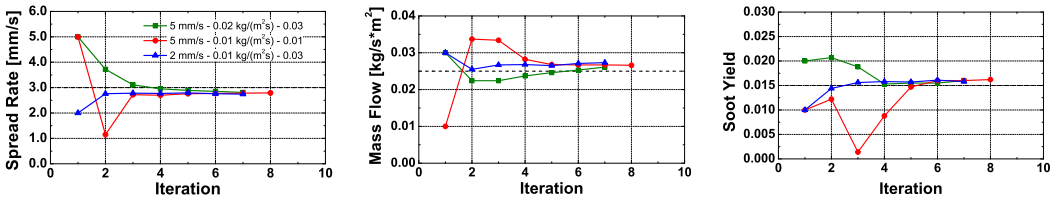

Figure 5.15: Characterization of a compartment fire. Graph a) shows the convergence of the spread rate. b) shows the convergence of the burning rate, and c) shows the estimation of the soot yield of the fire.

The thermocouple data together with the obscuration provided the necessary information for the estimation of all three parameters, as shown in Fig. 5.15. The spread rate (Fig. 5.15a) and the soot yield of the fire (Fig. 5.15c) are estimated with acceptable accuracy after 4 to 5 iterations. Convergence of the fuel mass flow rate (Fig. 5.15b) can take more than 6 iterations for certain combinations of first guesses.

5.6 Forecasting Fire Growth in a Compartment

The forecast of a physical process relies on a good estimation of the invariant parameters. A typical forecast cycle thus includes a data collection period, an assimilation period where the boundary and initial conditions are estimated, and finally a forecast based on those estimated parameters.

In the previous sections the estimation of invariant parameters is demonstrated (which corresponds to the assimilation of data). Generally it takes 6 to 8 iterations of the optimization cycle to obtain convergence. Each iteration involves many parallel executions of the CFD model (in this case FDSv5), so that each iteration lasts as long as it takes to run the slowest of the parallel CFD runs. Bearing in mind that a detailed CFD model can take several hours and even days to run, it would not be practical to use them for forecasting, as the lead time will be negative (i.e. the prediction arrives after the event has taken place).

However, since measured data are assimilated into the model, the fire could be

modelled in a much cruder way. The observations from the fire will provide the information lost by the approximations of the model. Computations can thus be accelerated considerably. Using grid cells with an edge of 25 cm will speed up the calculations over 100 times compared to grid cells with an edge of 5 cm.

The methodology presented in section 5.4 is independent of the size of grid cells that are used for the forward model, as long as it represents the flow field and temperature profiles within acceptable bounds. The CFD code (FDSv5) was tested for different grid sizes, and it was established that for a grid size with cell edges of 25 cm, temperature profiles were still in good agreement with simulations done with grid cells of 5 cm edges (compare chapter 2). It was thus decided to use 25 cm edged grid cells for the inverse model and the subsequent forecast.

Note that the lead times presented in the following sections refer to the time between the end of the assimilation window and the time where the forecast diverges from the true fire development. The assimilation time (i.e. the time it takes to estimate the parameters and to make a forecast) is not considered, since it would not be possible to obtain positive lead times considering these times in spite of the greatly reduced computation time. Using CFD to produce useful forecasts (that are available *a priori*, i.e. before events take place) of fire events is at the present far from being applicable. The goal of this paper is to illustrate that when observations from the fire are assimilated into the model, it is possible to reduce computation time considerably without losing accuracy.

Deciding the width of the assimilation window requires some analysis, since it has to be sufficiently large as to gather enough data, but small enough to still leave time to make a forecast.

The same fire scenario as presented in Fig. 5.4 was used to forecast fire growth with sensor locations as shown in Fig. 5.5. A fine grid (5 cm) FDSv5 simulation was run in order to produce the most realistic observations possible, and a coarse grid (25 cm) model was used to for assimilation and forecast. The true spread rate was fixed at 5 mm/s, which corresponds to a medium to fast fire typical in mattresses [4]. The geometry of the compartment is assumed known, as are fuel type, fuel location and fire origin.

As opposed to the previously discussed cases, where ceiling wall temperatures were

used, gas temperatures close to the ceiling were used for assimilation into the model in this case. In a CFD model temperatures are calculated in the center of each grid cell, representing thus the average temperature of the whole cell. This can lead to important underpredictions of the temperature close to the ceiling if the cell size is larger then the depth of the ceiling jet, resulting in an underprediction of the heat fluxes to the ceiling and a subsequent underprediction of the wall temperature.

The grid cell size in the forward model is 25 cm, which is more than the typical depth of the ceiling jet (less than 20 cm). In order to overcome the underprediction due to average temperatures in the forecast model, observations were taken inside and outside the ceiling jet in the true fire, and an average of both was used for assimilation.

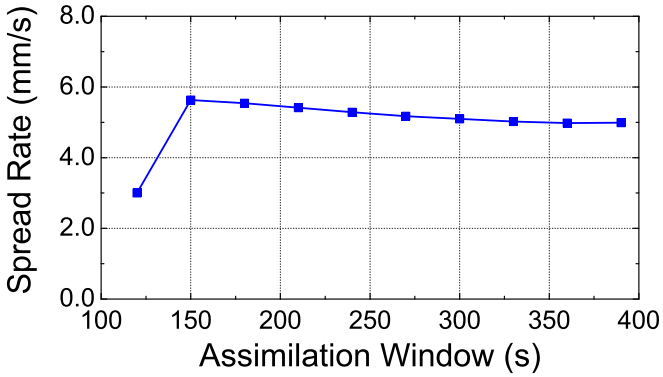

Figure 5.16: Spread rate as a function of the growing assimilation window.

Figure 5.16 shows the estimated spread rate of the fire as a function of the width of the assimilation window. With 150 s worth of data the spread rate is estimated to be 5.63 mm/s, 13% higher than the spread rate of the true fire. As more data come in a better estimation can be made, and after 330 s worth of data the estimated spread rate is within 1% of the true spread rate.

Figure 5.17 shows the forecast made with 150 s of data. The coarse grid simulation used for the assimilation cycle is not able to pick up the early fire growth correctly, producing an overprediction of the spread rate. As a consequence of this the HRR is overpredicted (Fig. 5.17a), which results in forecasted temperatures higher than the true fire development (Fig. 5.17b). The lead time, defined as the time ahead of the event during which the forecasted temperature is less than 15% off the true temperature, is only approximately 50 s.

Figure 5.18 shows the forecast made with 330 s worth of data. The HRR is in very

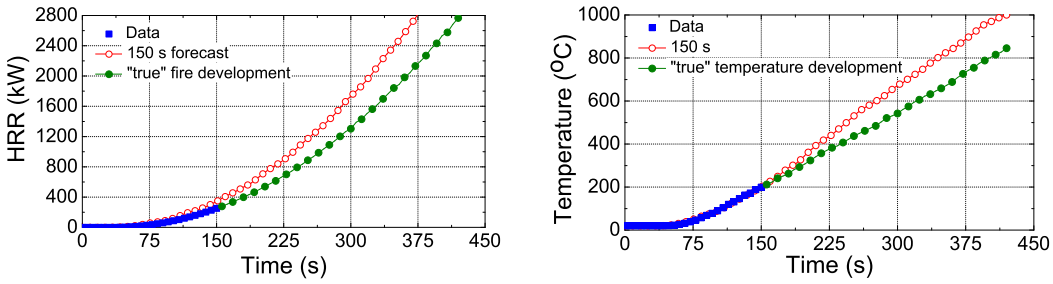

Figure 5.17: Forecast after 150 s of assimilated data. The observed data is shown together with the future development and the forecast of the fire; a) HRR b) Average Ceiling Jet temperature.

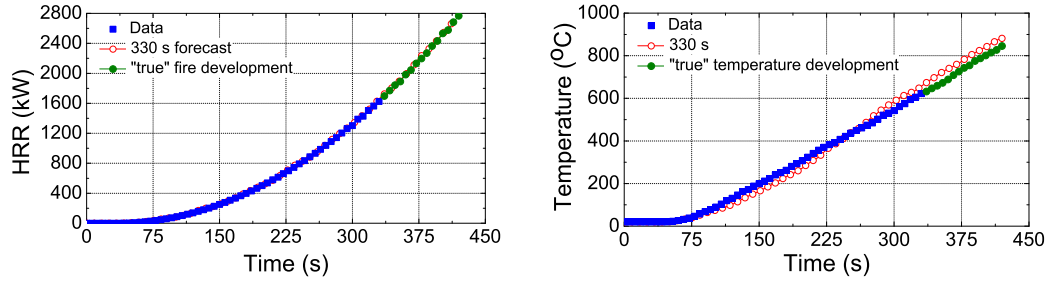

Figure 5.18: Forecast after 330 s of assimilated data. The observed data is shown together with the future development and the forecast of the fire; a) HRR b) Average Ceiling Jet temperature.

good agreement with the true fire (Fig. 5.18a), and although forecasted temperatures are slightly higher than the true fire development (9%), the slope of the temperature curve is equal to the true fire development (Fig. 5.18b). The lead time in this case is thus limited only by the next critical event that will change the burning behaviour fundamentally.

The assimilation and forecast cycle using 330 s of data took around 10 minutes on a standard dual core PC. If a blind prediction of the same fire scenario (without feedback from the fire) were to be made, it would require grid cells with edges of the order of less than a centimeter in order to be able to reproduce the underlying physics with enough accuracy. Such a simulation would take several weeks to run (compare [19]).

5.6.1 Unknown Fuel Source

Although the geometry of the room (walls, windows, doors) does usually not change and might therefore assumed to be known, the exact location and size of the fuel source

might not be well defined beforehand. Desks, chairs, bed and other potential fire loads can be moved freely within the compartment, and their exact composition and layout at the moment of a fire event are not easy to establish.

The sensitivity of a forecast to the assumptions regarding the fuel load are investigated. Note that the fire origin is relatively easy to obtain (as a first order approximation it would be enough to select the location of the thermocouple with the highest temperature reading), and can therefore always be assumed as known. The exact dimensions and location of the fuel load on the other hand are unknown.

As more detailed information is missing, the surface of the fuel load in the forward model is assumed to cover all the area of the compartment, although at an elevated level (0.4 m above the floor, at the height of the fire origin). The fire is thus not restricted to the area of the bed. This will obviously lead to a larger fire size than in the true fire once all the surface of the bed is burning, and subsequent divergence of the forecast from the true fire later on, as the fire growth is only limited by the walls of the compartment.

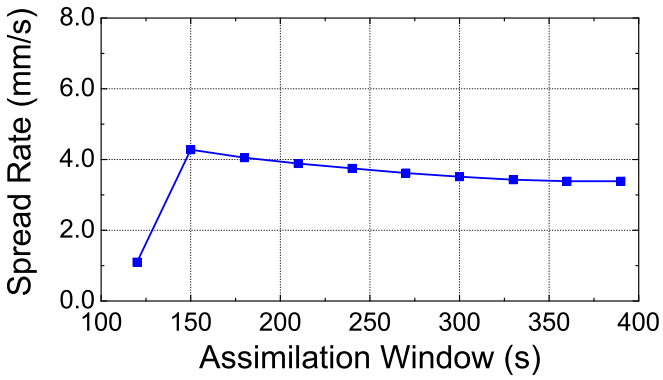

Figure 5.19: Spread rate as a function of the growing assimilation window with unknown fuel load.

Figure 5.19 shows the estimated spread rate of the fire as a function of the width of the assimilation window. The estimated spread rate is much smaller than the true spread rate. This is due to the layout of the true fire, which starts at the corner of the bed. Thus the initial fire area grows as the quarter of a circle. In the forward model without prior knowledge of the fuel source the fire does not start at a corner (although still at the wall) and can grow as a half-circle. For the same fire area the forward model without prior knowledge of the fuel has thus a smaller radius (i.e. smaller spread rate).

Figure 5.20 shows the forecast made with 330 s worth of data. Although the HRR is

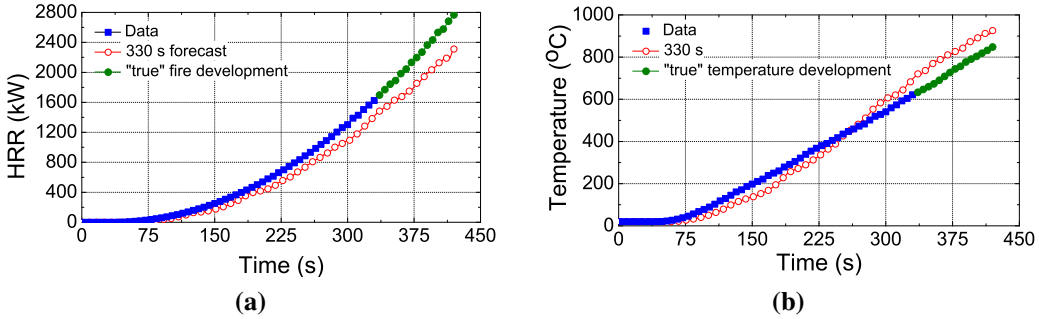

(a) **(b)**

Figure 5.20: Forecast after 330 s of assimilated data with no prior knowledge of the fuel load. The observed data is shown together with the future development and the forecast of the fire; a) HRR b) Average Ceiling Jet temperature.

underpredicted by around 15% (Fig. 5.20a), the temperatures are in good agreement with the true fire (Fig. 5.18b), and the forecast lies within 13% of the true fire development. Note that temperatures are only recorded close to the ceiling, and that the lower HRR leading to higher temperatures is thus not necessarily a contradiction. It is conjectured to be the result of a different flow pattern due to a different fire area [15].

5.7 Conclusions

Fire dynamics combine a series of complex physical processes that are closely coupled to each other by nonlinear relations and are therefore hard to model. Predictive modelling of fire dynamics gives rise to further complications, as very different length and timescales have to be solved simultaneously and the computational resources are limited, so that it is impossible to solve the entire physics in reasonable time (let alone with positive lead time). In state-of-the-art fire modelling the HRR is thus an input into the model rather than a result of the modelling. Therefore the forecast capabilities of fire modelling tools are limited, and it has been shown that blind predictions of real scale fire tests are not possible [5].

The proposed methodology was implemented in a real-scale fire simulation, and different parameters were estimated with a reasonable computational effort.

It was shown that it is possible to estimate the parameters that govern fire growth using CFD fire modelling together with measured data from the fire, and thus to decouple the highly complex processes of heat transfer from the flame and pyrolysis

in the solid phase. This approach allows for the use of relatively coarse grids, as mass and heat transfer from the fire to the sensor locations are the model outputs of interest, and the high resolution in the flaming region (which would be needed for an accurate description of the coupling between gas and solid phase) is not necessary. It was shown that several invariants can be estimated simultaneously and the effect of sensor density and distribution was investigated. It was further shown that the methodology presented does not require an exact knowledge of the fuel layout in the compartment, although the location of the fire origin is assumed known.

A relatively coarse CFD simulation was used to assimilate temperature observations, and useful forecasts could be produced in a time comparable to a characteristic fire duration. While this is still not practical for real world applications, the computation time could be reduced by several orders of magnitude compared to an equivalent fully detailed simulation, by substituting details that were lost as a consequence of the coarse grid with observations from the fire. The 10 minutes assimilation time obtained in this work is deemed by the authors to be reducible in another order of magnitude in the near future by advances in computational power. The methodology presented in this paper constitutes thus a feasible step towards useful fire scenario forecasts with a positive lead time.

References

[1] W. Davis, R. Vettori, P. Reneke, and L. Brassel. Workshop on the Evaluation of a Tactical Decision Aid Display. NIST report NISTIR 7268, 2005.

[2] R. Upadhyay, G. Pringle, G. Beckett, S. Potter, S. Han, S. Welch, A. Usmani, and J.L. Torero. An Architecture for an Integrated Fire Emergency Response System for the Built Environment. *Fire Safety Science*, 9:427–438, 2008. DOI:10.3801/IAFSS.FSS.9-427, http://www.era.lib.ed.ac.uk/handle/1842/2703.

[3] A. Cowlard, W. Jahn, C. Abecassis-Empis, G. Rein, and J.L. Torero. Sensor Assisted Fire Fighting. *Fire Technology*, in press, 2008. DOI:10.1007/s10694-008-0069-1.

[4] D. Drysdale. *An Introduction to Fire Dynamics*. ISBN 0-471-97290-8. Wiley & Sons, New York, 2nd edition, 1998.

[5] G. Rein, J.L. Torero, W. Jahn, J. Stern-Gottfried, N.L. Ryder, S. Desanghere, M. Lazaro, F. Mowrer, A. Coles, D. Joyeux, Alvear D., J. Capote, A. Jowsey, C. Abecassis-Empis, and P. Reszka. Round–Robin Study of *a priori* Modelling Predictions of the Dalmarnock Fire Test One. *Fire Safety Journal*, 44(4):590–602, 2009. DOI:10.1016/j.firesaf.2008.12.008, http://www.era.lib.ed.ac.uk/handle/1842/2704.

[6] E. Lorenz. Deterministic Nonperiodic Flow. *Journal of the Atmospheric Sciences*, 20(2):130–141, 1963.

[7] E. Kalnay. *Atmospheric Modeling, Data Assimilation and Predictability*. ISBN 978-0-521-79629-3. Cambridge University Press, Cambridge, 1st edition, 2003.

[8] T. Schlatter. Variational Assimilation of Meteorological Observations in the Lower Atmosphere: A Tutorial on How it Works. *Journal of Atmospheric and Solar–Terrestial Physics*, 62(17):1057–1070, 2000.

[9] J. Hoke and R. Anthes. The Initialization of Numerical Models by a Dynamic–Initialization Technique. *Monthly Weather Review*, 104(12):1551–1556, 1976.

[10] D. Harms, S. Raman, and R. Madala. An Examination of Four–Dimensional Data Assimilation Techniques for Numerical Weather Prediction. *Bulletin Amercian Meteorolical Society*, 73(4):425–440, 1992.

[11] R. Richards, B. Munk, and O. Plumb. Fire Detection, Location and Heat Release Rate Trough Inverse Problem Solution. Part I: Theory. *Fire Safety Journal*, 28(4):323–350, 1997. DOI:10.1016/S0379-7112(97)00005-2.

[12] M. Leblanc and A. Trouvé. Inverse Modeling of Enclosure Fire Dynamics. In *Proceedings of the 6th U.S. National Combustion Meeting*, 2009.

[13] S. Koo, J. Fraser-Mitchell, and S. Welch. Sensor-steered fire simulation. *Fire Safety Journal*, 45(3), 2010. DOI:10.1016/j.firesaf.2010.02.003.

[14] A. Cowlard, L. Auersperg, J.B. Richon, G. Rein, S. Welch, A. Usmani, and J.L. Torero. A Simple Methodology for Sensor Driven Prediction of Upward Flame Spread. *Turkish Journal of Engineering and Environmental Sciences*, 31(6):403–413, 2007.

[15] W. Jahn, G. Rein, and J.L. Torero. The Effect of Model Parameters on the Simulation of Fire Dynamics. *Fire Safety Science*, 9:1341–1352, 2008. DOI:10.3801/IAFSS.FSS.9-1341, http://www.era.lib.ed.ac.uk/handle/1842/2696.

[16] K. McGrattan, R. Rehm, and H. Baum. Large Eddy Simulations of Smoke Movement. *Fire Safety Journal*, 30(2):161–178, 1998.

[17] H. Forkel and J. Janicka. Large–Eddy Simulation of a Turbulent Hydrogen Diffusion Flame. *Flow, Turbulence and Combustion*, 65(2):163–175, 2000. DOI:10.1023/A:1011497715385.

[18] W. Xie and P. DesJardin. An Embedded Upward Flame Spread Model using 2D Direct Numerical Simulations. *Combustion and Flame*, 156(2):522–530, 2009. DOI:10.1016/j.combustflame.2008.11.011.

[19] J.W. Kwon, N. Dembsey, and C. Lautenberger. Evaluation of FDS v.4: Upward Flame Spread. *Fire Technology*, 43(4):255–284, 2007. DOI:10.1007/s10694-007-0020-x.

[20] C. Fernandez-Pello. The Solid Phase. In G. Cox, editor, *Combustion Fundamentals of Fire*, chapter 2. Academic Press Ltd., 1995.

[21] L. Cooper. Compartment Fire-Generated Environment and Smoke Filling. In P. DiNenno, editor, *SFPE Handbook of Fire Protection Engineering*, chapter 3–10, pages 3–243–3–267. National Fire Protection Association, Quincy, MA 02269, 3 edition, 2002.

[22] S.N. Sivanandam and S.N. Deepa. *Introduction to Genetic Algorithms*. ISBN 978-3-540-73189-4. Springer Verlag, Berlin, Heidelberg, 1st edition, 2008.

[23] J. Nocedal and S. Wright. *Numerical Optimization*. ISBN 978-0387-30303-1. Springer, USA, 2nd edition, 2006.

[24] F. Bouttier and P. Courtier. Data Assimilation Concepts and Methods. Technical report, European Centre for Medium-Range Weather Forecasts, 2001.

[25] V. Babrauskas. Heat Release Rates. In P. DiNenno, editor, *SFPE Handbook of Fire Protection Engineering*, chapter 3–1, pages 3–1–3–37. National Fire Protection Association, Quincy, MA 02269, 3 edition, 2002.

[26] W. Jahn, G. Rein, and J. L. Torero. Data Assimilation in Enclosure Fire Dynamics - Towards Adjoint Modelling. In T. Burczynski and J. Périaux, editors, *Evolutionary Methods for Design, Optimization and Control*. CIMNE, Barcelona, Spain, 2009.

[27] A. Cowlard. *Sensor and Model Integration for the Rapid Prediction of Concurrent Flow Flame Spread*. PhD thesis, The University of Edinburgh, 2009. http://www.era.lib.ed.ac.uk/handle/1842/2753.

[28] J.B. Moss, C. Stewart, and K. Young. Modelling Soot Formation and Burnout in a High Temperature Laminar Diffusion Flame Buning under Oxygen-Enriched Conditions. *Combustion and Flame*, 101(4):491–500, 1995. DOI:10.1016/0010-2180(94)00233-I.

6

Estimation of the Fire Growth Rate in a Real-Scale Fire Test

6.1 Introduction

Forecasting fire dynamics is conjectured to lead to a paradigm shift in the response to fire emergencies in buildings, providing the fire service with essential information about the development of the fire with some lead time (i.e. seconds or minutes ahead of the event) [1]. An attempt to apply a forecasting methodology to fire dynamics of a real fire is presented in this chapter using the inverse model methodology developed in chapter 5, and using the real scale experiment of Dalmarnock Test One. The spread rate of a fire on a burning sofa in a full scale compartment is estimated using an inverse modelling approach, and a forecast of the fire development is made.

The term 'forecast' is used in the context of this chapter as a theoretical process of predicting fire development based on comparison to observations from the evolving fire scenario, i.e. based on (automatic) tuning of the model with information received from observations. In reality positive lead times can not yet be provided if numerical fire models are used for the forecast, as the assimilation process alone still takes longer

than a typical fire scenario (15-20 min assimilation compared to 5 min fire), despite important simplification and resulting speed-up (see chapter 5).

The experimental set up, procedure and results of the Dalmarnock Tests are presented elsewhere ([2, 3], chapter 2), and will not be discussed here.

In chapter 2 the early HRR development of Dalmarnock Test One, which had not been measured during the test, was estimated by comparing field model output to observations from the test. Based on laboratory experiments, two HRR curves were established that provided an upper and a lower bound for a possible HRR. Although the modelling work was done *a posteriori*, it suggested that CFD type modelling could be used to recover to a certain extent the underlying physics of the fire growth in a real compartment fire. However, the lead time of that approach was in the order of months (that is the time it took to establish the HRR bounds), which is far from a positive lead time.

6.1.1 Simplified Forecast

The technology of forecasting fire dynamics based on numerical simulation of the underlying physics is currently non-existent because available fire simulation tools cannot predict fire growth in a fast, precise and robust manner.

Nevertheless, a very simple and fast way of forecasting fire development is to analyze the time history of the average temperature in the compartment (which can be estimated from live observations from the fire scenario). An adequate curve can be fitted to the available data and, assuming that the temperatures grow following the same curve, it is possible to forecast the average temperature with some acceptable uncertainty.

Figure 6.1 shows the average compartment temperature during the first 300 s of Dalmarnock Test One. After an initial rapid increase the temperatures follow a relatively slow linear growth until about 220 s. If a forecast was made 200 s after ignition, the temperatures would be well approximated by a linear fit as indicated in Fig. 6.1. Due to the decoupling from the underlying physics, the forecast can not anticipate changes in the growth pattern and is limited to short times (in this case until 220 s). The usefulness of this approach for assisting the decision making process of commanding fire service

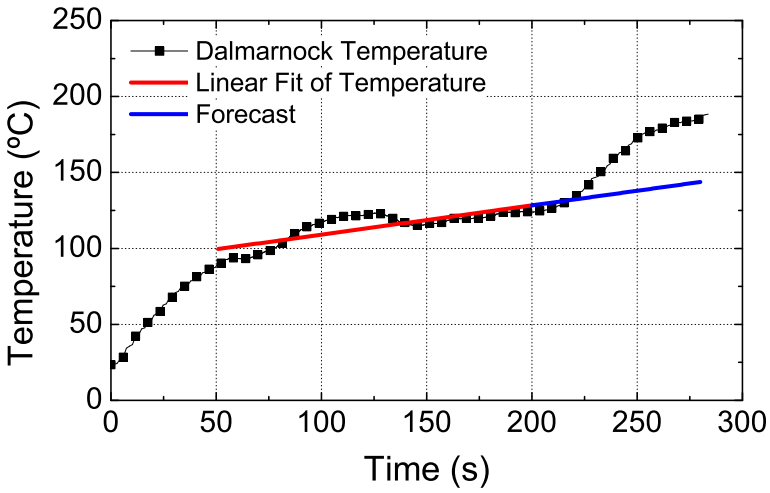

Figure 6.1: Forecast based on simple curve fitting.

officers is equally limited, especially considering that the forecast is only valid for those sensor locations whose readings are included in the observations (if thermocouples are only installed close to the ceiling, the forecasted development is only for temperatures close to the ceiling, not for general temperatures). However, the forecast is almost instantly available without the use of extensive computational resources, and any more sophisticated forecasting system will have to outperform this approach (at least in some way) in order to be considered for implementation.

The methodology presented in chapters 4 and 5 if applied to real data could provide a useful, physics based forecast within a reasonable time frame.

The simplified and decoupled fire growth model presented in chapters 4 and 5 is thus implemented, estimating the spread rate of the fire on the sofa. Other parameters necessary for the simulation of a complex fire scenario such as Dalmarnock Test One were taken from previous analysis and are assumed to be known.

6.2 Prior analysis

The ignition and early burning of the sofa in the Dalmarnock Fire Tests was reproduced in several laboratory experiments in order to provide an input HRR for numerical modelling of the Tests (see chapter 2). The first of these experiments was conducted before the Dalmarnock Test series was carried out, and the ignition protocol differed somewhat from the protocol finally adapted in Dalmarnock. In the laboratory experiments the

ignition source (a basket filled with crumpled waste paper and some accelerant) was standing next to the sofa without direct contact to the sofa, whereas in Dalmarnock both items (bin and sofa) were connected by means of a blanket placed over the armrest and hanging into the waste paper basket. Accelerant had been spilled in the bin and on the blanket in order to assure reasonably rapid ignition of the seating area of the sofa.

A second series of laboratory experiments was conducted after the Dalmarnock Tests. In these experiments the ignition protocol was reproduced as closely as possible based on layout information, photographs and video recordings from Dalmarnock.

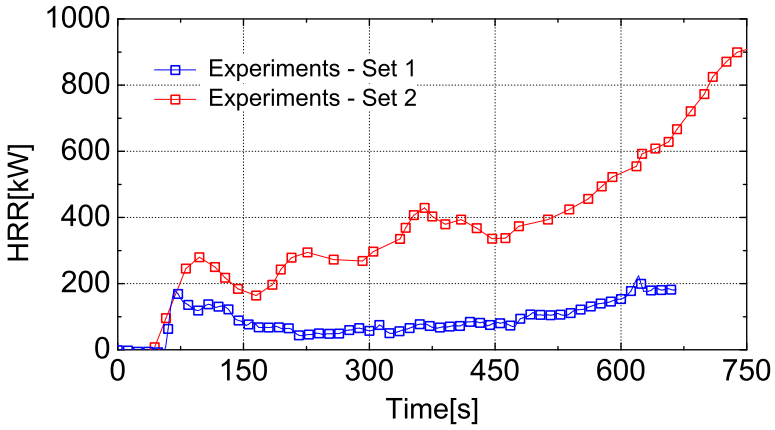

Figure 6.2: HRRs for sofa as measured in laboratory experiments.

Figure 6.2 shows the HRRs as estimated using oxygen depletion calorimetry in the laboratory experiments. The blue data correspond to the first experiment (Set 1, carried out before the Dalmarnock Tests), while the red correspond to the second series of experiments (Set 2, carried out after the Tests). The blanket, included in Set 2, is conjectured to have acted as a bridge between the burning bin and the seating area of the sofa, bypassing the barrier of the armrest. The fire could thus spread to the seating area of the sofa more easily.

The HRR curves presented in Fig. 6.2 show two distinct patterns in time (this is discussed with more detail in chapter 2). The initial peak, that can be attributed to the burning of the waste paper bin, is followed by a slower growth which is conjectured to correspond to the sofa itself. The growth on the sofa can be approximated to good agreement by a quadratic curve.

Figure 6.3 shows the HRRs with their respective t^2-fit and the HRR of the waste paper bin together with the blanket (which is obtained by resting the t^2-fit from the

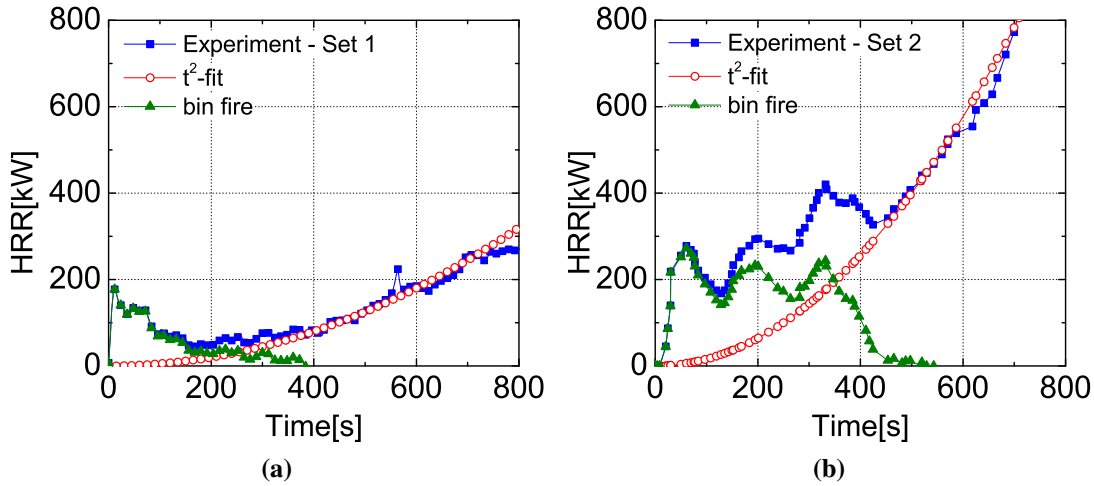

Figure 6.3: Quadratic fit of the HRR curves measured in the laboratory experiments with estimated bin fire; a) experiment prior to Dalmarnock (Set 1 according to chapter 2), b) second series of experiments, conducted after Dalmarnock (Set 2 according to chapter 2).

original data). The contribution of the bin fire is negligible after about 400 s in both cases.

The t^2-curve that can be fitted to both laboratory experiments confirms the validity of a fire growth consistent with the growth model proposed in chapter 5, where the HRR is assumed to be proportional to the fire area,

$$\dot{Q} = \Delta h_c \dot{m} = \Delta h_c \dot{\omega} A(r, t). \tag{6.1}$$

Here Δh_c is the effective heat of combustion (in kJ/kg), r (m/s) is the spread rate of the fire (assumed constant), and $\dot{\omega}$ (kg/s$\cdot$m^2) is the fuel burning rate per unit area. As long as the fire does not reach the boundaries of the fuel surface the fire area is circular ($A(r,t) = \pi(r(t-t_0))^2$), and the resulting HRR follows a quadratic growth.

The fire spread model presented in equation (6.1) is thus used in this approach to characterize the fire growth, and the growth rate is estimated.

6.3 Model Details

The fire specific CFD code Fire Dynamics Simulator version 5.1.6 (FDSv5) [4] is used for the fire simulations in the forward model. FDS solves a form of the Navier-Stokes equations adequate for low-speed thermally driven flows.

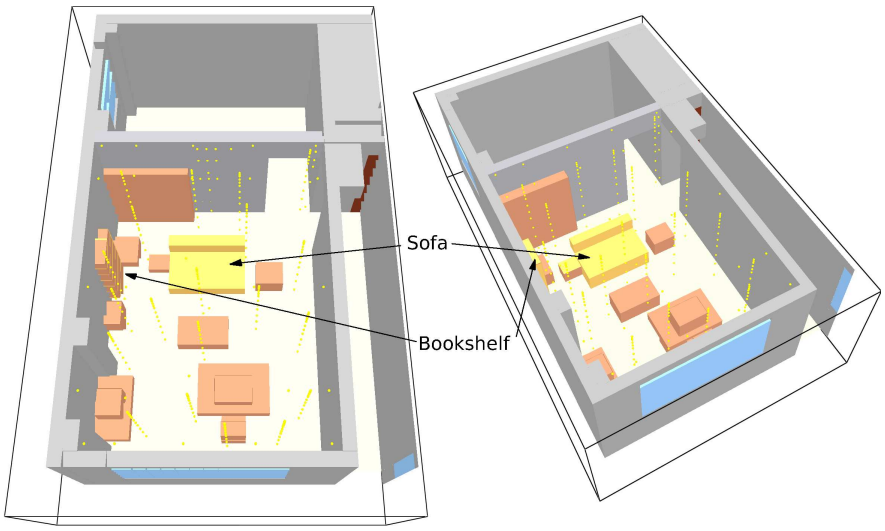

Figure 6.4: Computational domain and fuel items used in the FDS simulations.

6.3.1 Computational Domain

Detailed information about the experimental set-up of Test One can be found elsewhere [2, 3]. Test One was held in a two-bedroom single family flat, with the living room set up as the main experimental compartment.

In order to make the modelling more efficient in terms of computational time, the computational domain concentrated on the main compartment room of Dalmarnock Test One and its vent openings (Figure 6.4). This compartment was 3.50 m by 4.75 m wide and 2.45 m high with a 2.35 m by 1.18 m two-pane window. A detailed account of the model set up is given in chapter 2. For eventual fluid dynamic effects on the ventilation flows, the kitchen and an artificial hallway adjacent to the main compartment are included as shown in Fig. 6.4. The other rooms of the apartment were not considered, since they did not contribute to the fuel load nor significantly affected the ventilation flows.

The fuel load in the main compartment included the sofa and two bookshelves in the corner behind the sofa as shown in Figure 6.4. Although the coffee table, chairs and desks also contributed to the fuel load, this occurred only after flashover, and will not be considered here.

6.3.2 Grid Size

A grid sensitivity study for FDS applied to the Dalmarnock Test One was conducted by Jahn et al. [5], where it was shown that the results from a simulations with 20 cm grid are still in good agreement with the experiments, although the plume is not well resolved. In the context of this work computational speed is the primary goal, as details that are lost by the insufficient numerical resolution can be recovered from observations from the fire, and a 20 cm grid is thus chosen for the forward model simulations.

6.3.3 Modelling of the Fire

According to the analysis presented above, the fire is modelled in a twofold way. The area of the bin fire is assumed as constant, and its intensity is modelled as a constant HRR per unit area that decreases linearly to zero between 150 s and 250 s. This is a crude approximation of the contribution of the bin to the total HRR as shown by the green data in Fig. 6.3b. The fire growth on the sofa is modelled by subsequent ignition of surface cells according to a prescribed spread rate, starting from a point on the edge of the sofa closest to the burning bin (at the same time the bin ignites). By doing this the fire spread is decoupled from the heat feedback from the flame, and the spread rate becomes the invariant parameter to estimate.

Exact modelling of the fire spread over the sofa is not possible with this approach, due to the complicated geometry of the sofa that can not be captured by the coarse grid. It must be kept in mind however that the exact dimensions of the fuel source are not generally known to the forecasting system, and it is more realistic to assume some kind of equivalent fuel (the determination of a general equivalent fuel load that represents the greatest possible number of fuel sources is as yet a pending issue). In the present case it was assumed that the sofa is a plane surface of 1.44 m^2, which corresponds to the sum of the areas of the sofa's different surfaces (within the restriction that it has to be consistent with the grid). The sofa (i.e. the plane surface that represents it) in the forward model is located in approximately the same place as in the real scenario.

6.3.4 Data Assimilation

The high density of instrumentation in the Dalmarnock Tests and the relatively fine grid of gas phase temperature measurements provide a fairly high number of observations that can be assimilated into the forecasting system. And although it might be argued that sensor distributed as uniformly as seen in the Dalmarnock Tests is not realistic, those sensors that provide the most useful information during the early stages of the fire are the ones close to the ceiling, where the highest temperatures are recorded. Therefore using only sensors close to the ceiling might be sufficient (which is feasible from a operational point of view). In this attempt of using CFD to forecast fire dynamics of a real scale fire test, gas phase temperature observations at locations higher than 1 m were assimilated.

6.4 Forecast Result

The parameter to be estimated was the spread rate of the fire on the sofa. The bin fire was defined based on the results presented in Fig. 6.3b, as mentioned above. All other input parameters that needed to be defined in order to produce a forecast (radiative fraction, soot yield etc) of the fire were set to values within the ranges given in chapter 2 and [6] or to default FDSv5 values if applicable. Two hundred seconds of data were used for assimilation.

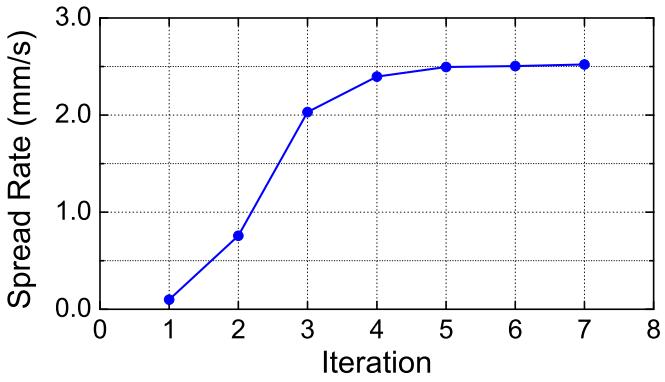

Figure 6.5: Convergence of the spread rate as function of iterations.

Figure 6.5 shows the estimated spread rate as a function of the iterations. The process is started with only a bin fire (spread rate on the sofa is set to zero). After four iterations it has converged to 2.5 mm/s.

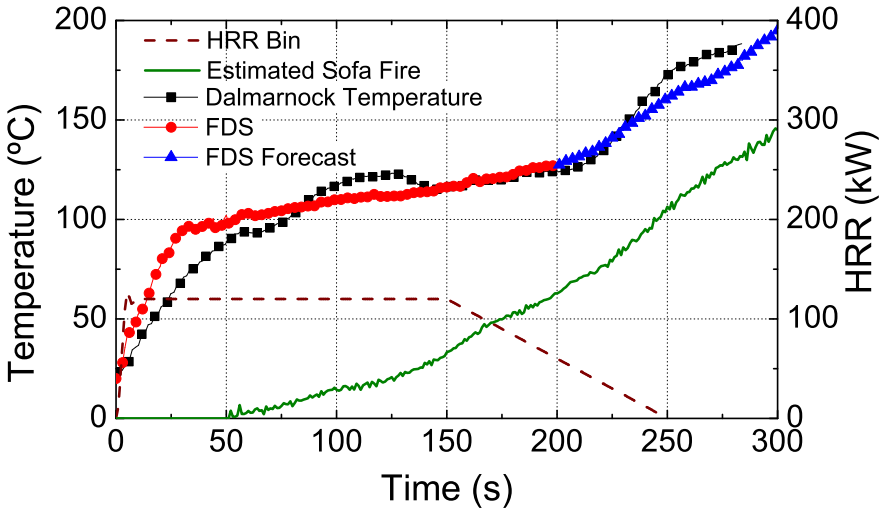

Figure 6.6: Forecast of fire development in Dalmarnock Test One.

The result of the analysis is shown in Fig. 6.6, where a forecast is made with a spread rate of 2.5 mm/s over the sofa. The temperature presented is an average of all the temperature observations considered for assimilation. The black squares represent the observations from Dalmarnock Test One, while the red dots is the model output within the assimilation window (less than 200 s). The blue triangles represent the forecast of the average temperature made based on the information of the assimilated data. The total HRR of the forecast is a combination of the bin fire (dashed line) and the estimated sofa fire (green line). The upwards trend of the observed temperature in Dalmarnock after 220 s is forecasted correctly.

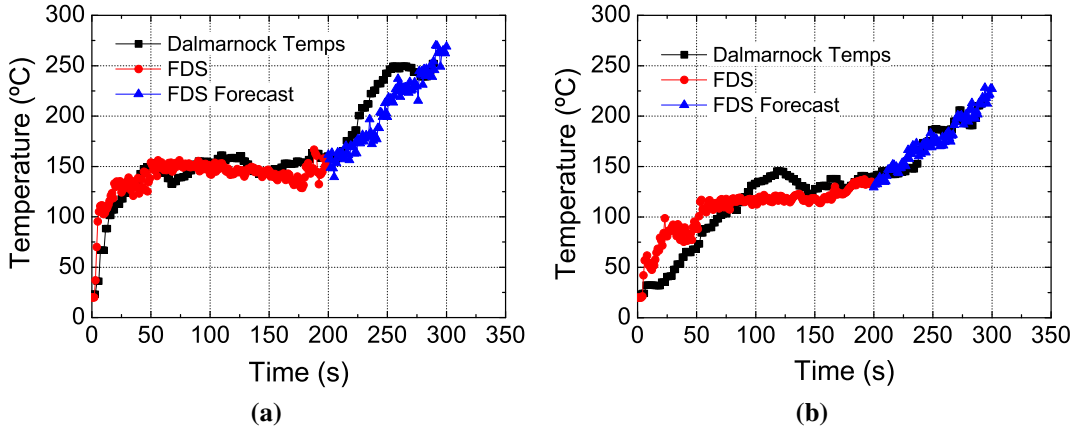

Figure 6.7: Forecast of the temperature at Rack 1 (see Fig 2.1 for sensor location); a) at 230 cm above floor level (15 cm from ceiling) and b) at 160 cm.

The temperature forecasts at six localized points of comparison are presented in

the following sections. Figure 6.7 shows the forecast of temperature development in the north east corner of the compartment (thermocouple rack 1, see Fig 2.1). Although the increase in temperature after 200 s is forecasted with a slightly less steep slope at 230 cm above floor level, the differences between true development and forecast remain within 10%. At the thermocouple at 160 cm above the floor the forecasted temperatures show the same growth rate as the true temperatures.

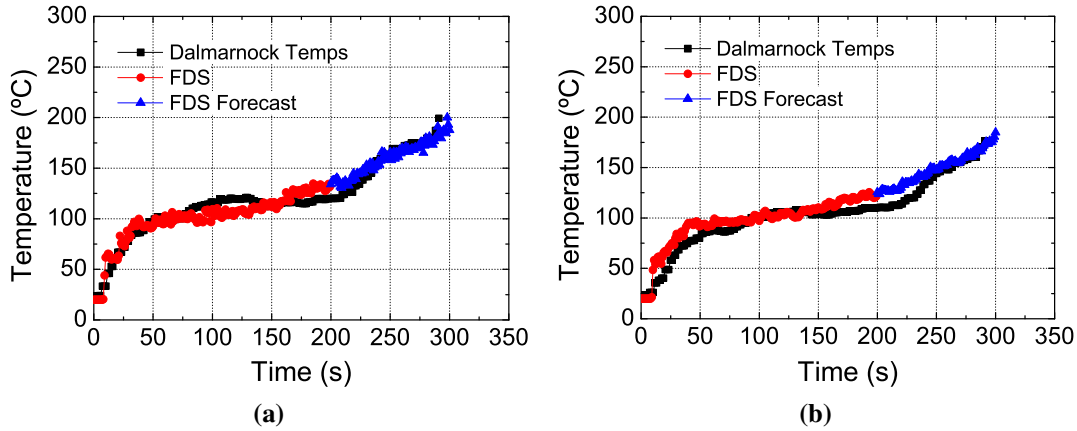

Figure 6.8: Forecast of the temperature at Rack 19 (see Fig 2.1 for sensor location); a) at 230 cm above floor level (15 cm from ceiling) and b) at 160 cm.

Figure 6.8 shows the temperature development at rack 19 in the south west corner of the compartment, close to the window (see Fig. 2.1 for exact location). At 230 cm above the floor the forecasted temperature rise coincides with the true development, providing good agreement until 300 s. At 160 cm above floor level the temperature is slightly overpredicted during the assimilation period (until 200 s), but the forecast is within 10% of the true development.

Close to the flaming region the forecast is expected to be of less quality, due to the low resolution of the numerical grid. Figure 6.9 shows the temperature development at rack 7 located next to the burning waste paper basket. Especially during the early stages of the fire, when the contribution of the basket is considerable and combustion takes place in the cells where the thermocouples are located, the temperatures produced by FDS show great fluctuations and do not agree well with the data from the true fire. The forecasted temperatures present a lower rate of increase compared to the true temperature development.

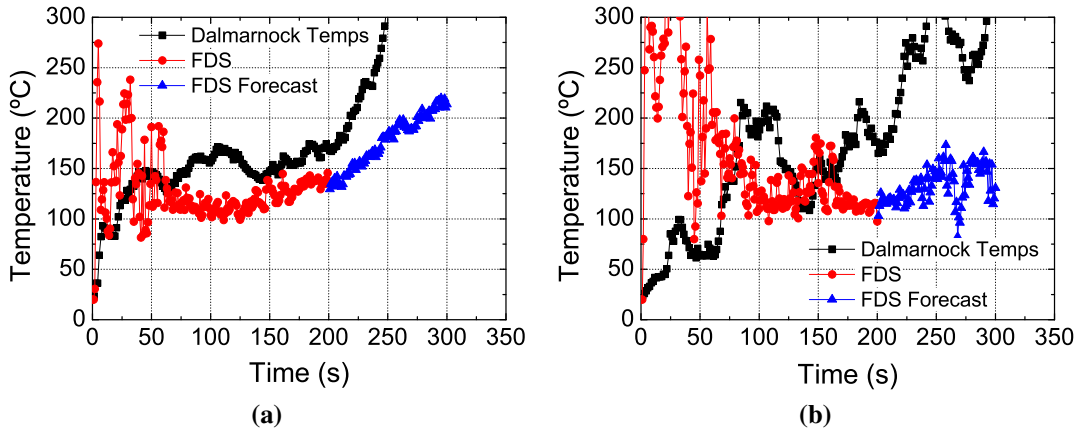

Figure 6.9: Forecast of the temperature at Rack 7 (see Fig 2.1 for sensor location); a) at 210 cm above floor level (35 cm from ceiling) and b) at 140 cm.

6.5 Conclusions

It was possible to find a good fit between the observation and the simulations, and estimate a spread rate that lies within the possible range of values. A forecast of future fire development could be made with a lead time of around 50 s.

A realistic fire spread rate could be estimated based on comparison of model output to measurements of the fire scenario, although it could not be compared to the true value, as no estimation of the spread rate on the sofa was made in the Dalmarnock Tests.

A forecast of a real fire event could be made with a potentially longer lead time than a forecast based on the gradient of the temperature measurements (if, of course, it is assumed that the assimilation time is negligible). While the temperature gradient method predicts a constant growth of 0.19 ^{o}C/s after 200 s, the method presented is able to predict the change in the gradient after 220 s.

Another advantage of this method over the curve fit forecast presented in Fig. 6.1 is that the CFD based forecast is also able to predict localized temperatures, not only average. Here the real strength of the proposed forecast methodology was shown. The forecasted temperature at localized points in the compartment was shown to be in very good agreement with the true development of the temperatures, as long as measurements were compared outside the flaming region. Within the flaming region the forecast is, as expected, of much less quality. Although only a few points of comparison are shown here, the good agreement of the forecast with the true temperature development was

generally observed throughout the compartment. Thus, using this CFD based forecast methodology the temperature at locations away from measurements can be extrapolated, and the spatial distribution of temperatures in the room can be forecasted.

Many issues have still to be addressed. Dalmarnock Test One is a very challenging set of data for the tested methodology. The predominance of the bin fire in the early stages of the fire makes it difficult to correctly estimate the spread rate of the fire on the sofa. Indeed, assuming a different burning pattern for the bin fire (variable instead of constant) would change the estimation of the spread rate of the fire on the sofa, and the robustness of the method has to be investigated in this context.

Another pending matter is the fact that the assimilation time with this forecasting methodology is still not negligible. Although the CFD model could be run with a very coarse grid, it took between 15 to 20 min to estimate the parameters correctly and to produce a forecast. Compared, however, to run times that would be required by traditional CFD based fire spread models with no information feedback from the fire scenario, these results are very close to positive lead times, and it is conjectured by the author that positive lead times will be possible in the near future with this methodology.

References

[1] A. Cowlard, W. Jahn, C. Abecassis-Empis, G. Rein, and J.L. Torero. Sensor Assisted Fire Fighting. *Fire Technology*, in press, 2008. DOI:10.1007/s10694-008-0069-1.

[2] C. Abecassis-Empis, P. Reszka, T. Steinhaus, A. Cowlard, H. Biteau, S. Welch, and G. Rein. Characterisation of Dalmarnock Fire Test One. *Experimental Thermal and Fluid Science*, 32(7):1334–1343, 2008. http://www.era.lib.ed.ac.uk/handle/1842/2513.

[3] Rein, Abecassis-Empis, and Carvel, editors. *The Dalmarnock Fire Tests: Experiments and Modelling*. ISBN 978-0-9557497-0-4. The University of Edinburgh, Accesible at www.era.lib.ed.ac.uk/handle/1842/2037, 1st edition, 2007.

[4] K. McGrattan, R. Rehm, and H. Baum. Large Eddy Simulations of Smoke Movement. *Fire Safety Journal*, 30(2):161–178, 1998.

[5] W. Jahn, G. Rein, and J. Torero. The Dalmarnock Fire Tests: Experiments and Modelling. In Cecilia Abecassis Empis Guillermo Rein and Richard Carvel, editors, *The Dalmarnock Fire Tests: Experiments and Modelling*, chapter 11. The University of Edinburgh, Edinburgh, 2007. http://www.era.lib.ed.ac.uk/handle/1842/2404.

[6] W. Jahn, G. Rein, and J.L. Torero. The Effect of Model Parameters on the Simulation of Fire Dynamics. *Fire Safety Science*, 9:1341–1352, 2008. DOI:10.3801/IAFSS.FSS.9-1341, http://www.era.lib.ed.ac.uk/handle/1842/2696.

7

Conclusions and Future Work

7.1 Conclusions

Fire dynamics combine a series of complex physical processes that are closely coupled to each other by nonlinear relations and are therefore hard to model. Predictive modelling of fire dynamics raises further complications, as very different length and timescales have to be solved simultaneously and the computational resources are limited, so that it is impossible to solve the entire physics in reasonable time (let alone in real time). In state-of-the-art fire modelling the HRR is thus an input into the model rather than a result of the modelling. Therefore the forecast capabilities of fire modelling tools are limited. It was shown in chapter 2, however, that using engineering criteria it is possible to establish lower and upper bounds for possible HRR curves in a real case fire compartment, if access to detailed observations form the fire is available. Although the process was tedious and required extensive time, it confirmed the conjecture that incoming observations from an evolving fire scenario can help to initialize and update forecasts.

A new methodology to effectively forecast fire growth based on assimilation of measured data is thus presented and illustrated in this document. It was shown that simple and robust (zone- or field-type) fire models that are able to deliver an output

in the order of a few minutes can be used to recover detailed information about the ongoing fire event by means of assimilating live recorded data from the emergency scenario. With this information a well informed forecast of the future fire development can be made.

The core of this methodology is a simplified fire growth model which consists of decoupling the gas phase modelling (flame) from the solid phase (pyrolization). Measurements from the fire are used to estimate the parameters that govern fire growth. These parameters are assumed to be constant for a certain period of time, and allow thus for a forecast of future fire development. The methodology is widely independent of the forward model to be used. As long as it represents the fire dynamics to be modelled satisfactorily, any existing model, zone- or field-type, may be used, as it is a 'black box' to the methodology. The methodology was implemented in a real-scale fire simulation, first using a zone type model (chapter 4), and then using a coarse grid CFD model (chapter 5). Finally, in chapter 6, the proposed methodology was tested with data from a real scale fire test.

It was shown in chapter 4 that a simple zone model, based on mass and heat balances between the layers, together with plume correlations, is enough to satisfactorily recover information of the main features of a fire. It was possible to estimate the fire growth invariants correctly and to find a physical basis for their values. It was further possible to provide positive lead times for the growth phase of a fire in the order of 30 s.

When used with a CFD type fire model, the methodology showed that it is possible to estimate the fundamental invariants that govern fire growth such as spread rates and burning rate, and other parameters associated to fire. Relatively coarse grids could be used in the assimilation and forecast, as a high resolution in the flaming region (which would be needed for an accurate description of the coupling between gas and solid phase) is not necessary. Although temperature measurements are the most obvious observations to be assimilated, other measurements, e.g. smoke obscuration, proved to be essential as a complement for parameters that are largely insensitive to temperatures.

A useful, physics based forecast of a fire development could be produced in a time comparable to a characteristic fire duration using a CFD type forward model. While this is still not practical for real world applications, the computation time could be reduced by several orders of magnitude compared to an equivalent fully detailed simulation, by

substituting details that were lost as a consequence of the coarse grid with observations from the fire. The assimilation time obtained in this work (of the order of 10 minutes) is expected to be reducible by at least an order of magnitude within the coming decade by advances in computational power. The methodology presented in this thesis constitutes thus a feasible step towards useful fire scenario forecasts with a positive lead time.

An obvious limitation of the proposed methodology is given by the capability of the forward model to represent the true fire. A zone type forward model is a very crude approximation of the governing physics and its applicability (and/or associated uncertainty) to each individual scenario has to be established before implementation. CFD type forward models generally are sufficiently detailed, even with coarse grids, to account with reasonable accuracy for the necessary features (mass and heat transport), but the maximum grid size that can be used without losing the link to the underlying physics needs to be addressed in order to assure acceptable results.

Although the viability of installing and implementing the required sensors in a real building was considered and discussed in this work, this remains an unsolved issue. When using a zone type forward model it is necessary to have a good estimation of the hot layer average temperature, which can be difficult to obtain from a practical point of view. It has to be investigated whether temperatures from thermocouples close to the compartment boundaries can provide enough information for an estimation of the hot layer temperature. If this is not the case, using a zone type forward model will not be possible in this context. A similar problem arises when using a coarse grid CFD type model as forward model. Only one temperature value is reported (and calculated) in each grid cell. This value represents an average of local temperatures. In order to compare the output of a coarse grid CFD model to real data, an average of several measurements has to be made. This results in a large amount of sensors which, although they can be placed close to the boundaries, can result in practical complications when implementing the presented methodology.

Another limitation that will have to be investigated further is the additional information that has to be provided in order to run the simulations. The more detailed the requested output of the forward model, the more details about the compartment to be modelled are required. If the forward model is a zone type fire model, the only required information about the compartment is its area and height, and the geometry

of vent openings. When using a CFD type forward model, additional to the detailed geometry, it is necessary to establish the location of the fire origin and the potential fuel load before starting the assimilation cycle. While the fire origin can be located easily (as a first approximation the location of the highest temperature reading can be used), the fuel load is potentially very variable and its exact distribution might be impractical to continually keep track of. Fortunately it was shown in chapter 5 that for relatively small compartments the exact fuel distribution is not essential in order to produce an adequate forecast, and the fuel load could for example be established based on a statistical analysis of typical compartment layouts. In larger compartments (relative to the fuel load), however, an unknown fuel load might lead to early divergence between forecast and true fire due to a change in the growth pattern of the fire once the fire has reached the physical boundaries of the fuel. Note that this change can potentially be assimilated, and the forecast can be readjusted. Thus, it does not constitute a limitation *per se* to the proposed methodology, but needs to be further investigated.

In summary, the work presented in this thesis, together with the work of Cowlard [1] and Koo [2], establishes the basis for sensor assisted fire fighting, but the envisioned system is not yet fit for operational implementation. It was demonstrated that fire dynamics can be forecasted if combined with information feedback from the evolving fire scenario. The observations allow for the use of simplified models that can run in much shorter time than fully detailed fire models, and can thus provide a forecast in times comparable to typical fire durations without losing the required accuracy. Further research has to be done in order to investigate and assure the robustness of the methodology in real life applications.

The work presented in this document considers only the growth stage of the fire. For fully developed fires the methodology illustrated here has to be modified in order to account for the special features of post-flashover fires. An introduction of the future steps in that direction are given in the next section.

7.2 Future Work

7.2.1 Experimental Testing

The methodology presented in this document needs to be tested extensively with experimental data. While the Dalmarnock Tests provide an obvious set of data with potential for much more exhaustive application of inverse modelling (chapter 6 presents only an example), they are at the very applied end of the spectrum and it is also necessary to design and to conduct specific (medium- or small-) scale experiments in order to assess the robustness of the TLM. In those tests the parameters to be estimated will have to be measured explicitly, in order to establish convergence rates and error bars.

7.2.2 Inverse Modelling of pre- and post-flashover

Fire dynamics are fundamentally different during the growth phase of the fire and the fully developed phase of the fire. During the growth phase the flames are localized and close to the original fuel source of the fire. Heat from the flame is radiated back to the surface of the fuel feeding the pyrolysis process. The amount of combustible gases produced depends mostly on the flame geometry and the thermal properties (heat conduction) of the fuel. The effect of the far field is only important if it affects for instance the flame geometry (wind blowing in tilting the flame towards a certain direction), but it can normally be assumed that the boundary conditions of a fire simulation (walls, ventilation conditions) have only a negligible effect on the fire growth.

In the fully developed phase of the fire the opposite is the case. Due to the lack of oxygen the combustible gases cannot burn close to the fuel source and have to travel until they find the right amount of oxygen to initiate combustion. Thus the flames are no longer localized, and flaming can occur anywhere within the compartment. Ventilation conditions of the compartment become the main parameter that governs fire development.

Due to these fundamental differences, the modelling approach is different, and both phases of the fire have to be modelled independently.

During the growth phase of the fire the parameters that govern fire development are

related to the pyrolysis process in the solid phase and the flame geometry. The details of how to estimate the relevant parameters are given in chapters 4 and 5. There might be a number of different spread rates (e.g. if the fire spreads vertically over a wall, the upwards spread rate will be much faster than the sidewards spread rate), and even several surfaces burning at different spread rates and different burning rates. But the number of parameters to estimate will not exceed, under any practical circumstances, the order of 10.

Once the fire is fully developed, and a change in the environment forces the modeller to update the model with the new information, the simulation has to be restarted. The initial conditions for the new simulation are not ambient any more, as the fire has developed for several minutes in the compartment. These initial conditions have to be considered in the new simulation. In other words, the initial conditions have to be estimated based on sensor measurements in the compartment. This means that at least one (normally more than one) parameter (e.g. temperature) has to be estimated for each grid cell. Depending on the size of the compartment, and the numerical grid considered for the simulations, the number of initial conditions to be estimated can easily reach several millions.

7.2.2.1 Gradient based optimization

For gradient based optimization, it is necessary to calculate the derivative of the output of the model at each point of comparison with respect to each parameter. Let N be the number of points of comparison (i.e. number of outputs, N = Number sensors × times of comparison), and M the number of parameters to be estimated. The matrix of derivatives (Jacobian Matrix) of the model $\mathscr{M}$ is

$$\nabla\mathscr{M} = \begin{bmatrix} \frac{\partial\mathscr{M}_1}{\partial\alpha_1} & \frac{\partial\mathscr{M}_1}{\partial\alpha_2} & \cdots & \frac{\partial\mathscr{M}_1}{\partial\alpha_M} \\ \\ \frac{\partial\mathscr{M}_2}{\partial\alpha_1} & \frac{\partial\mathscr{M}_2}{\partial\alpha_2} & \cdots & \vdots \\ \vdots & \cdots & \ddots & \vdots \\ \frac{\partial\mathscr{M}_N}{\partial\alpha_1} & \cdots & \cdots & \frac{\partial\mathscr{M}_N}{\partial\alpha_M} \end{bmatrix}. \tag{7.1}$$

In practical applications the number of points of comparisons N will be of the order of 10^3 (e.g. 50 sensors × 30 times of comparison).

7.2.2.2 Adjoint modelling

There are several ways of calculating the derivative of a CFD model. The simplest approach, which is implemented in this thesis, is to use finite differences (FD). In order to obtain the whole Jacobian using FD, it is necessary to run the model $M+1$ times (one for each row).

A different, more sophistic approach is to use algorithmic differentiation [3]. This technique is based on the fact that a CFD code is nothing else than a (very large) number of algebraic operations that represent a discretization of the system of partial differential equations (PDEs) that govern the flow. Thus, the CFD code takes an input (parameters, initial and boundary conditions), performs a number of algebraic operations, and gives an output which is an approximation of the solution to the PDEs. It is relatively easy to calculate the derivative of algebraic operations, so that each of the statements in the code can be differentiated. The derivative of the code with respect to the input parameter is then obtained using the chain rule for differentiation. This approach yields the exact derivative of the model output to one requested parameter (input), and is thus superior to the FD approach at a similar (probably lower) computational cost [4]. Implementing algorithmic differentiation could result in an improvement of the efficiency when computing the TLM. It would however still be necessary to run the differentiated code $M+1$ times (one for each parameter, i.e. for each row of the Jacobian).

An alternative approach is to run the algorithmic differentiation backwards instead of forwards, and thus obtaining the adjoint of the optimization problem. This is explained in detail in appendix A. The difference is that in the backwards differentiation (adjoint modelling) the derivative of one output of the code with respect to all parameters (input), i.e. one column of the Jacobian, is obtained with one model run. In order to obtain the whole Jacobian the backwards differentiated code has to be run $N+1$ times (one for each output, i.e. for each column of the Jacobian).

7.2.2.3 Summary

During the growth phase of the fire only a few parameters need to be estimated (of the order of at most 10). Once the fire has developed and flashover has taken place, changes in the ventilation condition can affect the course of the fire in such a way that it is necessary to restart the simulations with new boundary conditions. The necessary initial conditions can be obtained by assimilating measured data into the model. As the variable values at each grid point have to be estimated, the number of parameters can reach several millions.

Forward differentiation (which includes finite differences) calculates one row of the Jacobian with each extra model run. Backwards differentiation (adjoint) calculates one column of the Jacobian with each extra run. Thus, if more measurement points for comparison than parameters exist in the model (typically growth phase of the fire), then it is preferable to use forward differentiation, while if more parameters than measurement points exist in the model (typically fully developed fire), backwards differentiation is more efficient.

Automatic differentiation has important advantages over finite differences (accuracy and efficiency), and it would be desirable to implement the presented methodology with a forward model that allows for algorithmic differentiation. Forward algorithmic differentiation can be implemented with reasonable effort with any existing code. Backwards differentiation, however, is currently limited by the programming scheme used in the code to be differentiated (pointers and dynamic allocation of variables are prohibitive). For an efficient estimation of initial conditions, the adjoint of the forward model would have to be constructed.

References

[1] A. Cowlard. *Sensor and Model Integration for the Rapid Prediction of Concurrent Flow Flame Spread*. PhD thesis, The University of Edinburgh, 2009. http://www.era.lib.ed.ac.uk/handle/1842/2753.

[2] S. Koo, J. Fraser-Mitchell, and S. Welch. Sensor-steered fire simulation. *Fire Safety Journal*, 45(3), 2010. DOI:10.1016/j.firesaf.2010.02.003.

[3] A. Griewank. *Evaluating Derivatives – Prinicples and Techniques of Algorithmic Differentiation*. SIAM, Philadelphia, USA, 2000.

[4] L. Hascoet and V. Pascual. TAPENADE 2.1 User's Guide. Technical report, INRIA, 2004.

Appendix

A

Details of the Tangent Linear Model

A.1 Cost Function

Parameters are estimated by minimizing the following cost function that describes the distance between the model and observations

$$J(\mathbf{p}) = \sum_{i=1}^{N} \left(\mathbf{y}_i - \mathscr{M}_i(\mathbf{x}_0, \mathbf{p})\right)^T \left(\mathbf{y}_i - \mathscr{M}_i(\mathbf{x}_0, \mathbf{p})\right), \tag{A.1}$$

where $\mathscr{M}_i(\mathbf{x}_0, \mathbf{p})$ denotes the model (in this case FDS), $\mathbf{p} \in \mathbb{R}^P$ are the parameters to be estimated, and $\mathbf{y}_i$ are the observations at time i. Note that $\mathbf{y}_i$, $\mathscr{M}_i \in \mathbb{R}^M$, where M is the number of observations that is used for assimilation.

Minimization of this cost function can be obtained using a numerical optimization procedure, such as the Newton–Raphson method for example. The problem with this method is that it requires the gradient of the cost function to be computed at each step of the iteration.

A.2 Tangent Linear Model

If the model is only weakly non-linear close to the parameters that are being estimated, $\mathscr{M}(\mathbf{x}_0, \mathbf{p})$ can be approximated by a linear function around the first guess for the parameter. This is called the Tangent Linear Model (TLM). The cost function (A.1) becomes thus a quadratic function that can be minimized efficiently and without the need of an updated gradient.

The linear approximation is obtained from a Taylor expansion around the first guess $\mathbf{p}^b$.

$$\mathscr{M}(\mathbf{x}_0, \mathbf{p}) \simeq \mathscr{M}(\mathbf{x}_0, \mathbf{p}^b) + \nabla_{\mathbf{p}} \mathscr{M}(\mathbf{x}_0, \mathbf{p}^b) \left(\mathbf{p} - \mathbf{p}^b\right), \tag{A.2}$$

where $\nabla_{\mathbf{p}} \mathscr{M}(\mathbf{x}_0, \mathbf{p}^b) \in I\!R^{P \times M}$ is the Jacobian matrix evaluated at $\mathbf{p}^b$.

This can then be replaced in the cost function (A.1)

$$\begin{aligned} \tilde{J}(\mathbf{p}) = \sum_{i=1}^{N} \Big(\mathbf{y}_i - \Big[\mathscr{M}(\mathbf{x}_0, \mathbf{p}^b) + \nabla_{\mathbf{p}} \mathscr{M} \ \ (\mathbf{x}_0, \mathbf{p}^b) \left(\mathbf{p} - \mathbf{p}^b\right)\Big]\Big)^T \\ \Big(\mathbf{y}_i - \Big[\mathscr{M}(\mathbf{x}_0, \mathbf{p}^b) + \nabla_{\mathbf{p}} \mathscr{M}(\mathbf{x}_0, \mathbf{p}^b) \left(\mathbf{p} - \mathbf{p}^b\right)\Big]\Big), \end{aligned} \tag{A.3}$$

As opposed to the Newton–Raphson method, where the minimum of a quadratic function that is tangent to the original function that is minimized is searched for, the TLM of the forward model converts the cost function into a quadratic function with a minimum that is close to the exact minimum of the cost function. Figure A.1 illustrates the difference between a linearization of the forward model and the Newton–Raphson method using a nonlinear cost function ($f(x) = (\ln(x))^2$).

A.3 Gradient of the Cost Function

The gradient of the linearized cost function (A.3) is as follows

$$\nabla_{\mathbf{p}} \tilde{J}(\mathbf{p}) = 2 \sum_{i=1}^{N} \left(\nabla_{\mathbf{p}} \mathscr{M}_i(\mathbf{x}_0, \mathbf{p}^b)\right)^T \left(\mathbf{y}_i - \left[\mathscr{M}_i(\mathbf{x}_0, \mathbf{p}^b) + \nabla_{\mathbf{p}} \mathscr{M}_i(\mathbf{x}_0, \mathbf{p}^b) \left(\mathbf{p} - \mathbf{p}^b\right)\right]\right) \tag{A.4}$$

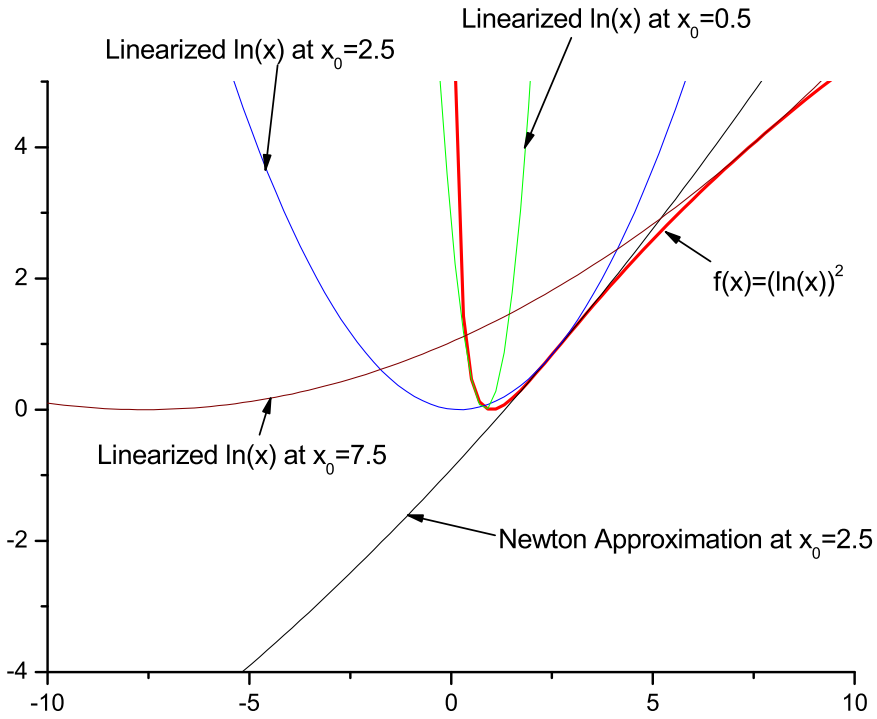

Figure A.1: Comparison of Newton–Raphson method for minimization and linearization of the forward model.

The first order condition for minimization of (A.3) requires the gradient (Eq. (A.4)) to be zero. Introducing the following notation,

$$\begin{aligned} \mathbf{M}_i &= \mathscr{M}_i(\mathbf{x}_0, \mathbf{p}^b), \\ \mathbf{H}_i &= \nabla_{\mathbf{p}} \mathscr{M}_i(\mathbf{x}_0, \mathbf{p}^b), \\ \tilde{\mathbf{p}} &= \left(\mathbf{p} - \mathbf{p}^b\right) \end{aligned}$$

the first order condition can be written as

$$\sum_{i=1}^{N} \mathbf{H}_i^T \left(\mathbf{y}_i - \left[\mathbf{M}_i + \mathbf{H}_i \tilde{\mathbf{p}}\right]\right) = 0. \tag{A.5}$$

The matrix $\mathbf{H}_i$ is often referred to as the "Tangent Linear" to the model, while its transpose, $\mathbf{H}_i^T$ is the "Adjoint" to the TL matrix.

Developing and rearranging Eq. (A.5) results in

$$\begin{aligned}
\sum_{i=1}^{N} \mathbf{H}_i^T \left(\mathbf{y}_i - \left[\mathbf{M}_i + \mathbf{H}_i\tilde{\mathbf{p}}\right]\right) &= \mathbf{H}_1^T \left(\mathbf{y}_1 - \left[\mathbf{M}_1 + \mathbf{H}_1\tilde{\mathbf{p}}\right]\right) + \mathbf{H}_2^T \left(\mathbf{y}_2 - \left[\mathbf{M}_2 + \mathbf{H}_2\tilde{\mathbf{p}}\right]\right) + \\
&\qquad \cdots + \mathbf{H}_N^T \left(\mathbf{y}_N - \left[\mathbf{M}_N + \mathbf{H}_N\tilde{\mathbf{p}}\right]\right) = 0 \\
&= \mathbf{H}_1^T \left(\mathbf{y}_1 - \mathbf{M}_1 - \mathbf{H}_1\tilde{\mathbf{p}}\right) + \mathbf{H}_2^T \left(\mathbf{y}_2 - \mathbf{M}_2 - \mathbf{H}_2\tilde{\mathbf{p}}\right) + \\
&\qquad \cdots + \mathbf{H}_N^T \left(\mathbf{y}_N - \mathbf{M}_N - \mathbf{H}_N\tilde{\mathbf{p}}\right) = 0 \\
&= \mathbf{H}_1^T \left(\mathbf{y}_1 - \mathbf{M}_1\right) - \mathbf{H}_1^T\mathbf{H}_1\tilde{\mathbf{p}} + \mathbf{H}_2^T \left(\mathbf{y}_2 - \mathbf{M}_2\right) - \mathbf{H}_2^T\mathbf{H}_2\tilde{\mathbf{p}} + \\
&\qquad \cdots + \mathbf{H}_N^T \left(\mathbf{y}_N - \mathbf{M}_N\right) - \mathbf{H}_N^T\mathbf{H}_N\tilde{\mathbf{p}} = 0.
\end{aligned}$$

This can be rearranged as

$$\sum_{i=1}^{N} \mathbf{H}_i^T\mathbf{H}_i\tilde{\mathbf{p}} = \sum_{i=1}^{N} \mathbf{H}_i^T \left(\mathbf{y}_i - \mathbf{M}_i\right).$$

Defining

$$\begin{aligned}
\mathbf{A} &= \sum_{i=1}^{N} \mathbf{H}_i^T\mathbf{H}_i \quad \text{and} \\
\mathbf{b} &= \sum_{i=1}^{N} \mathbf{H}_i^T \left(\mathbf{y}_i - \mathbf{M}_i\right),
\end{aligned}$$

Eq. (A.5) results in a linear system of the form

$$\mathbf{A}\tilde{\mathbf{p}} = \mathbf{b}, \tag{A.6}$$

which can be solved using a numerical scheme such as the conjugate gradient method.

A.4 For a Single Parameter

In the case that only one parameter is being estimated, Eq. (A.6) reduces to $a \cdot p = b$, and can be solved directly. Rearranging and setting equal to zero Eq. (A.4), p can be

obtained from the initial guess p^b

$$p = p^b + \frac{\sum_{j=1}^{N}\sum_{i=1}^{M} \frac{\partial \mathscr{M}_i^j(p^b)}{\partial p}\left(y_i^j - \mathscr{M}_i^j(p^b)\right)}{\sum_{i=1}^{N}\sum_{j=1}^{M}\left(\frac{\partial \mathscr{M}_i^j(p^b)}{\partial p}\right)^2} \tag{A.7}$$

A.5 Efficiency Considerations

Obtaining the Jacobian matrix of the model, which is equivalent to the Tangent Linear Model $\mathbf{H}_i$, can be computationally very expensive. There are different ways of calculating the derivatives, and the efficiency of choosing one or another can result in important improvements regarding time and efficiency. The different ways of calculating the Jacobian matrix consist in using one of the following techniques:

- Finite Difference approximation.
- Tangent Differentiation.
  - → First discretize, then differentiate.
  - → First differentiate, then discretize.
- Adjoint Model
  - → First discretize, then differentiate.
  - → First differentiate, then discretize.

A.5.1 Finite Difference

The simplest way of calculating a derivative numerically is taking the finite difference approach,

$$\frac{\partial \mathscr{M}_i^j(\mathbf{p}^b)}{\partial p_k} \simeq \frac{\mathscr{M}_i^j(\mathbf{p}^b + \boldsymbol{\varepsilon}_k) - \mathscr{M}_i^j(\mathbf{p}^b)}{||\boldsymbol{\varepsilon}_k||}, \tag{A.8}$$

where $\boldsymbol{\varepsilon}_k \in \mathbb{R}^P = \{0, 0, \ldots, \varepsilon, \ldots, 0\}$ with a perturbation ε in position k. While this approach is easy to implement, its accuracy depends on the size of the perturbation and it requires an additional run of the model for each parameter to be estimated.

A.5.2 Tangent Differentiation

Alternatively to the finite difference approach, the Jacobian matrix can be obtained by differentiating the model equations. This can be done either before the equations are discretized, or afterwards differentiating the discretized equations.

A.5.2.1 Differentiate then discretize

The model equations are differentiated with respect to a parameter p_k, yielding an additional differential equation for each model equation. These can then be discretized alongside with the model equations.

A.5.2.2 Discretize then differentiate

If the model equations are already discretized, it can often be easier to differentiate the discrete model equations. Generally a discretized model has the form

$$x_i = f(x_{i-1}, x_{i-2}, \ldots, x_{i-l}, p_k), \tag{A.9}$$

i.e. the value at time (or position) i is obtained based on previously computed x. Therefore the chain rule can be applied to obtain the derivative

$$x_i' = \frac{\mathrm{d}x_i}{\mathrm{d}p_k} = \frac{\partial x_i}{\partial x_{i-1}} \frac{\mathrm{d}x_{i-1}}{\mathrm{d}p_k} + \frac{\partial x_i}{\partial x_{i-2}} \frac{\mathrm{d}x_{i-2}}{\mathrm{d}p_k} + \cdots + \frac{\partial x_i}{\partial x_{i-l}} \frac{\mathrm{d}x_{i-l}}{\mathrm{d}p_k} + \frac{\partial x_i}{\partial p_k}. \tag{A.10}$$

This can then be solved recursively. There are several open source programs that can transform a computer coded model into a tangent linear model using automatic differentiation.

As a matter of example, let us assume that the model code takes just one parameter, and that the underlying equation is of the form $f(x) = sin(x^2)$. It is of interest to obtain $\mathrm{d}f/\mathrm{d}x$.

The code would be as follows:

Listing A.1: Code example

```
start program
read 'input'
x1=input
x2=x1*x1
x3=sin(x2)
end program
```

Algorithmic differentiation reads each statement of the code, and applies the chain rule to it, as shown in Table A.1.

$x_0 = 2$	$x_0' = \partial x_0 / \partial x_0 = 1$
$x_1 = x_0 = 2$ $x_2 = x_1^2 = 4$ $x_3 = \sin(x_2) = \sin(4)$ $= -0.7568$	$x_1' = \partial x_1 / \partial x_0 = 1$ $x_2' = \partial x_2 / \partial x_1 \cdot \partial x_1 / \partial x_0 = 2x_1 \cdot x_1' = 2 \cdot 2 \cdot 1 = 4$ $x_3' = \partial x_3 / \partial x_2 \cdot \partial x_2 / \partial x_0 = \cos(x_2) \cdot x_2' = \cos(4) \cdot 4$ $= -2.6146$
$f(x) = x_3 = -0.7568$	$f'(x) = \partial f / \partial x_0 = \partial f / \partial x_3 \cdot \partial x_3 / \partial x_0 = x_3' = -2.6146$

Table A.1: Forward algorithmic differentiation evaluated in $x = 2$. The first row corresponds to the assignment of input parameters, the last row is the output of the code, and the rows in between are the body of the code.

This code transformation can be done automatically, and the differentiated code `program` would be as follows:

Listing A.2: Forward mode differentiated code

```
start d_program
read 'input'
x1=input
dx1=1.0
x2=x1*x1
dx2=2*x1*dx1
x3=sin(x2)
dx3=cos(x2)*dx2
end d_program
```

The derivative of $f(x)$ with respect to x is `dx3`. It can be seen that the number of statements is doubled in code `d_program` with respect to `program`. Thus it can be expected that the time to run `d_program` will take twice as long, which is comparable to the finite difference approach. Note that this approach also yields one entire row of the Jacobian matrix for each run. It is always possible to find the algorithmic differentiation of an existing code, as long as the source files are available. For codes written in `FORTRAN` and C++, there are a vast amount of programs available that transform the original code into differentiated code.

Note that both of the tangent methods are as accurate as the discretization of the model equations, i.e. no extra truncation error is present. The tangent differentiation has to be run once for each parameter.

A.5.3 Adjoint Model

When the number of parameters to be estimated is much larger than the observations the model is compared to, the adjoint approach presents some important advantages. While the tangent method (the same as the finite differences method) propagates an initial perturbation of a parameter and yields the sensitivity of the model to this parameter, the adjoint runs "backwards" and yields the set of perturbations of parameters that are required to produce a certain perturbation of the model. In terms of efficiency this means that with one run of the adjoint model the derivative of one model variable with respect to as many parameters as desired can be obtained. This is particularly interesting if the initial conditions of the model need to be estimated. In that case the number of derivatives needed is the number of degrees of freedom of the model. When the adjoint is obtained, the Tangent Linear is created by transposing the matrix $\mathbf{H}_i^T$

A.5.3.1 Differentiate then discretize

The adjoint of a system of partial differential equations (PDE) can be interpreted as the Lagrange multiplier of a minimization problem, where the model acts as a constraint. Although the adjoint of any system of PDE always exists, it can be mathematically very demanding to find it, requiring advanced skills in integral calculus.

If it is found, an additional differential equation is obtained that has to be solved alongside the original model equations by some kind of discretization.

A.5.3.2 Discretize then differentiate

Alternatively it is possible to find the adjoint of the discrete model equations. This is done by applying the chain rule, although in backwards mode. If N is the time at which the derivative is to be calculated, then $\bar{x}_i$ denotes the derivative of x_N with respect to x_i

$$\bar{x}_i = \frac{\mathrm{d}x_N}{\mathrm{d}x_i} = \frac{\partial x_N}{\partial x_i} + \frac{\mathrm{d}x_N}{\mathrm{d}x_{N-1}}\frac{\partial x_{N-1}}{\partial x_i} + \frac{\mathrm{d}x_N}{\mathrm{d}x_{N-2}}\frac{\partial x_{N-2}}{\partial x_i} + \cdots + \frac{\mathrm{d}x_N}{\mathrm{d}x_{i+1}}\frac{\partial x_{i+1}}{\partial x_i}. \tag{A.11}$$

This can again be solved recursively. Many of the automatic differentiation softwares can produce the adjoint model in backwards mode. However, there are some fundamental problems when the original code is programmed using advanced programming tools. Since for the adjoint all the information of the forward integration of the model has to be saved, it requires an important amount of memory space, and dynamic allocation of variables and pointers are still subject to active research for adjoint code generation and are not supported by current automatic differentiation tools [1].

Let us consider again the example of the model code with the underlying equation of the form $f(x) = sin(x^2)$. The reverse mode differentiation is shown in Table A.2.

$x_0 = 2$	$\bar{x}_0 = \partial f/\partial x_0 = \partial f/\partial x_1 \cdot \partial x_1/\partial x_0 = \bar{x}_1 \cdot 1 = -2.6146$
$x_1 = x_0 = 2$	$\bar{x}_1 = \partial f/\partial x_1 = \partial f/\partial x_2 \cdot \partial x_2/\partial x_1 = \bar{x}_2 \cdot 2x_1$
	$= -0.6536 \cdot 2 \cdot 2 = -2.6146$
$x_2 = x_1^2 = 4$	$\bar{x}_2 = \partial f/\partial x_2 = \partial f/\partial x_3 \cdot \partial x_3/\partial x_2 = \cos(x_2) = \cos(4)$
	$= -0.6536$
$x_3 = \sin(x_2) = \sin(4)$	$\bar{x}_3 = \partial f/\partial x_3 = 1$
$f(x) = x_3 = -0.7568$	$\bar{f}(x) = \partial f/\partial f = 1$

Table A.2: Reverse algorithmic differentiation evaluated in $x = 2$. The first row corresponds to the assignment of input parameters, the last row is the output of the code, and the rows in between are the body of the code.

This code transformation can be done automatically, and the reversely differentiated code `program` would be as follows:

Listing A.3: Reverse mode differentiated code

```
start b_program
read 'input'
x1=input
x2=x1*x1
x3=sin(x2)
bx3=1.0
bx2=cos(x2)*bx3
bx1=bx2*2*x1
end b_program
```

In this case the desired derivative is stored in `bx1` which corresponds to $\bar{x}_0$ in Table A.2. It is important to notice that for the reverse mode to work, it is necessary to run the whole code normally before calculating the derivative. This means that potentially a large amount of memory is necessary to store all the variables (the needed memory is proportional to the size of the variable, i.e. indirectly to the number of grid cells). Although the methodology is based on the same assumptions of chain rule use as the forward differentiation, it has the additional requirement that the variables have to be stored during the whole run of the code (i.e. pointers cannot be used in the code).

Note that in the reverse mode one run of the model gives one entire column of the Jacobian matrix. In the case that there are more parameters than points of measurements ($M > N$), it is preferable to use the reverse mode, as only N runs of the model are needed to obtain the Jacobian, whereas the forward mode needs M runs of the model. Equivalently, if there are more points of measurement than parameters to estimate, it is more convenient to use the forward or tangent linear approach.

A.5.4 Minimizing a Quadratic Function

If the dimension of the parameter vector $\tilde{\mathbf{p}}$ is greater than one, it can be cheaper to solve the resulting linear system (A.6) using an iterative method rather than inverting the matrix $\mathbf{A}$.

The conjugate gradient method finds the minimum of a quadratic system in P iterations, P being the dimension of matrix $\mathbf{A}$.

References

[1] L. Hascoet and V. Pascual. TAPENADE 2.1 User's Guide. Technical report, INRIA, 2004.